

SHEAR BEHAVIOR OF GEOSYNTHETIC ENCASED COLUMNS EMBEDDED
IN SOFT SOILS

by

Murat Cenk Erdurak

B.S., Civil Engineering, Boğaziçi University, 2008

M.S., Civil Engineering, Boğaziçi University, 2011

Submitted to the Institute for Graduate Studies in
Science and Engineering in partial fulfillment of
the requirements for the degree of
Doctor of Philosophy

Graduate Program in Civil Engineering
Boğaziçi University

2020

SHEAR BEHAVIOR OF GEOSYNTHETIC ENCASED COLUMNS EMBEDDED
IN SOFT SOILS

APPROVED BY:

Prof. Erol Güler
(Thesis Supervisor)

Assist. Prof. I. Emrah Kılıç
(Thesis Co-supervisor)

Prof. Ayşe Edinçliler

Assoc. Prof. Özer Çinicioğlu, Not Approved

Assist. Prof. Murat Hamderi

Assist. Prof. Berrak Teymur

DATE OF APPROVAL: 03.10.2019

ACKNOWLEDGEMENTS

I would like to express my heart felt gratitude to my thesis supervisor, Prof. Erol Güler for his continuous support, precious guidance and encouragement. Without his endless patience this study would not be completed.

I would like to thank Cihan Cengiz for inventing the Unit Cell Shear Device and making possible to conduct this graduate study. I am grateful to him for his encouragement and support. I would also thank, my thesis co-supervisor, Asst. Prof. İsmail Emrah Kılıç for his support and helpful suggestions.

I would like to thank members of my thesis committee, Asst. Prof. Murat Hamderi, Prof. Ayşe Edinçliler, Asst. Prof. Berrak Teymür and Assoc. Prof. Özer Çinicioğlu who devoted their invaluable time for reading and commenting on my thesis.

I owe my friends Musa Rahmanlar and Yusuf Eşidir a debt of gratitude. Their precious support made it possible to accomplish this thesis.

I would to thank all my friends in the department and in the civil engineering laboratories. Many heartfelt thank are to Ayşe Aydın and Yener Aydın for their support and guidance.

Finally, I extremely indebted to my mother Türkan and my sister Ceren for their immense support and patience throughout my life.

This thesis is dedicated in loving memory of my father and grandparents.

ABSTRACT

SHEAR BEHAVIOR OF GEOSYNTHETIC ENCASED COLUMNS EMBEDDED IN SOFT SOILS

In this study, the static and cyclic shear behavior of ordinary and geosynthetic encased columns embedded in soft soils are investigated. In the former researches, it was seen that the shear behavior of geosynthetic encased columns were not studied sufficiently. In these few studies, the scale ratio is not considered, and the other field conditions are not represented in the models. Although the shear and bending failure mechanism are also common, the lack of research might be explained by the lack of sufficient and required experimental setups and models and by the newly recognition of these failure modes. Therefore this study was focused on the shear behavior of the ordinary and geosynthetic encased columns and the Unit Cell Shear Device was used. This is the first time that UCSD is used to investigate the shear behavior of GECs and OSCs in clay. The Unit Cell Shear Device can shear unit cells prepared with stone columns that are slender and have relatively high model to prototype diameter ratios (approximately 1:3.5). 5 types of unit cells were used in this study, namely, benchmark unit cell, unit cell with ordinary stone column and the unit cells with encasements made by 3 different types of geotextiles. The surrounding soil in these unit cells were prepared in 3 different consolidation loads, namely 15 kPa, 25 kPa and 35 kPa. All these unit cells were prepared as 2 sets and they were tested under static and cyclic loading. During the experiments, horizontal displacement and shear loading readings were taken. For the experiments with geosynthetic encased columns, strain readings in 3 levels were, also, taken. The equivalent friction angles at different horizontal displacements for both static and cyclic shearing were calculated in order to evaluate the soil improvement capacity for geosynthetic encased columns using geotextiles with different stiffnesses.

ÖZET

GEOSENTETİK İLE MANTOLANMIŞ TAŞ KOLONLARIN YUMUŞAK ZEMİNLERDEKİ KESME DAVRANIŞI

Bu çalışmada, taş kolonların ve geosentetik ile mantolanmış taş kolonların yumuşak zeminlerdeki, statik ve döngüsel kesme davranışları incelenmiştir. Daha önceki çalışmalarda geosentetik ile mantolanmış taş kolonların kesme davranışının yeterince araştırılmadığı görülmüştür. Bu çalışmalarda ölçek oranının dikkate alınmadığı ve diğer zemin koşullarının modellere yeterince aktarılmadığı görülmüştür. Kesme ve eğme nedenli göçmeler yaygın olmasına rağmen, ilgili araştırmaların azlığı, yeterli ve gerekli deneysel düzeneklerin ve modellerin olmaması, bu göçme modlarının yeni tanınması ile açıklanabilir. Bu çalışma, taş kolon ve geosentetik ile mantolanmış taş kolonların kesme davranışına odaklandığından, Birim Hücre Kesme Cihazı (BHKC) kullanılmıştır. İlk kez bu çalışmada BHKC geosentetikle mantolanmış taş kolonların ve taş kolonların kildeki kesme davranışını incelemekte kullanılmıştır. BHKC, narin ve model/prototip çap oranları yüksek (yaklaşık 1: 3.5) taş kolonlarla hazırlanmış birim hücreleri keşebilir. Bu çalışmada 5 tip birim hücre (kontrol amaçlı kil model birim hücresi, taş kolonla hazırlanmış birim hücre ve 3 farklı tipte geotekstil ile hazırlanmış geosentetik ile mantolanmış taş kolonlu birim hücre) kullanılmıştır. Bu birim hücrelerdeki taş kolonlar etrafındaki zemin 15 kPa, 25 kPa ve 35 kPa olmak üzere 3 farklı konsolidasyon yükünde hazırlanmıştır. Bütün bu birim hücreler 2 takım olarak hazırlanmış, statik ve döngüsel yükleme altında test edilmiştir. Deneyler sırasında yatay deplasman ve kesme yükleri kaydedilmiştir. Geosentetik ile mantolanmış taş kolonlu deneyler için, 3 seviyedeki gerinim değerleri alınmıştır. Hem statik hem de döngüsel kesme deneylerinde farklı deplasman değerlerindeki eşdeğer sürtünme açıları hesaplanmış, bu sayede farklı rijitlik değerlerine sahip geotekstiller kullanarak hazırlanmış geosentetik ile mantolanmış taş kolonların zemin iyileştirme kapasiteleri değerlendirilmiştir.

TABLE OF CONTENTS

ACKNOWLEDGEMENTS	iii
ABSTRACT	iv
ÖZET	v
LIST OF FIGURES	viii
LIST OF TABLES	xv
LIST OF SYMBOLS	xix
LIST OF ACRONYMS/ABBREVIATIONS	xxi
1. INTRODUCTION	1
2. LITERATURE REVIEW	6
3. METHODOLOGY	15
3.1. Materials	15
3.1.1. Clay and Clay Slurry	15
3.1.2. Gravel	16
3.1.3. Geosynthetic Reinforcement	17
3.1.4. Latex Membrane	18
3.2. Unit Cell Shear Device	19
3.2.1. Unit Cell Shear Device Design Considerations	21
3.2.2. Operating and Measurement Systems	23
3.2.2.1. Actuators	23
3.2.2.2. Load Cell, Laser Displacement Sensors and Strain Rosettes	23
3.2.2.3. Data Logger	24
3.2.3. Unit Cell Model Preparation	24
3.2.4. The Preparation and Placement of GECs in the Unit Cell	26
3.3. Experimental Scheme	29
4. TEST RESULTS AND EVALUATION	32
4.1. Tests to Determine Material Properties	32
4.1.1. Consolidation Properties	32
4.1.2. Shear Strength Properties	34
4.2. Unit Cell Shear Device Tests	36

4.2.1. Monotonic Shear Loading	36
4.2.2. Cyclic Shear Loading	41
4.2.3. Evaluation of Test Results	43
4.2.4. Strain Measurements	48
5. CONCLUSION	57
REFERENCES	61
APPENDIX A: MOHR-COULOMB ENVELOPES	65



LIST OF FIGURES

Figure 1.1.	Scheme of GEC (Murugesan and Rajagopal, 2010).	2
Figure 1.2.	Displacement method for GEC installation (Alexiew et al., 2005, after Huesker).	3
Figure 1.3.	Replacement method for GEC execution (Gniel and Bouazza, 2010).	4
Figure 2.1.	Analytical Axisymmetric Calculation Model (Raithel and Kempfert, 2000).	8
Figure 2.2.	Design Chart for OSC (modified from Ambily and Gandhi, 2007, taken from Najjar, 2013).	11
Figure 2.3.	(a) Failure Modes Identified in the Literature, (b) Nature of the Problem (Cengiz <i>et al.</i> , 2019).	12
Figure 2.4.	Cross sections of calculation models for the finite difference analysis of (a) individual columns and (b) an equivalent area (all dimensions are in meters).	13
Figure 3.1.	Hydrometer Analysis of Clay.	15
Figure 3.2.	Clay Slurry Placement.	16
Figure 3.3.	Unit Cell Shear Device (UCSD).	20
Figure 3.4.	(a) Pneumatic Piston for Static Shearing, (b) Actuator for Cyclic Loading.	21

Figure 3.5.	Partial Sketch of the UCSD Illustrating Cyclic Loading Unit and Vessels (Cihan <i>et al.</i> , 2019).	22
Figure 3.6.	Unit Cell with Latex Membrane.	25
Figure 3.7.	Sand Bed at the Bottom of the Benchmark Unit Cell.	25
Figure 3.8.	Geotextile for Bottom Filtration in Benchmark Unit Cells.	26
Figure 3.9.	Top Sealing of the Benchmark Unit Cell.	27
Figure 3.10.	The Stainless-steel on the top of Geotextile Filter.	28
Figure 3.11.	Strain Rosettes glued onto a geotextile encasement.	28
Figure 3.12.	A GEC in the Unit Cell.	29
Figure 3.13.	112 Channel Data Logger with the UCSD.	30
Figure 3.14.	Taken Before Cyclic Shearing Begins.	31
Figure 4.1.	Vertical Settlement vs. Log Time (min) during Consolidation under 15 kPa, 25 kPa and 35 kPa Vertical Loading in Direct Shear Apparatus.	33
Figure 4.2.	Vertical Settlement vs. Log Time (min) during Consolidation under 15 kPa, 25 kPa and 35 kPa Vertical Loading of the Unit Cells with OSC.	33
Figure 4.3.	Vertical Settlement vs. Log Time (min) during Consolidation under 15 kPa, 25 kPa and 35 kPa Vertical Loading of Benchmark Unit Cells.	34

Figure 4.4.	Shear Stress vs. Horizontal Displacement Results in Direct Shear Tests after 15 kPa, 25 kPa and 35 kPa Consolidation.	34
Figure 4.5.	Failure Envelope from the Direct Shear Test Results.	35
Figure 4.6.	Vertical Displacement vs. Horizontal Displacement Results in Direct Shear Tests after 15 kPa, 25 kPa and 35 kPa Consolidation.	35
Figure 4.7.	Shear Stress vs. Displacement Graph for Monotonic Benchmark Unit Cell Shearing.	36
Figure 4.8.	Failure Envelope from the Unit Cell Shear Device Benchmark Test Results.	37
Figure 4.9.	Shear Stress vs. Displacement Graph for Monotonic Unit Cell Shearing Conducted after Consolidation under 35 kPa Load.	38
Figure 4.10.	Shear Stress vs. Displacement Graph for Monotonic Unit Cell Shearing Conducted after Consolidation under 25 kPa Load.	39
Figure 4.11.	Shear Stress vs. Displacement Graph for Monotonic Unit Cell Shearing Conducted after Consolidation under 15 kPa Load.	40
Figure 4.12.	Shear Stress vs. Displacement Graph for Monotonic Unit Cell Shearing Conducted with all Benchmark Unit Cells, all Unit Cells with OSC and Unit Cell with J1000 after Consolidation of 15 kPa Loading.	41
Figure 4.13.	10 th Cycle of Shear Stress versus Displacement Loop with Cyclic Shear Loading after Consolidation under 35 kPa Load.	42

Figure 4.14.	10 th Cycle of Shear Stress versus Displacement Loop with Cyclic Shear Loading after Consolidation under 25 kPa Load.	42
Figure 4.15.	10 th Cycle of Shear Stress versus Displacement Loop with Cyclic Shear Loading after Consolidation under 15 kPa Load.	43
Figure A.1.	Mohr-Coulomb Envelope for the Benchmark Unit Cell at +5 mm Horizontal Displacement during Monotonic Shearing.	65
Figure A.2.	Mohr-Coulomb Envelope for the Benchmark Unit Cell at +10 mm Horizontal Displacement during Monotonic Shearing.	65
Figure A.3.	Mohr-Coulomb Envelope for the Benchmark Unit Cell at +35 mm Horizontal Displacement during Monotonic Shearing.	66
Figure A.4.	Mohr-Coulomb Envelope for the Benchmark Unit Cell at +60 mm Horizontal Displacement during Monotonic Shearing.	66
Figure A.5.	Mohr-Coulomb Envelope for the Unit Cell with OSC at +5 mm Horizontal Displacement during Monotonic Shearing.	67
Figure A.6.	Mohr-Coulomb Envelope for the Unit Cell with OSC at +10 mm Horizontal Displacement during Monotonic Shearing.	67
Figure A.7.	Mohr-Coulomb Envelope for the Unit Cell with OSC at +35 mm Horizontal Displacement during Monotonic Shearing.	68
Figure A.8.	Mohr-Coulomb Envelope for the Unit Cell with OSC at +60 mm Horizontal Displacement during Monotonic Shearing.	68
Figure A.9.	Mohr-Coulomb Envelope for the Unit Cell with J35 at +5 mm Horizontal Displacement during Monotonic Shearing.	69

Figure A.10. Mohr-Coulomb Envelope for the Unit Cell with J35 at +10 mm Horizontal Displacement during Monotonic Shearing.	69
Figure A.11. Mohr-Coulomb Envelope for the Unit Cell with J35 at +35 mm Horizontal Displacement during Monotonic Shearing.	70
Figure A.12. Mohr-Coulomb Envelope for the Unit Cell with J35 at +60 mm Horizontal Displacement during Monotonic Shearing.	70
Figure A.13. Mohr-Coulomb Envelope for the Unit Cell with J400 at +5 mm Horizontal Displacement during Monotonic Shearing.	71
Figure A.14. Mohr-Coulomb Envelope for the Unit Cell with J400 at +10 mm Horizontal Displacement during Monotonic Shearing.	71
Figure A.15. Mohr-Coulomb Envelope for the Unit Cell with J400 at +35 mm Horizontal Displacement during Monotonic Shearing.	72
Figure A.16. Mohr-Coulomb Envelope for the Unit Cell with J400 at +60 mm Horizontal Displacement during Monotonic Shearing.	72
Figure A.17. Mohr-Coulomb Envelope for the Unit Cell with J1000 at +5 mm Horizontal Displacement during Monotonic Shearing.	73
Figure A.18. Mohr-Coulomb Envelope for the Unit Cell with J1000 at +10 mm Horizontal Displacement during Monotonic Shearing.	73
Figure A.19. Mohr-Coulomb Envelope for the Unit Cell with J1000 at +35 mm Horizontal Displacement during Monotonic Shearing.	74
Figure A.20. Mohr-Coulomb Envelope for the Unit Cell with J1000 at +60 mm Horizontal Displacement during Monotonic Shearing.	74

Figure A.21. Mohr-Coulomb Envelope for the Benchmark Unit Cell at +5 mm Horizontal Displacement during Cyclic Shearing.	75
Figure A.22. Mohr-Coulomb Envelope for the Benchmark Unit Cell at +10 mm Horizontal Displacement during Cyclic Shearing.	75
Figure A.23. Mohr-Coulomb Envelope for the Benchmark Unit Cell at +35 mm Horizontal Displacement during Cyclic Shearing.	76
Figure A.24. Mohr-Coulomb Envelope for Unit Cell with OSC at +5 mm Horizontal Displacement during Cyclic Shearing.	76
Figure A.25. Mohr-Coulomb Envelope for Unit Cell with OSC at +10 mm Horizontal Displacement during Cyclic Shearing.	77
Figure A.26. Mohr-Coulomb Envelope for Unit Cell with OSC at +35 mm Horizontal Displacement during Cyclic Shearing.	77
Figure A.27. Mohr-Coulomb Envelope for Unit Cell with J35 at +5 mm Horizontal Displacement during Cyclic Shearing.	78
Figure A.28. Mohr-Coulomb Envelope for Unit Cell with J35 at +10 mm Horizontal Displacement during Cyclic Shearing.	78
Figure A.29. Mohr-Coulomb Envelope for Unit Cell with J35 at +35 mm Horizontal Displacement during Cyclic Shearing.	79
Figure A.30. Mohr-Coulomb Envelope for Unit Cell with J400 at +5 mm Horizontal Displacement during Cyclic Shearing.	79
Figure A.31. Mohr-Coulomb Envelope for Unit Cell with J400 at +10 mm Horizontal Displacement during Cyclic Shearing.	80

Figure A.32. Mohr-Coulomb Envelope for Unit Cell with J400 at +35 mm Horizontal Displacement during Cyclic Shearing. 80

Figure A.33. Mohr-Coulomb Envelope for Unit Cell with J1000 at +5 mm Horizontal Displacement during Cyclic Shearing. 81

Figure A.34. Mohr-Coulomb Envelope for Unit Cell with J1000 at +10 mm Horizontal Displacement during Cyclic Shearing. 81

Figure A.35. Figure A.34. Mohr-Coulomb Envelope for Unit Cell with J1000 at +35 mm Horizontal Displacement during Cyclic Shearing. 82

LIST OF TABLES

Table 3.1.	Engineering Properties of Infill Materials.	16
Table 3.2.	Model and Prototype Comparison.	17
Table 3.3.	Scaling Relationships used for Model to Prototype Scaling.	17
Table 3.4.	Tensile Stiffness Parameters of the Geotextiles.	18
Table 3.5.	The Characteristics of Latex Membrane.	19
Table 3.6.	Experimental Scheme.	30
Table 4.1.	Monotonic Shear Strength Results of Benchmark Unit Cell, Unit Cell with OSC, J35, J400, J1000 after 15 kPa consolidation at +5 mm, +10 mm, +35 mm and +60 mm Displacement.	44
Table 4.2.	Monotonic Shear Strength Results of Benchmark Unit Cell, Unit Cell with OSC, J35, J400, J1000 after 25 kPa consolidation at +5 mm, +10 mm, +35 mm and +60 mm Displacement.	44
Table 4.3.	Monotonic Shear Strength Results of Benchmark Unit Cell, Unit Cell with OSC, J35, J400, J1000 after 35 kPa consolidation at +5 mm, +10 mm, +35 mm and +60 mm Displacement.	45
Table 4.4.	Cyclic Shear Strength Results of Benchmark Unit Cell, Unit Cell with OSC, J35, J400, J1000 after 15 kPa consolidation at +5 mm, +10 mm and +35 mm Displacement.	45

Table 4.5.	Cyclic Shear Strength Results of Benchmark Unit Cell, Unit Cell with OSC, J35, J400, J1000 after 25 kPa consolidation at +5 mm, +10 mm and +35 mm Displacement.	45
Table 4.6.	Cyclic Shear Strength Results of Benchmark Unit Cell, Unit Cell with OSC, J35, J400, J1000 after 35 kPa consolidation at +5 mm, +10 mm and +35 mm Displacement.	46
Table 4.7.	ϕ Angles of Benchmark Unit Cells, Unit Cells with OSC, J35, J400 and J1000 at +5 mm, +10 mm, +35 mm and +60 mm Horizontal Displacement in Monotonic Shearing.	47
Table 4.8.	ϕ Angles of Benchmark Unit Cells, Unit Cells with OSC, J35, J400 and J1000 at +5 mm, +10 mm and +35 mm Horizontal Displacement in Cyclic Shearing.	48
Table 4.9.	Vertical Strain Values (%) after Normal Loading at 700 mm depth (Before Monotonic Shear Loading).	49
Table 4.10.	Vertical Strain Values (%) after Normal Loading at 600 mm depth (Before Monotonic Shear Loading).	49
Table 4.11.	Vertical Strain Values (%) after Normal Loading at 500 mm depth (Before Monotonic Shear Loading).	49
Table 4.12.	Horizontal Strain Values (%) after Normal Loading at 700 mm depth (Before Monotonic Shear Loading).	50
Table 4.13.	Horizontal Strain Values (%) after Normal Loading at 600 mm depth (Before Monotonic Shear Loading).	50


Table 4.14.	Horizontal Strain Values (%) after Normal Loading at 500 mm depth (Before Monotonic Shear Loading).	50
Table 4.15.	Vertical Strain Values (%) at +60 mm Displacement at 700 mm depth (After Monotonic Shear Loading).	51
Table 4.16.	Vertical Strain Values (%) at +60 mm Displacement at 600 mm depth (After Monotonic Shear Loading).	51
Table 4.17.	Vertical Strain Values (%) at +60 mm Displacement at 500 mm depth (After Monotonic Shear Loading).	51
Table 4.18.	Horizontal Strain Values (%) at +60 mm Displacement at 700 mm depth (After Monotonic Shear Loading).	52
Table 4.19.	Horizontal Strain Values (%) at +60 mm Displacement at 600 mm depth (After Monotonic Shear Loading).	52
Table 4.20.	Horizontal Strain Values (%) at +60 mm Displacement at 500 mm depth (After Monotonic Shear Loading).	52
Table 4.21.	Vertical Strain Values (%) after Normal Loading at 700 mm depth (Before Cyclic Shear Loading).	53
Table 4.22.	Vertical Strain Values (%) after Normal Loading at 600 mm depth (Before Cyclic Shear Loading).	53
Table 4.23.	Vertical Strain Values (%) after Normal Loading at 500 mm depth (Before Cyclic Shear Loading).	53
Table 4.24.	Horizontal Strain Values (%) after Normal Loading at 700 mm depth (Before Cyclic Shear Loading).	54

Table 4.25.	Horizontal Strain Values (%) after Normal Loading at 600 mm depth (Before Cyclic Shear Loading).	54
Table 4.26.	Horizontal Strain Values (%) after Normal Loading at 500 mm depth (Before Cyclic Shear Loading).	54
Table 4.27.	Vertical Strain Values (%) at +35 mm Displacement at 700 mm depth (After Cyclic Shear Loading).	55
Table 4.28.	Vertical Strain Values (%) at +35 mm Displacement at 600 mm depth (After Cyclic Shear Loading).	55
Table 4.29.	Vertical Strain Values (%) at +35 mm Displacement at 500 mm depth (After Cyclic Shear Loading).	55
Table 4.30.	Horizontal Strain Values (%) at +35 mm Displacement at 700 mm depth (After Cyclic Shear Loading).	56
Table 4.31.	Horizontal Strain Values (%) at +35 mm Displacement at 600 mm depth (After Cyclic Shear Loading).	56
Table 4.32.	Horizontal Strain Values (%) at +35 mm Displacement at 500 mm depth (After Cyclic Shear Loading).	56

LIST OF SYMBOLS

A_c	Column area
A_e	Influence area
a_E	Relationship between column area (A_c) and its influence area (A_E)
a_r	Area Replacement Ratio
a_s	Area replacement ratio
B	Width of the Foundation
c	Undrained shear strength
G_s	Specific gravity
H/d_c	Height to diameter ratio
J	Modulus of elasticity
K_a	Active earth pressure coefficient
K_o	At rest earth pressure coefficient
K_{pc}	Coefficient of Passive Earth Pressure for the Column
K_p	Passive earth pressure coefficient
n	Stress Concentration Factor
p_c	Pressure Shared by the Stone Column
p_0	Pressure Caused by the Footing
p_s	Pressure Shared by the Surrounding Clay Layer
q	Surcharge on the Surrounding Clay
q_{ult}	Vertical Capacity of the Column
u_{s0}	Initial Pore Water Pressure at Depth h
u_s	Pore Water Pressure at Depth h After Yielding
γ	Unit weight of the material
ϕ	Internal angle of friction
σ	Normal Stress
τ	Shear Stress

σ_{r0}	Initial Radial Total Stress in the Clayey Soil before the Column is Constructed
δ_p	Angle of the Shear Plane in the Column
δ	Angle of the Shear Plane in the Matrix Soil
σ_3	Lateral Earth Pressure
γ_c	Unit Weight of the Surrounding Soil
σ_{suq}	Limiting Axial Capacity of the Column
σ_{su}	Limiting Axial Capacity of the Granular Column
ϕ'	Friction Angle of the Stone Column
ε_{ult}	Ultimate strain



LIST OF ACRONYMS/ABBREVIATIONS

AR	Elongation at Break
CR	Tensile Strength
GEC	Geosynthetic Encased Column
GT1	Tencate Polyfelt TS 10 Geotextile Reinforcement
GT2	HUESKER Sefitec PP 50 Geotextile Reinforcement
GT3	HUESKER Stablenka 100 Geotextile Reinforcement
Hz	Hertz
kN/m	Kilo-Newton Per Meter
kPa	Kilopascal
mm	Millimeter
OSC	Ordinary Stone Column
UCSD	Unit Cell Shear Device
UTS	Ultimate Tensile Strength

1. INTRODUCTION

When an embankment will be constructed on problematic soil with poor geotechnical characteristics, there are several ways to overcome this challenge. The most widely used techniques can be listed as follows: avoiding the site, replacing the soft soil with another soil, conducting a stage construction, using deep foundation or improving the soil (Hausmann, 1990). To avoid the location is getting more and more difficult because the availability for non-occupied places in the urban areas is very rear. The next options are expensive and time consuming in comparison with soil improvement techniques. Therefore, soil remediation is chosen more and more for enabling construction on problematic soils.

One of these soil remediation techniques are stone columns, also known as granular columns. The concept of ordinary stone columns (OSCs) emerged almost 50 years ago. The main working principle of this soil improvement technique is that most of the load applied by the foundation is concentrated on the columns with higher modulus of elasticity. So, most of the load exerted by the foundation is transferred to the stiffer columns. This can be also interpreted as the total modulus of elasticity of the soil strata with stone columns is increased and hence an increased bearing capacity is achieved. However, the stability of the columns is based upon the stiffness of the surrounding soft soil. The vertical load on the stone columns exerted by the foundation induce lateral active pressure in the same columns and they try to expand in the surrounding soil layer. The increased stresses on the soil exerted by the lateral active pressure of the stone columns are compensated by the passive pressure of the soil layer. If the capacity of the surrounding in terms of lateral confinement is not enough, bulging failure is very likely to occur in the soil column.

In order to avoid bulging failure in very soft soils, the concept of geosynthetic encased columns (GECs) emerged in the 1980s (van Impe, 1986 and 1989) and its application came to life at the beginning of 1990s. These geosynthetic encasements are giving the necessary confinement which cannot be provided by the surrounding soft

soil. In the soft soils that has in general less than 15 kPa of undrained shear strength, the column cannot be hold intact due to lack of the necessary confinement and stone column will most likely fail in the bulging mode. In Figure 1.1, the working mechanism of a GEC is given. Like in an OSC, the vertical load exerted on the GEC is transferred along the column. This concludes a lateral thrust in the granular material of the column, and it tries to expand. The geosynthetic encasement limits this expansion and provides the necessary lateral confinement.

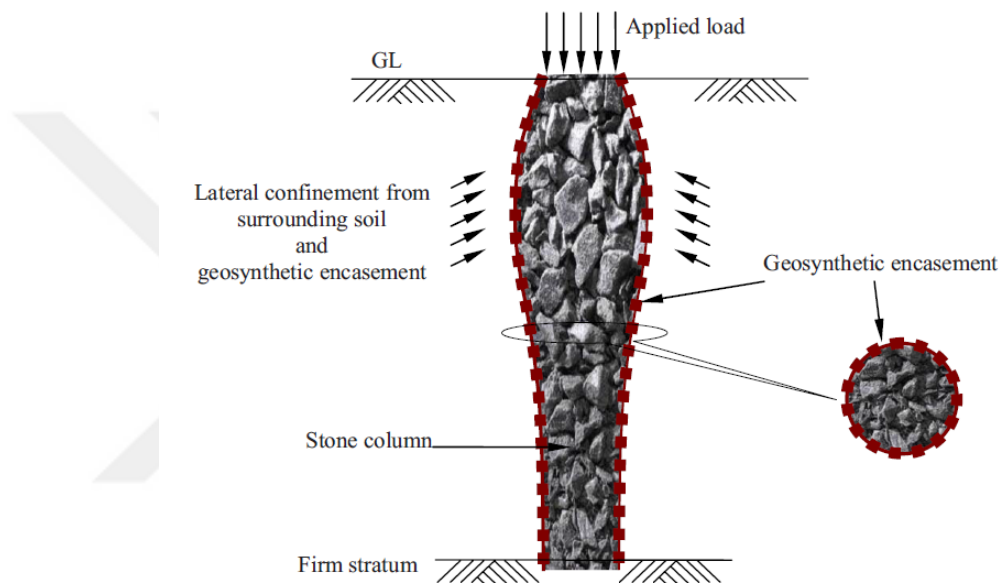


Figure 1.1. Scheme of GEC (Murugesan and Rajagopal, 2010).

Furthermore, granular columns, especially GECs, work as “mega-drains” (Almeida et al., 2019). Thus, the consolidation time in case of clayey soils decreases dramatically. However, the installation of OSCs and GECs do not create a densification like in sandy soils.

Lastly, it is also important to mention about the final and differential settlements in a site that is remediated by granular columns. Because the granular columns work as mega-drains, primary consolidation finishes quite fast, as stated above. Moreover, the settlements after construction is significantly reduced because most of the foundation load is transferred to the stiff columns and only a small percentage of the total load is transferred to the soft clay (Almeida et al., 2019). This enables us faster and safer

construction.

There are different techniques to install OSCs or GECs. Mainly, displacement and non-displacement (replacement) methods are used for installation. Vibro-floatation method is a widely used example for displacement methods for installing OSCs. For the GECs the most widely used displacement technique is seen in Figure 1.2. Here a closed-tip steel pipe is driven into the soil typically with the help of a vibrator. After it reaches the intended depth, the geosynthetic encasement is inserted in the tube. Then the encasement is filled with granular material and then the tip of the tube is opened, and the steel tube is pulled up again with the help of a vibrator. The displacement methods are preferred methods because of the advantage of compacting surrounding soil in granular soils and, also, the granular material of the column.

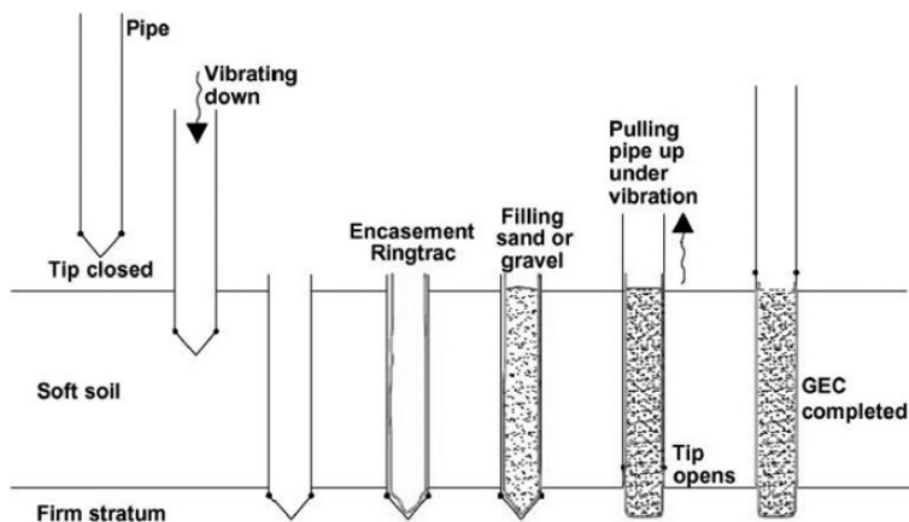


Figure 1.2. Displacement method for GEC installation (Alexiew et al., 2005, after Huesker).

Replacement method is mostly chosen when the driving of piles has the potential of harming close buildings or some strata that is hard to penetrate exists. In this method, an open steel tube is driven into the soil. The soil remained in the tube is excavated by augering. The geosynthetic encasement is placed inside of the tube and the geosynthetic encasement is filled with granular material. Casing is removed by pulling out with the help of a crane (Figure 1.3).

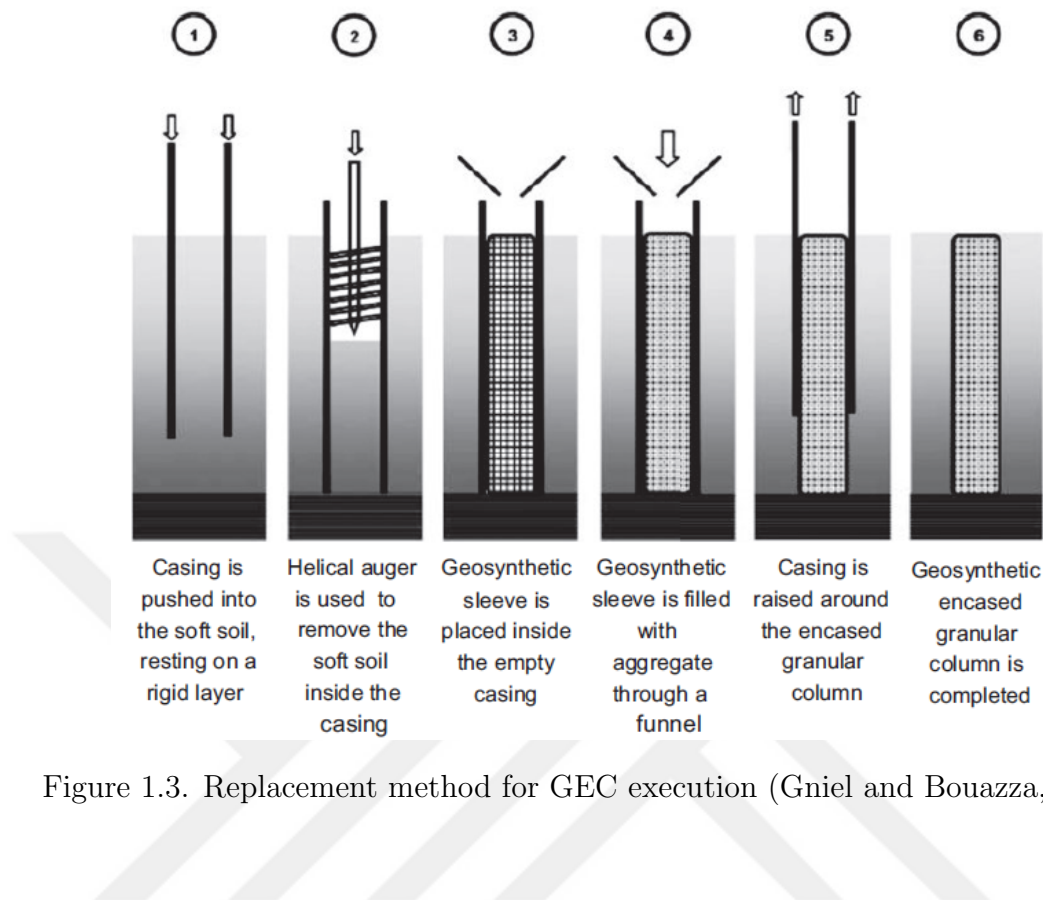


Figure 1.3. Replacement method for GEC execution (Gniel and Bouazza, 2010).

Commercially, GECs' diameter can be between 0,4-1,0 m and their height is mostly between 8-30 m (<https://www.huesker.co.uk/products/geosynthetics/woven/ringtrac.html>). The mostly used encasements have an ultimate tensile strength (UTS) between 100-400 kN/m, an ultimate strain (ε_{ult}) varying from 10% to 5%. The modulus of elasticity (J) of these mostly used geosynthetic encasements are from 1000 to 6000 kN/m (Alexiew et al., 2014). In a broader scale, 500 kN/m is the lowest value of stiffness for geosynthetic encasements used in GEC applications and 12500 kN/m is the upper value for PET geogrids, respectively (Cengiz et al., 2019).

In general, both OSCs and GECs are used to increase the bearing capacity of soft soils. However, when an embankment is constructed on soft clay soils, besides the overall bearing capacity problem, the most frequently encountered failure mode is the wedge failure. In this failure mode the soft soil as well as the rigid columns must be sheared. In the literature there is very limited information on the shear strength of GECs. In the scope of this dissertation, the Unit Cell Shear Device (UCSD) was used for the experiments with OSCs and GECs with a prototype diameter of

400mm in the field. The scale ratio was taken as 1:3,5 and the diameters of the model stone columns were therefore chosen as 113 mm. The scaling factor for the tensile modulus of the geosynthetic encasement was calculated as 12,5 (Baker et al., 1991). The model encasements had 35, 400 and 1000 kN/m as elastic modulus values. Thus, equivalent stiffness values for the prototype encasements were 440, 5000 and 12500 kN/m, respectively. These equivalent stiffness values are also in accordance with the mostly used commercial geosynthetic encasements.

As is evident from its name, UCSD is using the concept of “unit cell” in its assumptions. In the unit cell concept, it is assumed that there is an equilibrium for each column and some portion of its surrounding soil. There is an area replacement ratio (a_E) to define the relationship between column area (A_c) and its influence area (a_E). In this experimental study the area replacement ratio (a_E) is chosen as 6%. Furthermore, each column is in the center of this unit cell and spacing between unit cells is measured from center to center of each column. There are different meshes used to define unit cells in group. This corresponds to a square mesh the spacing of 1,445 m for the prototype equivalent and this is a typical spacing used in many real projects (Almeida et al., 2019).

The height to diameter ratio (H/d_c) in the model is about 14 with the height of 1550 mm and diameter of 113 mm. As stated before, the diameters and heights vary in the field. However, the height to diameter ratio (H/d_c) of 14 is large enough to represent the slenderness of the both the stone columns and geosynthetic encased columns.

In this study, totally 30 unit cells with different model columns under different consolidation loadings were tested. These unit cells are either sheared under static loading or cyclic loading is applied. The detailed experimental program is given in the Methodology section. In all experiments, the shear force and displacement are measured along the strains on the GECs. With the help of the strain gauges, the strains before and during shearing phase were measured.

2. LITERATURE REVIEW

The design of the ordinary stone columns and geosynthetic encase columns under vertical loads are well established in the literature. The stone columns in clay can be imagined as the samples in the triaxial chamber. The failure mechanisms of this system are the local shear failure in the surrounding clay or end bearing failure (Najjar, 2013).

In their study, Hughes and Withers (1974) proposed a formula to express the maximum vertical stress that can be carried by a stone column as follows:

$$q_{ult} = \frac{1 + \sin\phi'}{1 - \sin\phi'}(\sigma_{ro} - u + 4c) \quad (2.1)$$

where u is pore pressure, c is undrained shear strength, ϕ' is the angle of internal friction of the column material, q_{ult} is the vertical capacity of the column and σ_{ro} is the initial radial total stress in the clayey soil before the column is constructed.

Brauns (1978) established a model where it is assumed that the upper part of the stone column yields like a cohesionless cylindrical triaxial test specimen with a shear plane with the angle $\delta_p = 45 + \phi'/2$ and the surrounding soil has no internal friction angle. The final expression is as follows:

$$q_{ult} = \left(q + \frac{2c}{\sin 2\delta_p} \right) \left(1 + \frac{\tan \delta_p}{\tan \delta} \right) \tan^2 \delta_p \quad (2.2)$$

where c is the undrained shear strength of the surrounding clay, δ is the angle of the shear plane in the matrix soil (surrounding clay) that is calculated iteratively to minimize passive pressure and δ_p is the angle of the shear plane in the column. This approach considers that the clay applies an undrained passive pressure to the column.

Watts *et al.* (2000) improved the equation that was given by Hughes and Withers (1974) with the assumption of that the stone column is yielding at a depth of h as

follows:

$$q_{ult} = K_{pc}(K_o [\gamma_s h - u_{so}] + u_{so} - u_s + 4c_u) \quad (2.3)$$

where K_{pc} is the coefficient of passive earth pressure for the column. It is equal to $(1 + \sin \phi') / (1 - \sin \phi')$. K_o is the coefficient of earth pressure at rest for the surrounding clayey soil. u_{so} is the initial pore water pressure at depth h and u_s is the pore water pressure at depth h after yielding.

As mentioned before, the first studies about GECs appeared at end of 1980's. The idea behind geosynthetic encased columns is to confine granular columns with geosynthetic reinforcement in very soft soils. Without this confinement, granular material of the columns would bulge into the soft clay with increasing vertical pressure. In these early concepts of GECs, all the confining pressure was provided by the geosynthetic encasement and the contribution of surrounding soil was not taken into the consideration.

The first analytical model of geosynthetic encased columns with more accurate results to calculate vertical load capacity was suggested by Raithel and Kempfert (2000). This model was named as analytical axisymmetric calculation model and it was using the unit cell concept with iteration the loads acting on it. This model with essential boundary conditions is given in Figure 2.1. The further assumptions were that the settlements of the column and soft soil will be the same under the loading. It is also assumed that the earth pressure in the column is active and the lateral earth pressure in the clay soil is taken as at rest for replacement method and a bigger earth pressure is taken if the displacement method is used. It is further assumed that the geotextile encasement is linear-elastic and that the drained condition is governing. When the results of the model were compared with the results of the PLAXIS model it was determined that the analytical model was consistent with the FEM.

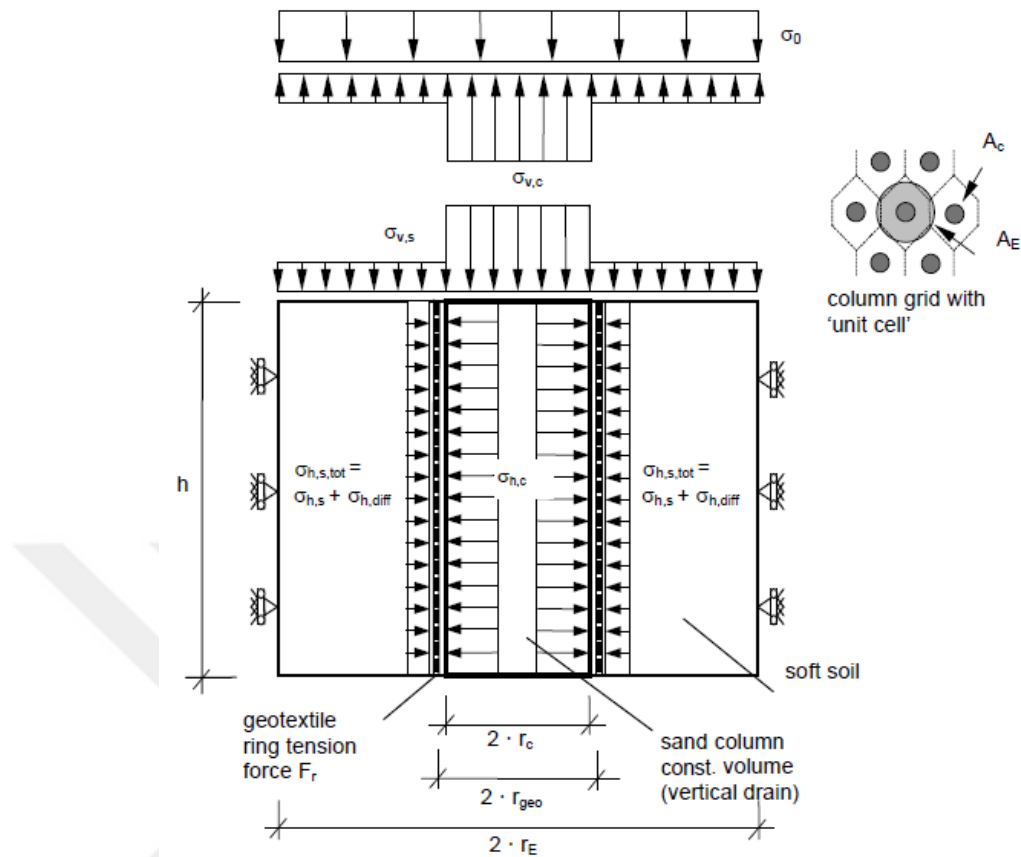


Figure 2.1. Analytical Axisymmetric Calculation Model (Raithel and Kempfert, 2000).

This calculation method suggested by Raithel and Kempfert (2000) was implemented in “Recommendations for Design and Analysis of Earth Structures using Geosynthetics Reinforcements-EBGEO” (2011) with minor modifications (Almeida *et al.*, 2019).

Our aim is to understand the shear resistance of the OSCs and GECs when they are exposed to direct shear stresses during the potential wedge failure mode of embankments. There is no established method or any proposal in the literature to address this issue. There were limited studies about this concept in the past but in the last two decades its importance was understood. It seems that more studies will be done with time. So, we used the same unit cell concept as was introduced in Figure 2.1 for the design of such inclusions under vertical loads and adapted it to the direct shear of column improved clays. The main experiments in the scope of this dissertation was

conducted in an apparatus which uses the “unit cell” concept. Hence the apparatus is named “Unit Cell Shear Device” or UCSD in short.

Because we take the unit cell model as a basis of our study to understand the shear behavior of soils, a brief summary of the limited studies about unit cell concept will be presented. Also, the research done with computer models on shear failure mode will be summarized.

The pioneers in the concept of unit cell were Baumann and Bauer. In their study, a method was established to calculate immediate settlement and consolidation settlement of surrounding clay layer of OSCs (Baumann and Bauer, 1974). The load exerted by the foundation was divided in unit cells. In the assumption, the pressure caused by the footing (p_0) was shared by the surrounding clay layer as p_s and by the stone column p_c . The load on the unit cell became:

$$p_0 A = p_s A_s + p_c A_c \quad (2.4)$$

Barksdale and Bachus (1983) suggested that the unit cell concept could be used to calculate the bearing capacity of a group of OSCs. They assumed that the mobilization of the shear strength in the OSC and surrounding clay would be at the same time and they added the shear strength parameters of the OSC to the shear strength parameters of the surrounding soil:

$$\phi_{avg} = \tan^{-1}(n * a_r * \tan\phi') \quad (2.5)$$

$$c_{avg} = (1 - a_r) c \quad (2.6)$$

where n is the stress concentration factor, a_r is the area replacement ratio that is calculated as the ratio of the area of OSC to the area of the unit cell. Moreover, it was assumed that the lateral earth pressure to overcome the failure wedge under a strip

footing could be calculated using the relation given in Equation 2.7 (Barksdale and Bachus, 1983).

$$\sigma_3 = 0.5\gamma_c B \tan(45 + \phi_{avg}/2) + 2c \quad (2.7)$$

where σ_3 is the lateral earth pressure, γ_c is unit weight of the surrounding soil and B is the width of the foundation. For the case with the lateral earth pressure under square footing, Barksdale and Bachus (1983) used an approximation of the square footing as a circular footing and they, also, used the cylindrical cavity expansion theory of Vesic (1972). The bearing capacity of a group of granular columns is expressed as given in Equation 2.8.

$$q_{ult,group} = \sigma_3 \tan^2\left(45 + \frac{\phi_{avg}}{2}\right) + 2c_{avg} \tan\left(45 + \frac{\phi_{avg}}{2}\right) \quad (2.8)$$

In their study, Ambily and Gandi (2007) conducted laboratory experiments with single or group of granular columns. In these experiments, stone columns with 100 mm diameter were used and parameters such as column spacing, shear strength of cohesive soil and vertical loading were changed. They, also, made finite-element analyses with the software program PLAXIS which they have calibrated using the results of the experimental study. So, they found out that the load carrying capacity of the stone columns is increasing with the effect of increasing surcharge load on the surrounding clay and decreasing with the increasing spacing between columns. After the column spacing to diameter ratio passed 3, the change in axial capacity and settlement was negligible. A design chart shown in Figure 2.2 was developed with the help of this FE analysis and experiments. Also, an equation to calculate the limiting axial capacity based on the strength parameters and surcharge on the surrounding soil was given (Equation 2.4)

$$\sigma_{suq} = \sigma_{su} + \left(0.0088\phi'^2 - 0.5067\phi' + 10.86\right) q \quad (2.9)$$

where σ_{suq} is the limiting axial capacity of the column, q is the surcharge on the surrounding clay, ϕ' is the friction angle of the stone in the column, σ_{su} is the limiting axial capacity of the granular column that is found without the effect of surcharge load on surrounding clay. Finally, it was proven in the study with the help of FEM analyses and tests that a single column with unit cell concept can model the field behavior of a group of columns successfully.

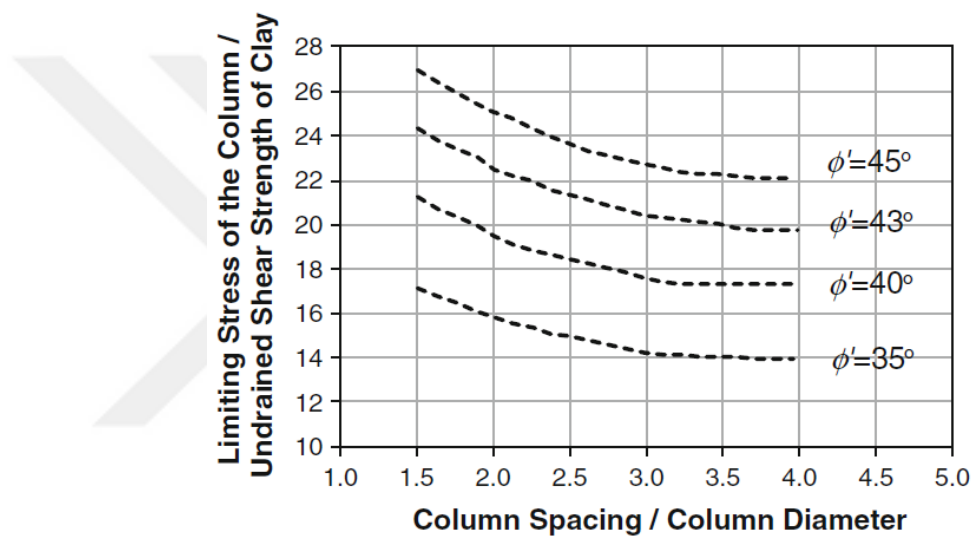


Figure 2.2. Design Chart for OSC (modified from Ambily and Gandhi, 2007, taken from Najjar, 2013).

Cimentada *et al.* (2011) undertook 1-g consolidation tests with unit cell concept in their study. For this purpose, two single OSCs with different diameters were prepared in kaolinite slurry and were consolidated. The area replacement ratios were 6.25% and 11.11%. The models were vertically loaded with 100 kPa increments. It was found that the ratio of stress on the clay to the stress on OSCs varied from 0.68 to 0.75 respectively.

As mentioned before, there is very limited research about shear and bending failure mechanisms of GECs. Most of the studies are on the performance of OSCs and GECs under vertical loads. Figure 2.3a gives an illustration about the shear-type

and bending failure mechanisms. Figure 2.3b shows the global stability issue with the potential slip circle.

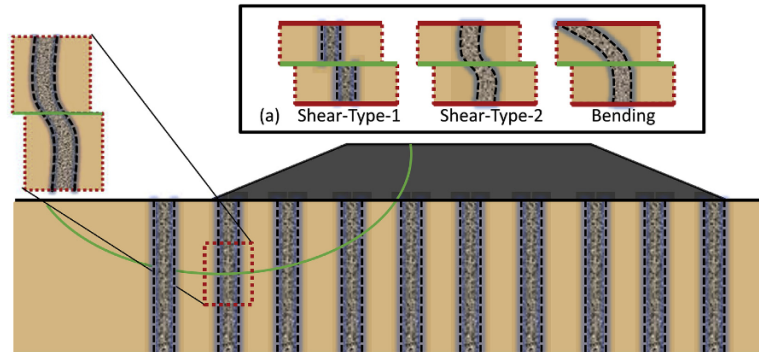


Figure 2.3. (a) Failure Modes Identified in the Literature, (b) Nature of the Problem (Cengiz *et al.*, 2019).

Murugesan and Rajagopal (2009) performed some large direct shear tests to investigate the shear behavior of stone column models. In the large direct shear box (300 mm x 300 mm), 3 series of tests were conducted: only with clay, granular column models in clay and GEC models in clay. Also, the plan of columns was changed in the test series: with only one column and with 4 columns at a time. From these test results, it was seen that the GECs had better performance than OSCs. The drawback of the study was that the columns were not slender like in the field and the scaling ratio was not taken into the consideration.

Abusharar and Han (2011) used a two-dimensional finite difference model to investigate the factor of safety against slope failure of embankments over soft clay enhanced by OSCs. The important relevance of their study for our study is that the equivalent area model and individual column model were used in the modelling of the system under the embankment. In the equivalent area model, the soil parameters for the enhanced area are estimated as the average of soil parameters of granular column and clay with their area replacement ratio taken into the consideration. The equivalent parameters of the equivalent area are given in the following equations:

$$c_{eq} = c_c a_s + c_s (1 - a_s) \quad (2.10)$$

$$\phi_{eq} = \tan^{-1} (a_s \tan \phi_c + (1 - a_s) \tan \phi_s) \quad (2.11)$$

$$\gamma_{eq} = \gamma_c a_s + \gamma_s (1 - a_s) \quad (2.12)$$

where a_s is the area replacement ratio, the terms with “eq” subscript are equivalent area parameters, the terms with “c” subscript are stone column parameters and the terms with “s” subscript are surrounding soil parameters.

In Figure 2.4, the cross sections of both models can be seen. In the comparison of the results of the models with individual column model and equivalent area model, it is seen that the factor of safety values with the equivalent area model was slightly higher than those by the individual column model. Thus, the factor of safety results by the equivalent area model needs to be reduced by a reduction factor of 0.90 as suggested in the study.

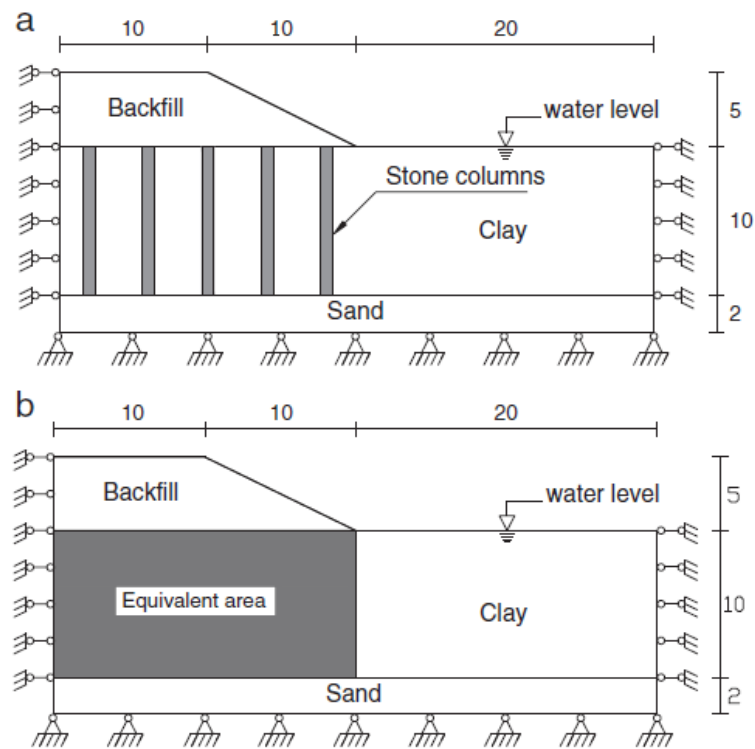


Figure 2.4. Cross sections of calculation models for the finite difference analysis of (a) individual columns and (b) an equivalent area (all dimensions are in meters).

In the study of Castro (2017), the main modeling techniques of OSCs and GECs were discussed. These techniques included unit cell modelling, longitudinal gravel trenches in plane strain conditions, cylindrical rings of gravel in axial symmetry conditions, equivalent area model and three-dimensional models. The advantages and disadvantages of these techniques and recommendation regarding where those techniques were used, were reviewed. As a conclusion unit cell modelling was recommended for numerical analyses, calibrating and tuning the parameters of both OSCs and GECs. They suggested that longitudinal gravel trenches in plane strain conditions can be used for settlement, consolidation and stability calculations of OSC. Furthermore, they concluded that cylindrical rings of gravel in axial symmetry conditions are modelling the confining conditions and drained properties well but encasement properties, e.g. GEC modeling is not satisfactory like with the longitudinal gravel trenches in plane strain condition models. Equivalent area model was only recommended as a first approximation. So, based on the findings of this study only unit cell modeling gives satisfactory results for GEC modelling.

For the study of Cengiz *et al.* (2019), a Unit Cell Shear Device was designed and constructed to provide monotonic and cyclic loading. As the surrounding soil, sand was used. The models were subjected to monotonic and 1 Hz. cyclic loading. It was determined that the resistance of the unit cells against shear forces were increasing with increasing encasement stiffness values of GECs in monotonic loading. Also, in cyclic loading, the shear strengths were increasing with the increasing encasement stiffnesses.

In the light of above findings, it was determined that the most promising technique to model both OSC and GEC improved soft clays is the “Unit Cell Approach”. Furthermore, there is a very limited number of studies about the shear failure mechanism of GECs. In this study, experimental models were used to shed light to this failure mechanism with the Unit Cell Shear Device which is using unit cell approach.

3. METHODOLOGY

In this chapter, the materials which are used in the experiments, the process of preparing the models and the experimental setups that were chosen are explained. The aim is to determine the behavior of the OSC or GEC improved foundation soil under static shear loading or cyclic shear loading.

3.1. Materials

3.1.1. Clay and Clay Slurry

The clay used to model the soft foundation soil is kaolinite. The kaolinite was in powder form. Its hydrometer analysis is given in Figure 3.1. As seen in Figure 3.1, the particle size of kaolinite is smaller than 100 microns.

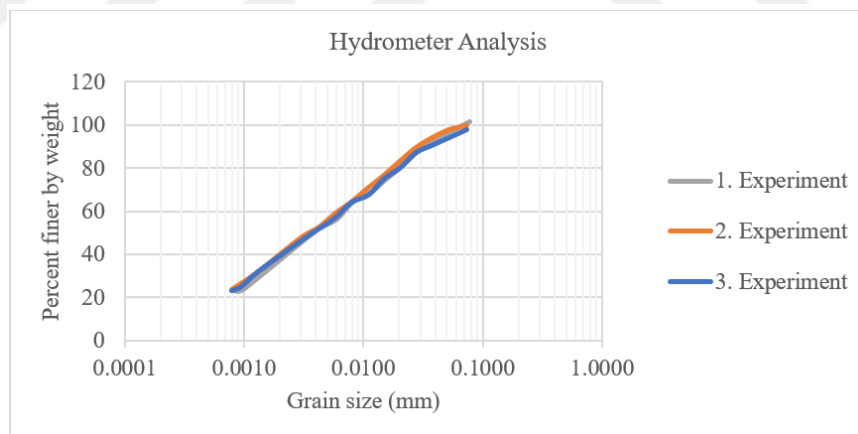


Figure 3.1. Hydrometer Analysis of Clay.

The specific gravity (G_s), of the clay was found as 2,58. The Plastic Limit and Liquid Limit values were obtained as 26% and 37%, respectively.

In the container seen in Figure 3.2, the clay slurry was mixed with the help of a drill with mixer head. In literature, the water content of clay slurries is typically recommended as 1.5 times the Liquid Limit (Murugesan and Rajagopal, 2010; Black *et*

al., 2011; Frikha *et al.*, 2013; Miranda *et al.*, 2017). For one batch, 300 kg of kaolinite clay powder is mixed with 150 kg tap water. This corresponds to a water content of 50% and 50% of water content is chosen as the initial water content in all of the experiments.



Figure 3.2. Clay Slurry Placement.

3.1.2. Gravel

The gravel used in the infill of OSCs and GECs is a poorly graded gravel with D_{10} , D_{30} and D_{60} values of 5, 6.1 and 7.9 mm, respectively. Its internal friction angle is 44° determined by large scale direct shear tests. The engineering properties of gravel is presented in the Table 3.1.

Table 3.1. Engineering Properties of Infill Materials.

	D_{10} (mm)	D_{30} (mm)	D_{60} (mm)	c_u	e_{max}	e_{min}	$\phi(^{\circ})$
Gravel	5.0	6.1	7.9	1.58	0.94	0.43	44

3.1.3. Geosynthetic Reinforcement

Three different geotextiles have been used as encasement of GECs same as in Cengiz and Guler (2018a) and Cengiz *et al.*, (2019). The diameter of the model OSCs and GECs is chosen as 113 mm and the diameter of the prototype OSCs and GECs is taken as 400 mm. So, the scale ratio is 1:3.5 that is the ratio of the model diameter to prototype diameter. Furthermore, the scaling factor for stiffnesses is the square of the scale ratio (1:12.5) according to Buckingham Pi Theorem (Baker *et al.*, 1991). As presented in Table 3.2, the stiffnesses are 35, 400 and 1000 kN/m for the 1., 2. and 3. geotextile used for encasements, respectively. Because the scaling factor for the stiffness of the reinforcement is approximately 12.5, the prototype equivalents of these geotextiles have the stiffnesses of 440, 5000 and 12500 kN/m. Knowing that 500 kN/m is the lowest value for the stiffness of geosynthetics of GECs and 12500 kN/m is the upper stiffness value for PET geogrids, the stiffness values of the prototype equivalents are presented well in the models. The GECs constructed with GT1, GT2 and GT3 are called J35, J400 and J1000, respectively. The stiffness parameters for the geotextiles are given in Table 3.4.

Table 3.2. Model and Prototype Comparison.

	Diameter	Scale Ratio	Scaling Factor	GT1	GT2	GT3
Model	113 mm	1	1	35 kN/m	400 kN/m	1000 kN/m
Prototype	400 mm	3.5	12.5	440 kN/m	5000 kN/m	12500 kN/m

Table 3.3. Scaling Relationships used for Model to Prototype Scaling.

Diameter (m)	λ (=3.5)
Length (m)	λ (=3.5)
Stress (kN/m ²)	λ (=3.5)
Tensile Modulus (kN/m)	λ^2 (=12)
Displacement (m)	λ (=3.5)

Table 3.4. Tensile Stiffness Parameters of the Geotextiles.

Strain (%)	Tensile Force (kN/m)			Secant Modulus		
	GT1	GT2	GT3	GT1	GT2	GT3
2	0.72	7.6	21.6	36	380	1050
3	0.9	12.2	31.5	30	400	1050
5	1.25	21	60	25	420	1200
10	1.8	44	115	18	440	1150

3.1.4. Latex Membrane

The Unit Cell Shear Device (UCSD) chamber consists of 4 vessels. Specially since at one location shear stress needs to be applied to the model, some space had to be present to reduce the friction between the two vessel parts. Therefore, to prevent the leakage of the clay slurry these locations, a latex membrane with high elasticity was used. The membrane was commercially available as a plate with a standard width of 1500 mm and 10000 mm length. A 2000 mm long portion was taken for every experiment and glued on the long side. So, a cylinder with a height of 2000 mm and circumference of 1480 mm was obtained. The circumference of this cylinder was higher than the circumference of the vessels which is 1445 mm. This margin was necessary to reduce the contribution of the membrane to the resistance to the shearing force. Also, there was a margin in the longitudinal direction with the same purpose like at the circumference. This cylinder made from latex was used repeatedly till a discontinuity like a small rupture or a plastic state like a bulge occurred on it. The high elasticity of the membrane also contributed to the minimum disturbance at the loading when the unit cell was sheared.

The characteristics of the latex membrane such as tensile strength (CR) and elongation at break (AR) were determined according to ASTM D 412C, by the producer. Tensile strength was 20 MPa and elongation at break was 550%. All the characteristics are given in Table 3.5.

Table 3.5. The Characteristics of Latex Membrane.

Characteristics	Units of Measure	Specifications	Values
Hardness (H)	Sh. A3	ASTM D 2240	40
Tensile Strength (CR)	MPa	ASTM D 412C	20
Elongation at Break (AR)	%	ASTM D 412C	550
Tear Strength	N/mm (.)	ASTM D 624B	40
Specific Gravity	gr/cm ³	DIN 53479	0.97

3.2. Unit Cell Shear Device

The Unit Cell Shear Device (UCSD) has been designed by Cihan Cengiz and published in Cengiz *et al.* (2019). The purpose of UCSD is to study the shear behavior of OSCs and GECs under static and cyclic loading. It is possible to shear, like in direct shear apparatus, large unit cells with high height to diameter ratio (4:1) with the help of UCSD. In Figure 3.3, a photo of the UCSD can be seen. The static and cyclic actuators are presented in Figure 3.4.



Figure 3.3. Unit Cell Shear Device (UCSD).



Figure 3.4. (a) Pneumatic Piston for Static Shearing, (b) Actuator for Cyclic Loading.

3.2.1. Unit Cell Shear Device Design Considerations

In Figure 3.5, a partial sketch of UCSD is presented. The total height of the vessels is 1850 mm and the diameter of the vessels is 460 mm. The height to diameter ratio of the unit cell can be as high as 4:1. In the tests, the height of the specimens was 1550 mm before shearing because the clay slurry consolidated, and the upper part of the specimens settled down approximately 300 mm.

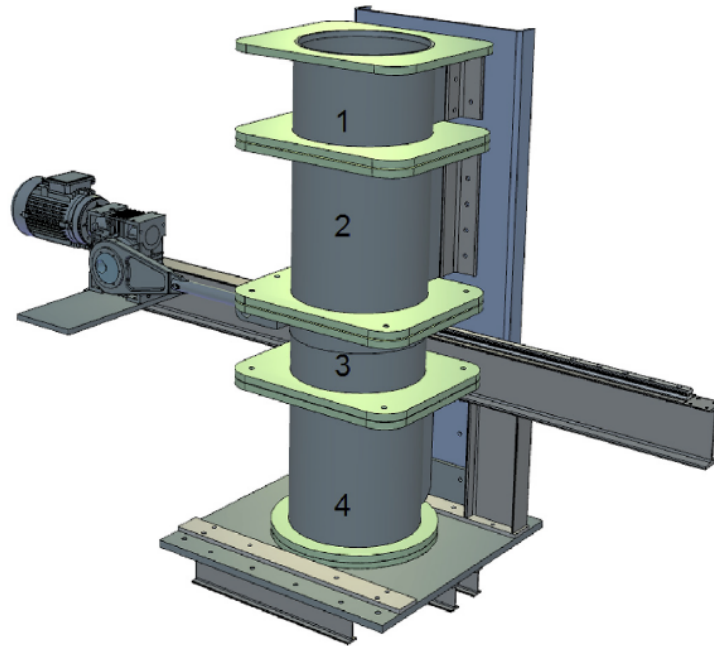


Figure 3.5. Partial Sketch of the UCSD Illustrating Cyclic Loading Unit and Vessels (Cihan *et al.*, 2019).

Vessel 4 is fixed, and the actuators are connected to vessel 3. The other vessels 1 and 2 are staying fixed on the vessel 3 during shearing. Thus, the shear plane ingenerates between vessel 4 and 3. The vessel 3 is placed on 4 carts that are moving on stainless steel rails that has low friction. Also, grease is used on the wheels of the carts to lower the friction.

The height of the columns was equal to the total height of the vessel 2, 3 and 4, namely 1550 mm. This height allowed the model to have a height to diameter ratio H/d_c well above 10, to be more specific 14. This H/d_c ratio is large enough to represent the slenderness of OSCs and GECs in the site.

At the bottom of the vessel 4, right in the middle of the base, there is a 10 mm deep intrusion with 113mm diameter where the steel tube used for columns fits. This intrusion enables with the hole in the plate of the vertical load actuator that the steel tube stands exactly in the middle of the unit cell during consolidation. At the bottom and in the middle of this intrusion, there is a half inch hole connected with a pipe

letting the water out of the steel tube during the consolidation.

3.2.2. Operating and Measurement Systems

3.2.2.1. Actuators. A total of 3 actuators are used to exert loads in this study. 2 of these actuators are pneumatic pistons with the same inner diameter of 160 mm and provided monotonic normal and shear load. These actuators are stress controlled. The actuator which is used to apply the lateral monotonic shear loading had a stroke of 160 mm and connected to a load cell which was fixed on the vessel 3. The shear load was increased with 0.25 kN steps and there were 1 minute of waiting time between these steps. This corresponds to a shear stress increment of 1.50 kN/m².

The pneumatic piston which is used for the vertical (normal) loading has a 700 mm stroke. It is connected to a circular steel plate with a diameter of 450 mm that was surrounded with a 1 cm thick gasket. Thus, the total diameter of the top cap was 460 mm providing smooth movement and no leakage at the edges. Both pneumatic actuators were controlled by a precision air regulator that has an accuracy of 0,05%.

The cyclic loading was applied by a displacement controlled electric motor, redactor and Scotch-yoke mechanism system. The excitation of the electric motor was controlled by a redactor to maintain the frequency of 1 Hz. The Scotch-yoke mechanism was converting the rotational movement to the cyclic bi-directional pure horizontal movement. The displacement provided by this system was ± 35 mm at a 1 Hz. frequency.

3.2.2.2. Load Cell, Laser Displacement Sensors and Strain Rosettes. A load cell with 5-ton capacity (CAS, LS5T) was used to measure the monotonic or cyclic shear load given to the vessel 3. During shearing, two laser displacement sensors (Leuze, ODSL 96B) were quantifying the lateral displacements. Two laser displacement sensors were used to monitor the lateral displacements in order to minimize the measurement errors. In the tests with GECs, the strains on the geotextile was measured by strain rosettes

(TML, WFRA-6-11-5L) in 3 axes (longitudinal, hoop and 45° skew from longitudinal). The 45° skew axis from longitudinal was providing extra data in case one of other axes would not work.

3.2.2.3. Data Logger. All the sensors were connected to a 112 channel cyclic data logger (Testbox) that had a maximum sampling rate of 2000 Hz. The data logger was connected with a laptop that was using the Testlab Network interface program. This program was working on the Labview program.

3.2.3. Unit Cell Model Preparation

As seen in Figure 3.6, the latex membrane was attached on the walls of the vessels with small magnets. The magnets were placed as far as possible from the shear plane and plate that is exerting the vertical loading on the unit cell, so that magnets would not affect the loadings by occluding the edges of moving parts.

For the Benchmark Unit Cells, a sand layer and a geotextile was used to prevent the slurry leakage from the bottom outlet. Also, for the unit cell with stone column, a smaller piece of geotextile fitting the intrusion at the bottom was used for filtration of water from clay during consolidation, so that the steel tube can fit in. For the unit cells with geosynthetic encasement there was no need for such prevention because the encasement geotextile itself was providing this filtration.

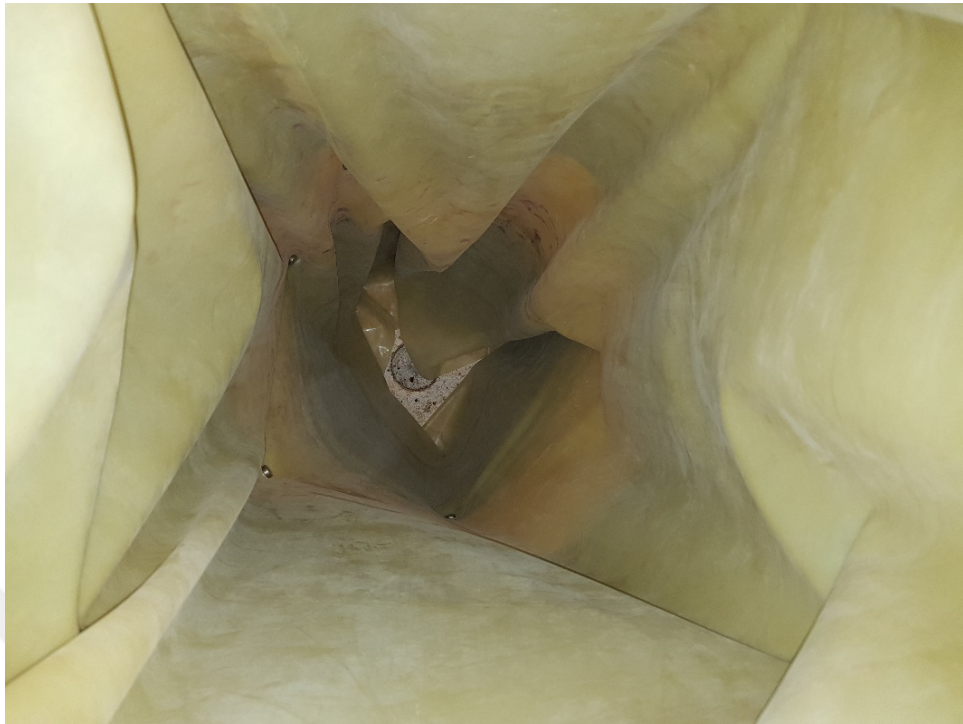


Figure 3.6. Unit Cell with Latex Membrane.



Figure 3.7. Sand Bed at the Bottom of the Benchmark Unit Cell.

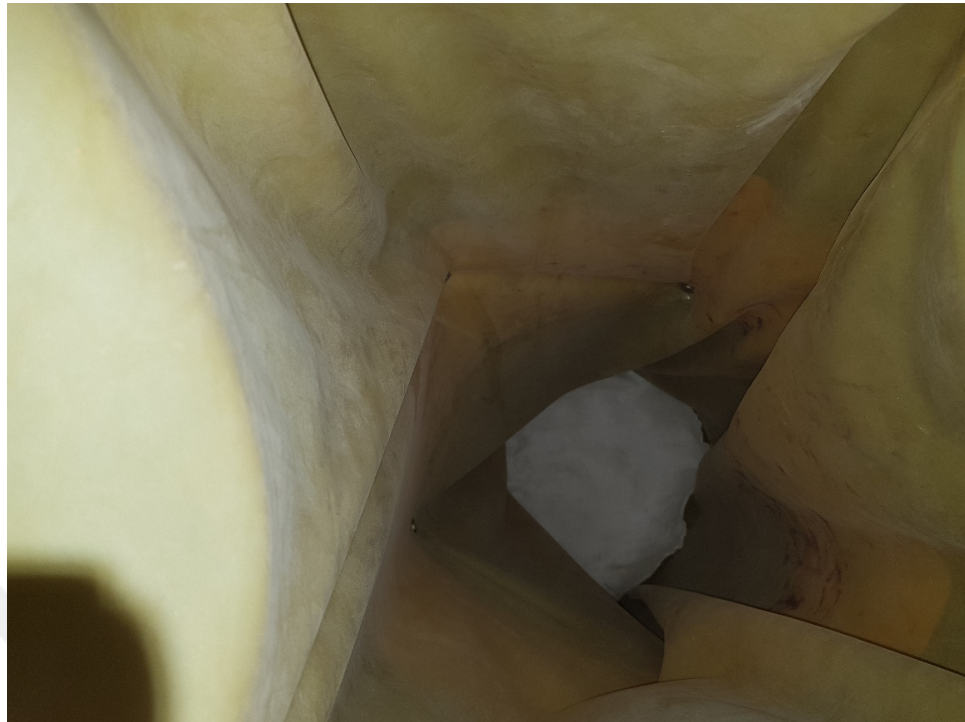


Figure 3.8. Geotextile for Bottom Filtration in Benchmark Unit Cells.

The top of the unit cell for benchmark experiments are covered with the same logic as bottom of the model. After the top of the membrane is covered loosely and a geotextile strip is put like a candlewick in the node, as seen in Figure 3.9, a geotextile disc is put on the top of it. A stainless-steel disc with four 1 cm-diameter holes is placed on the geotextile, as seen in Figure 3.10, so the 113 mm diameter reservation that allowed the installation of the GECs and OSCs will be closed. The disc is also used after the consolidation of unit cells with GECs and OSCs to give the vertical load on the GECs and OSCs.

3.2.4. The Preparation and Placement of GECs in the Unit Cell

For installation of the GEC's the steel tube inside the UCSD surrounded by clay slurry is used. The geotextile encasements are put inside this tube. During the consolidation phase, the steel tube was inside the encasement. On the tube, there were holes to drain the excess water. The holes were covered with filter papers to prevent the leakage of soil but to allow drainage.

After the consolidation phase, the steel tube is filled with gravel step by step. This is considered to better represent the field condition of the replacement method of the GEC installation. The weight of gravel that is expected to fill the encasement is measured before, and it is poured in 5 steps while light hammer strokes are pounded to assure that the gravel fill the voids better. At the same time the tube is pulled up gradually.

The shear plane was 600 mm higher than the bottom of the geotextile. So, the strain rosettes were glued at 500 mm, 600 mm and 700 mm height of the geotextiles. These strain rosettes were placed on the geotextiles along a single line and at a location closest to static actuator. This line was chosen for the strain gauges because it was obvious that the highest strain during shearing phase would be at this line.

The cables of the strain rosettes remain inevitably under the steel loading plate. Therefore, these cables are taken out of the model through the holes of the steel disc. With the help of steel disc, the normal load is exerted on the clay and stone column at the same time.



Figure 3.9. Top Sealing of the Benchmark Unit Cell.



Figure 3.10. The Stainless-steel on the top of Geotextile Filter.



Figure 3.11. Strain Rosettes glued onto a geotextile encasement.



Figure 3.12. A GEC in the Unit Cell.

3.3. Experimental Scheme

Totally 30 models are tested with UCSD. For static and cyclic shear tests different unit cells with same characteristics were prepared. Models of benchmark unit cell, unit cell with OCS and three unit cells with GECs having different types of geosynthetics were prepared. For each type three models are prepared, and each was consolidated under different consolidation pressures, namely 15, 25 and 35 kPa. Separate models were prepared to apply for each case static and cyclic loading. The scheme for experiments is presented in the Table 3.6.

Table 3.6. Experimental Scheme.

	STATIC			CYCLIC		
Sets of Tests	Consolidation Loadings before Shearing					
Benchmark	15 kPa	25 kPa	35 kPa	15 kPa	25 kPa	35 kPa
OSC	15 kPa	25 kPa	35 kPa	15 kPa	25 kPa	35 kPa
J35	15 kPa	25 kPa	35 kPa	15 kPa	25 kPa	35 kPa
J400	15 kPa	25 kPa	35 kPa	15 kPa	25 kPa	35 kPa
J1000	15 kPa	25 kPa	35 kPa	15 kPa	25 kPa	35 kPa



Figure 3.13. 112 Channel Data Logger with the UCSD.



Figure 3.14. Taken Before Cyclic Shearing Begins.

4. TEST RESULTS AND EVALUATION

The test results discussed in this chapter are to study the enhancement of the performance of the soil under shear stresses with Geosynthetic Encased Columns (GECs). First of all, geotechnical index tests were conducted to investigate the properties of the clay that would be used in the Unit Cell Shear Device. The shear strength results of the direct shear tests were compared with the benchmark test results of the Unit Cell Shear Device that were conducted just with clay. At the end, monotonic and cyclic shear loading were applied to the specimens with OSC and different GECs to see the improvement of the shear strength.

4.1. Tests to Determine Material Properties

4.1.1. Consolidation Properties

To determine the time necessary for the consolidation of the model, consolidation tests have been conducted. In the consolidation tests it has been seen that the consolidation process is faster than assumed. From Figure 4.1, the t_{50} values were determined as 0,15; 0,08 and 0,075 minutes for consolidation under loadings of 15, 25 and 35 kPa, respectively. Afterwards corresponding c_v values and the times needed for 90% consolidation for the clay in the Unit Cell Shear Device were calculated. The calculated consolidation times were 50 hours, 28 hours and 21 hours for consolidation under loading 15, 25 and 35 kPa, respectively. The time needed for the consolidation for models with OSCs and GECs decreases drastically because of the shortened drainage path. So, the time necessary for those models to complete the consolidation were calculated as 90, 50 and 38 minutes under loading 15, 25 and 35 kPa, respectively. In Figure 4.2 and Figure 4.3, the graphs of vertical settlement vs log time during the consolidation of one benchmark model and one OSC model are given. For each model, the vertical settlement - time graphs for 15 kPa, 25 kPa and 35 kPa vertical loads are given. As seen in Figure 4.2, the consolidation processes were finished for all loading levels in OSC model before 2 hours. As presented in Figure 4.3, the consolidation phase for the

benchmark unit cell were finished before 48 hours. To be on the safe side, the minimum time needed for the consolidation of benchmark unit cells was taken as 50 hours and for those with GECs and OSC, the consolidation time was taken as 2 hours.

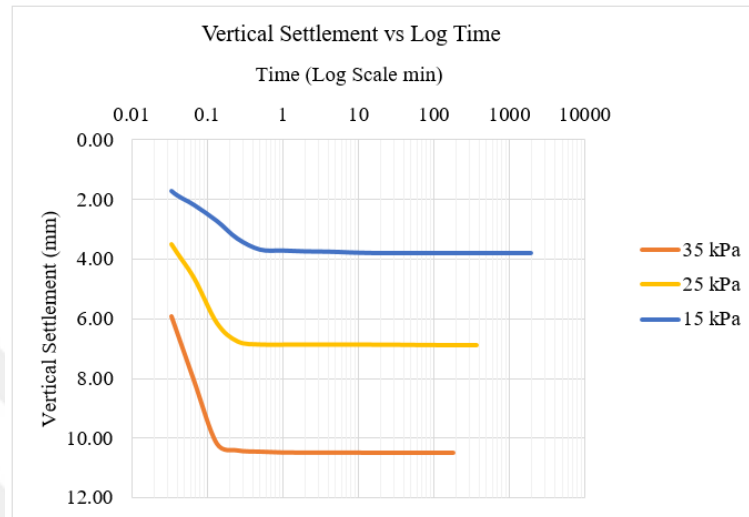


Figure 4.1. Vertical Settlement vs. Log Time (min) during Consolidation under 15 kPa, 25 kPa and 35 kPa Vertical Loading in Direct Shear Apparatus.

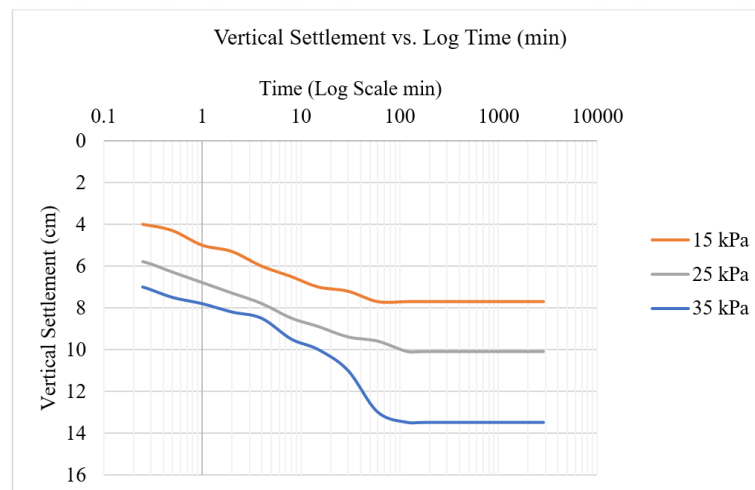


Figure 4.2. Vertical Settlement vs. Log Time (min) during Consolidation under 15 kPa, 25 kPa and 35 kPa Vertical Loading of the Unit Cells with OSC.

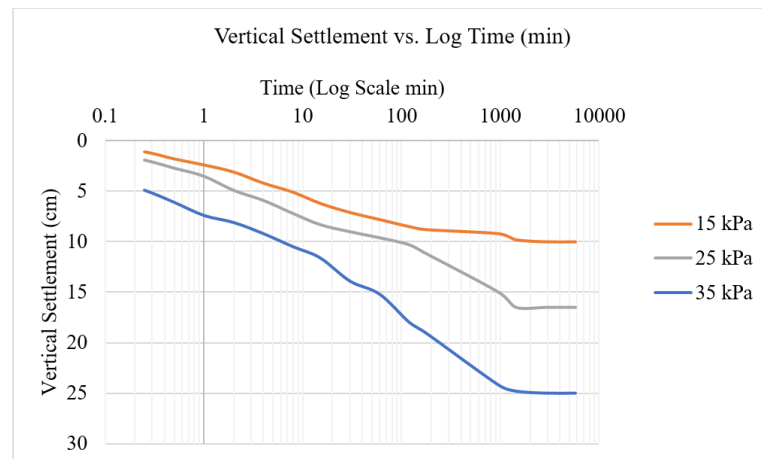


Figure 4.3. Vertical Settlement vs. Log Time (min) during Consolidation under 15 kPa, 25 kPa and 35 kPa Vertical Loading of Benchmark Unit Cells.

4.1.2. Shear Strength Properties

In order to determine the shear strength properties of the clay used, direct shear tests were conducted. The peak shear strength results of the direct shear tests were 5,89 kPa, 9,39 kPa and 13,69 kPa for specimens consolidated under 15 kPa, 25 kPa and 35 kPa vertical loading. The maximum mobilized shear resistance was reached in the early stages of shearing and didn't vary sizably throughout the experiments for all consolidation cases, as is seen in Figure 4.4. From these shear and normal stress results, a failure envelope in Figure 4.5 was drawn. The internal friction angle ϕ for this failure envelope was calculated as 21,3°.

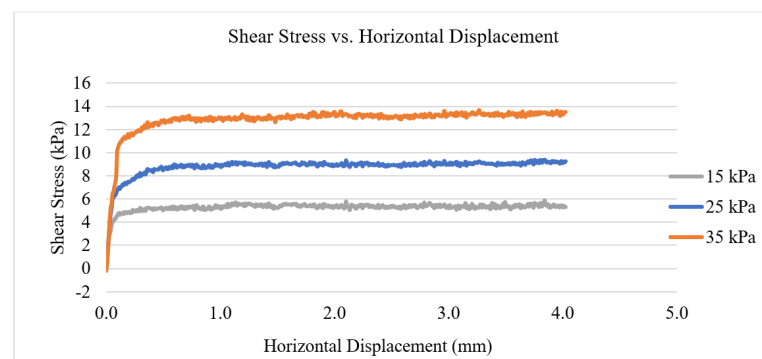


Figure 4.4. Shear Stress vs. Horizontal Displacement Results in Direct Shear Tests after 15 kPa, 25 kPa and 35 kPa Consolidation.

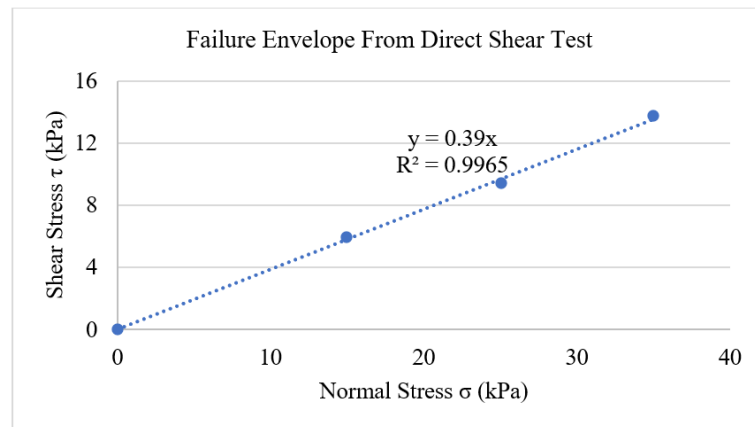


Figure 4.5. Failure Envelope from the Direct Shear Test Results.

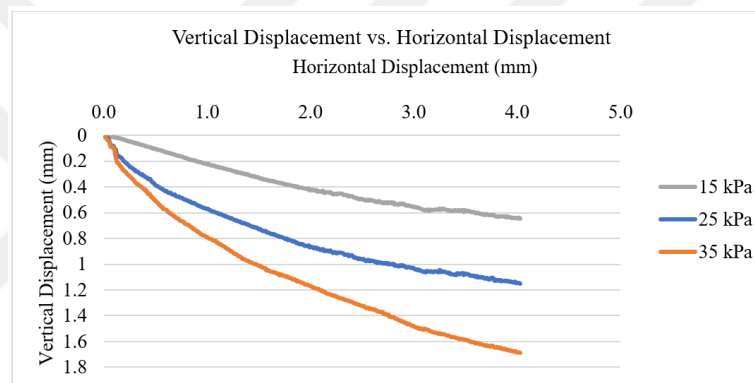


Figure 4.6. Vertical Displacement vs. Horizontal Displacement Results in Direct Shear Tests after 15 kPa, 25 kPa and 35 kPa Consolidation.

The vertical displacement results during shearing phase are represented in Figure 4.6. The total changes in height during the shearing were, approximately, 0,6, 1,2 and 1,7 mm for the specimens consolidated under 15, 25, 35 kPa, respectively. It is anticipated that further consolidation took place as a result of the increased porewater pressure during the shearing process.

4.2. Unit Cell Shear Device Tests

4.2.1. Monotonic Shear Loading

In Figure 4.7 shear stress vs. displacement graphs for Monotonic Benchmark Unit Cell tests are given. As can be seen from the graphs, the big portion of shear resistance was mobilized in smaller strain values in the unit cells consolidated under 35 kPa than the cells consolidated under 25 and 15 kPa. The strain value needed for the mobilization of the peak shear stress in the elastic region increased with decreasing consolidation loading.

The shear strength properties obtained from monotonic shear test results for benchmark unit cells (pure clay) after consolidation under 15, 25 and 35 kPa vertical loading were similar to the results from the direct shear tests. As seen in Figure 4.7, the mobilized peak shear stresses in the unit cell consolidated under 15 kPa, 25 kPa and 35 kPa vertical loading were 6, 10 and 14 kPa, respectively. The failure envelope is given in Figure 4.8. The internal friction angle ϕ for the benchmark unit cell shearing was calculated as 21.8° . This shows that the results obtained in the unit cell are consistent with the direct shear results.

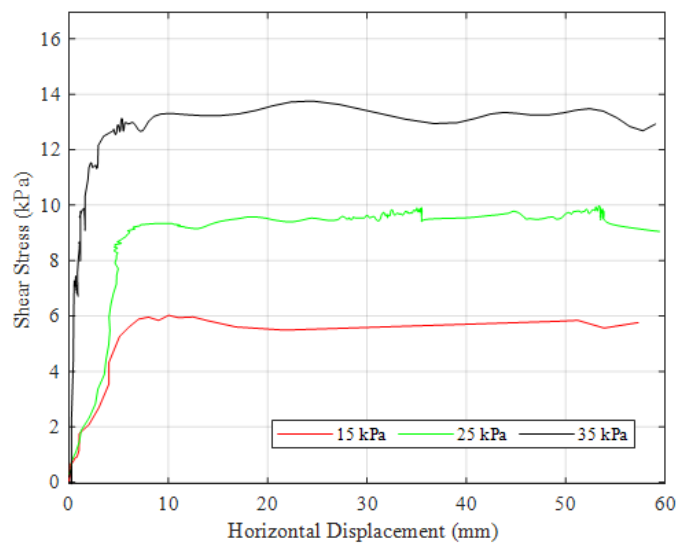


Figure 4.7. Shear Stress vs. Displacement Graph for Monotonic Benchmark Unit Cell Shearing.

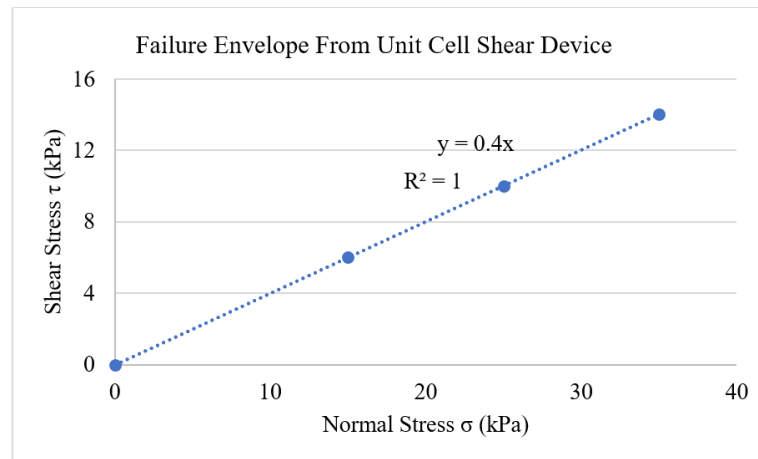


Figure 4.8. Failure Envelope from the Unit Cell Shear Device Benchmark Test Results.

After determining the shear properties of the pure clay as a benchmark, tests with GECs were conducted.

The shear stress - displacement graphs obtained under the vertical stress of 35 kPa can be seen in Figure 4.9. As can be seen from this figure, the shear strength is reached under minimal deformation. Therefore a comparison was made at the horizontal displacement of 5 mm. When the shear resistance at this deformation obtained for benchmark unit cell, OSC installed cell and GEC installed cells with a geotextile stiffnesses of 35 kN/m were compared, it was seen that the shear resistances measured were 12,75, 13,00 and 12,25 kPa, respectively. This shows that the OSC and GEC with very weak nonwoven geotextile does not provide an improvement to the shear strength. At the end of the shearing phase where the horizontal displacement reaches the maximum value of 60 mm, a differentiation between pure clay and improved soil was seen. The shear resistance of the pure clay remained almost constant with increasing displacement. However, for example the model with the GEC having geotextile with stiffness of 35 kN/m reached a shear strength of 20 kPa. There was also a minimal increase in the shear resistance of the OSC. These observations indicate that as the horizontal deformation increases, the granular infill started to provide an additional contribution as well, but the main contribution was obtained because of the tensile strength of the geotextile.

In Figure 4.9, the increasing behavior of stress with increasing strain after yielding can be seen also in the unit cells prepared with J400 and J1000 columns. For the GEC with J400 geotextile the shear resistance increased from 18.0 to 24.3 kPa as the horizontal displacement increased from 5 mm to 60 mm. Similarly for the GEC with J1000 geotextile the shear resistance increased from 27.8 to 35.8 kPa as the horizontal displacement increased from 5 mm to 60 mm.

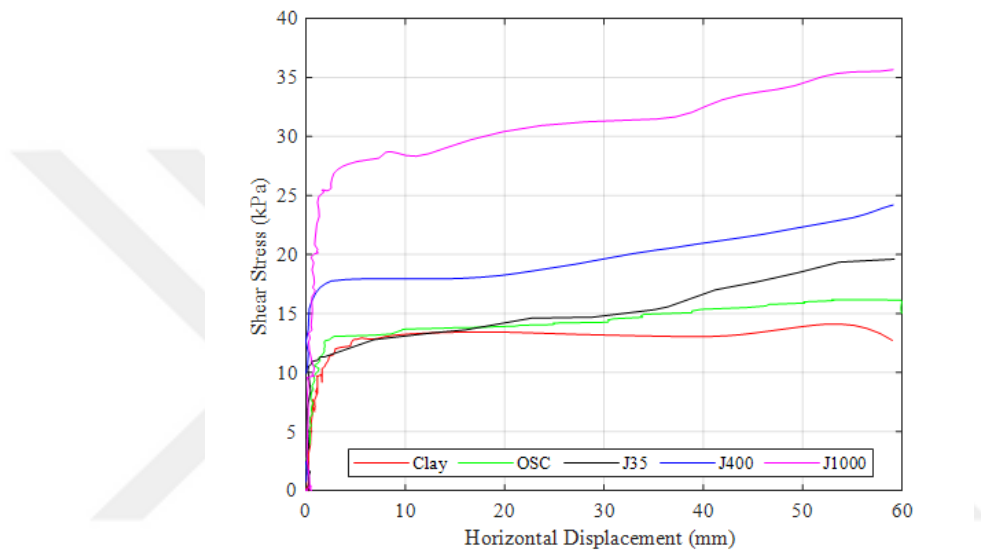


Figure 4.9. Shear Stress vs. Displacement Graph for Monotonic Unit Cell Shearing Conducted after Consolidation under 35 kPa Load.

The shear resistance versus horizontal displacement results for the models consolidated under 25 kPa are given in Figure 4.10. As seen in Figure 4.10, the mobilized shear strengths at 5 mm horizontal displacement were about 8,5; 9, 9; 25,0; 10,75 and 14,75 kPa for benchmark unit cell, unit cell with OSC, GECs with J35, J400 and J1000, respectively. Here also a similar trend like seen in Figure 4.9 is observed. There is no change in shear resistance in pure clay as the horizontal displacement increases. However for GECs, the final shear strength values at 60 mm horizontal displacement were 12, 15 and 19 kPa for the unit cells with J35, J400 and J1000 respectively. Again a marginal increase in OSC model have been observed with increasing horizontal displacement.

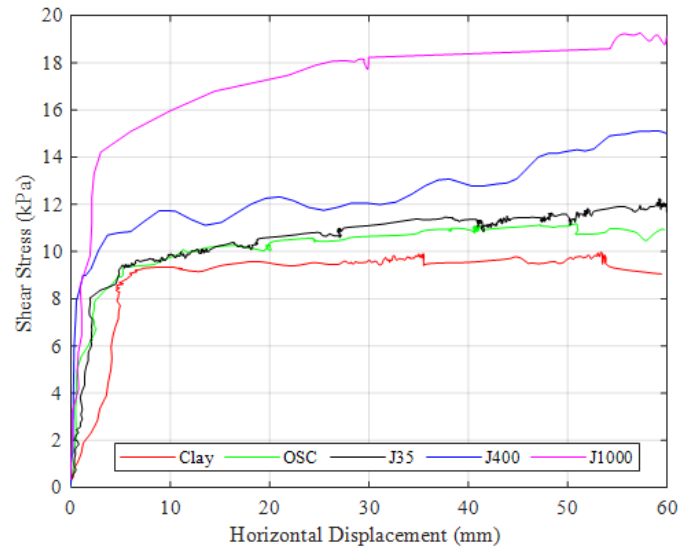


Figure 4.10. Shear Stress vs. Displacement Graph for Monotonic Unit Cell Shearing Conducted after Consolidation under 25 kPa Load.

The results obtained for 15 kPa vertical consolidation pressure are given in Figure 4.11. The trends are very similar to the trends observed for the models consolidated under 25 and 35 kPa vertical loads. As seen in Figure 4.11, the mobilized shear strength results at 5 mm horizontal displacement were 5,0; 4,5; 5,5; 7,5 and 11 kPa for the benchmark unit cell, unit cells with OSC, GECs with J35, J400 and J1000 respectively. At the end of horizontal displacement of 60 mm, the shear stresses were approximately 6 kPa for both benchmark unit cell and unit cell with OSC. For the unit cells GECs with encasement geotextiles of J35, J400 and J1000, the shear resistance values at 60 mm horizontal displacement were 7,5 kPa, 10,5 kPa and 15,75 kPa respectively.

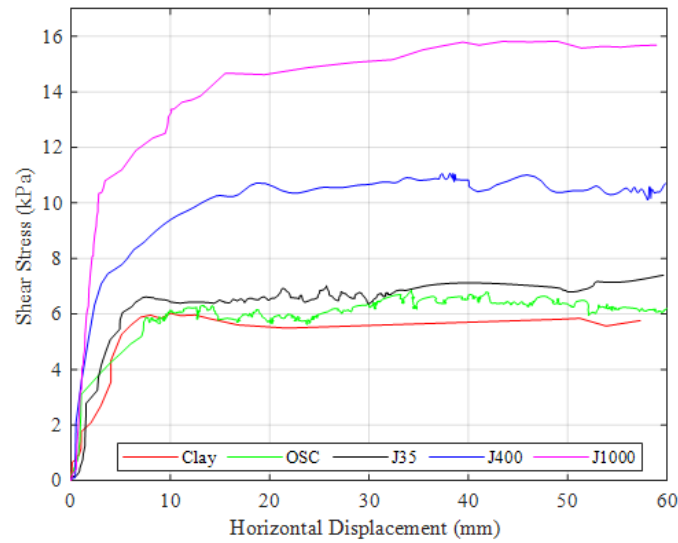


Figure 4.11. Shear Stress vs. Displacement Graph for Monotonic Unit Cell Shearing Conducted after Consolidation under 15 kPa Load.

The shear strength values of each unit cell after consolidation under 15 kPa were the lowest values among the other 2 cases of consolidation. However, the peak shear strength of the unit cell with J1000 was about 16 kPa and with this value it was even higher than all benchmark cells and cells with OSC consolidated even under 35 kPa, as seen in Figure 4.12. In the field, the shear strength of cohesive soils cannot be increased easily. But with the help of geosynthetic encased columns, a very weak soil consolidated even under 15 kPa and enhanced with a GEC can achieve the shear strength of a soil enhanced with OSC and consolidated under the load of 35 kPa.

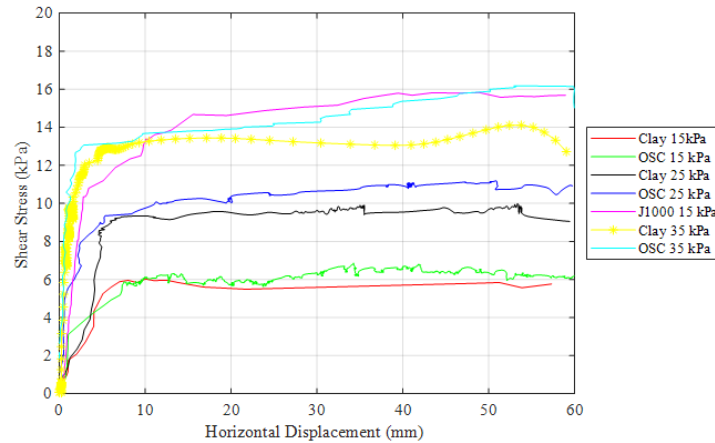


Figure 4.12. Shear Stress vs. Displacement Graph for Monotonic Unit Cell Shearing Conducted with all Benchmark Unit Cells, all Unit Cells with OSC and Unit Cell with J1000 after Consolidation of 15 kPa Loading.

4.2.2. Cyclic Shear Loading

In order to understand the behavior of the OSC or GEC improved soft soils in terms of global stability under earthquake loading conditions, a series of cyclic load tests were conducted. For these experiments, new models were constructed in order to avoid the effects of disturbance caused on previous models. The same model preparation methods were used for these models and the same vertical consolidation pressures were chosen. After the consolidation loading, in order to simulate an earthquake loading a cyclic strain of ± 35 mm has been applied. Evaluations were also made for the stress levels reached at ± 10 mm horizontal displacement.

In Figure 4.13, the results of the unit cells which are consolidated under a vertical load of 35 kPa are given. In cyclic shearing phase, the mobilized shear strengths at +10 mm displacement are 10,5 kPa for the unit cells prepared with clay, OSC and J35 respectively. At the same horizontal displacement the shear strengths for unit cells with J400 and J1000 were 13,75 and 14,5 kPa, respectively. This shows that the GECs with typical geotextile stiffnesses increase the resistance to cyclic loading. At 35 mm displacement, the mobilized shear strengths were 16; 18; 20; 24,5 and 33 kPa for the unit cells with only clay, enhanced with OSC, J35, J400 and J1000, respectively. Here

also it is observed that a GEC with stiff geotextile increases the cyclic shear resistance significantly.

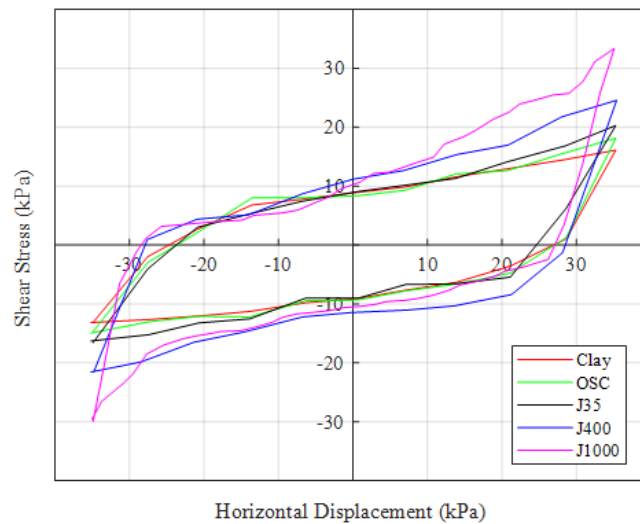


Figure 4.13. 10th Cycle of Shear Stress versus Displacement Loop with Cyclic Shear Loading after Consolidation under 35 kPa Load.

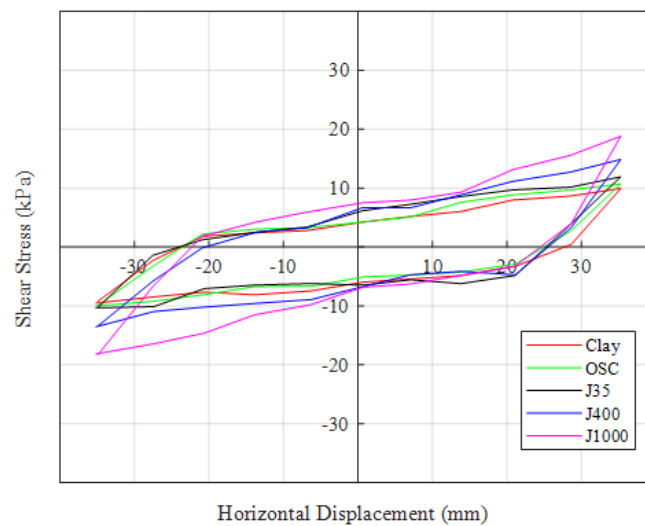


Figure 4.14. 10th Cycle of Shear Stress versus Displacement Loop with Cyclic Shear Loading after Consolidation under 25 kPa Load.

The results obtained on models consolidated under a vertical pressure of 25 kPa are given in Figure 4.14. As seen in this figure, the mobilized shear strengths resis-

tance at 10 mm displacement were 5,5 kPa, 6,25 kPa, 7,5 kPa, 7,75 kPa and 8,5 kPa respectively for the benchmark unit cell and unit cells with OSC, GECs J35, J400 and J1000. At +35mm displacement, the shear strengths were 10 kPa, 10,75 kPa, 12 kPa, 15 kPa and 19 kPa respectively for the benchmark unit cell and unit cells enhanced OSC, J35, J400 and J1000.

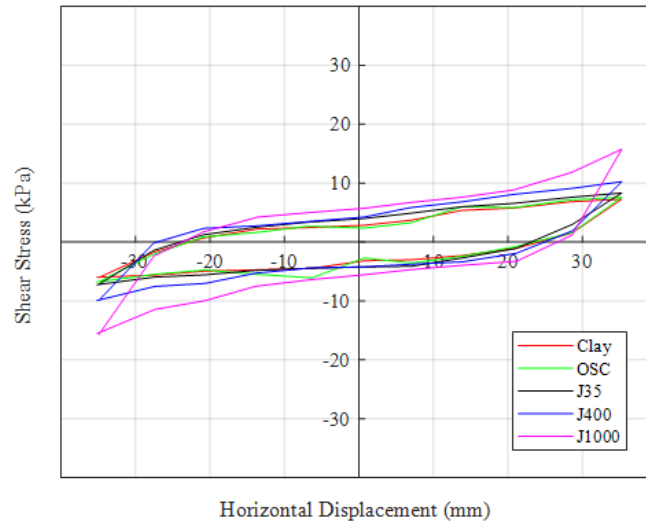


Figure 4.15. 10th Cycle of Shear Stress versus Displacement Loop with Cyclic Shear Loading after Consolidation under 15 kPa Load.

The unit cell models prepared with a vertical consolidation pressure of 15 kPa had naturally the lowest shear resistance values compared to the cases with higher consolidation loadings. At +10 mm of horizontal displacement, the mobilized shear strength values were 4,5 kPa, 4,5 kPa, 5,5 kPa, 6,25 kPa and 7 kPa for the benchmark unit cell and unit cells prepared with OSC, J35, J400 and J1000, respectively. The mobilized shear strengths at 35 mm horizontal displacement became 7,25 kPa, 7,5 kPa, 8 kPa, 10,25 kPa and 15,75 kPa.

4.2.3. Evaluation of Test Results

In Table 4.1-Table 4.6, all the shear strength results of the Unit Cell Shear Device are summarized. In order to understand the effect of the horizontal displacement are given for 5 mm, 10 mm, 35 mm and 60 mm. The first three levels were also chosen

in the given values to allow a comparison between monotonic and cyclic behavior. As can be seen from the tables, in the unit cells with J35, J400 and J1000, there was an increasing trend of shear strengths with increasing horizontal displacement under all consolidation loadings during monotonic shearing. In the unit cells with OSC, there was also an increasing trend of shear strength with horizontal displacement under all consolidation loadings except 15 kPa. In the benchmark unit cells, the shear strengths were mostly stable during monotonic shearing. During cyclic shearing, at +5 mm and +10 mm horizontal displacements, the shear strength values of all unit cells were very close to each other. However, at +35 mm horizontal displacement, the shear strength values were increasing drastically.

Table 4.1. Monotonic Shear Strength Results of Benchmark Unit Cell, Unit Cell with OSC, J35, J400, J1000 after 15 kPa consolidation at +5 mm, +10 mm, +35 mm and +60 mm Displacement.

	15 kPa Consolidation Loading			
	+5 mm	+10 mm	+35 mm	+60 mm
Benchmark	5 kPa	6.25 kPa	5.5 kPa	5.75 kPa
OSC	4.5 kPa	6 kPa	6.5 kPa	6 kPa
J35	5.5 kPa	6.5 kPa	7 kPa	7.5 kPa
J400	7.5 kPa	9.5 kPa	11 kPa	10.5 kPa
J1000	11 kPa	12.5 kPa	15.5 kPa	15.75 kPa

Table 4.2. Monotonic Shear Strength Results of Benchmark Unit Cell, Unit Cell with OSC, J35, J400, J1000 after 25 kPa consolidation at +5 mm, +10 mm, +35 mm and +60 mm Displacement.

	25 kPa Consolidation Loading			
	+5 mm	+10 mm	+35 mm	+60 mm
Benchmark	8.5 kPa	9.25 kPa	9.75 kPa	9 kPa
OSC	9 kPa	9.75 kPa	10.75 kPa	11 kPa
J35	9.25 kPa	10 kPa	11.5 kPa	12 kPa
J400	10.75 kPa	11.75 kPa	12.75 kPa	15 kPa
J1000	14.75 kPa	16 kPa	18.25 kPa	19 kPa

Table 4.3. Monotonic Shear Strength Results of Benchmark Unit Cell, Unit Cell with OSC, J35, J400, J1000 after 35 kPa consolidation at +5 mm, +10 mm, +35 mm and +60 mm Displacement.

	35 kPa Consolidation Loading			
	+5 mm	+10 mm	+35 mm	+60 mm
Benchmark	12.75 kPa	13.25 kPa	13 kPa	12.75 kPa
OSC	13 kPa	13.75 kPa	15 kPa	16 kPa
J35	12.25 kPa	13 kPa	15.25 kPa	19.5 kPa
J400	18 kPa	18 kPa	20.25 kPa	24.25 kPa
J1000	27.75 kPa	28.5 kPa	31.5 kPa	35.75 kPa

Table 4.4. Cyclic Shear Strength Results of Benchmark Unit Cell, Unit Cell with OSC, J35, J400, J1000 after 15 kPa consolidation at +5 mm, +10 mm and +35 mm Displacement.

	15 kPa		
	+5 mm	+10 mm	+35 mm
Benchmark	3,5 kPa	4,5 kPa	7.25 kPa
OSC	3 kPa	4,5 kPa	7,5 kPa
J35	4.5 kPa	5.5 kPa	8 kPa
J400	5.5 kPa	6.25 kPa	10.25 kPa
J1000	6.5 kPa	7 kPa	15.75 kPa

Table 4.5. Cyclic Shear Strength Results of Benchmark Unit Cell, Unit Cell with OSC, J35, J400, J1000 after 25 kPa consolidation at +5 mm, +10 mm and +35 mm Displacement.

	25 kPa		
	+5 mm	+10 mm	+35 mm
Benchmark	4.75 kPa	5,5 kPa	10 kPa
OSC	4.75 kPa	6.25 kPa	10.75 kPa
J35	7 kPa	7.5 kPa	12 kPa
J400	6.75 kPa	7,75 kPa	15 kPa
J1000	7.75 kPa	8,5 kPa	19 kPa

Table 4.6. Cyclic Shear Strength Results of Benchmark Unit Cell, Unit Cell with OSC, J35, J400, J1000 after 35 kPa consolidation at +5 mm, +10 mm and +35 mm Displacement.

	35 kPa		
	+5 mm	+10 mm	+35 mm
Benchmark	9.5 kPa	10.5 kPa	16 kPa
OSC	9 kPa	10.5 kPa	18 kPa
J35	9.75 kPa	10.5 kPa	20.25 kPa
J400	12.25 kPa	13.75 kPa	24.5 kPa
J1000	12.5 kPa	14.5 kPa	33.25 kPa

In Table 4.7 and Table 4.8 the ϕ angle values of benchmark unit cell, unit cell with OSC, J35, J400 and J1000 are given for monotonic shearing and cyclic shearing respectively. For the OSCs as well, but especially for GECs it is for sure that the increase to shear resistance is not derived only from frictional forces but also a major contribution is made by the tensile strength of the encasement geotextile. So here ϕ angle should not be considered as purely a friction angle but it is an equivalent shear strength parameter which incorporates the effect of the clay, stone infill and the geotextile encasement. It is our suggestion, that this equivalent ϕ value can be assigned to the area which is improved with GECs to represent the overall soil improvement. Since it was observed that the shear strength continuous to gradually increase specially for the GEC models, the ϕ angle values at +5 mm, +10 mm, +35mm and +60 mm horizontal displacement in monotonic shearing are given separately. It can be seen from Table 4.7 that the installation of an OSC or weak encasement (J35) does not significantly increase the shear resistance. However, GECs with stiffer encapsulation geotextiles cause a very important increase in the measured friction angle and this increase is also a function of the geotextile stiffness. Namely as the stiffness of the encapsulation stiffness increases from 400 kN/m to 1000 kN/m the friction angle increases from 26° to 36° for a 5 mm displacement and for example from 33.7° to 43.4° for 60 mm deformation. From these measured internal friction angles, we can also conclude that for the pure clay model (benchmark) there is no significant increase in the shear resistance after 5 mm displacement. However even for the weak encapsulation geotextile (J35)

the internal friction angle increases from 19.7° to 27.8° as the displacement increases from 5 to 60 mm. Similar trends were observed for stiffer geotextiles as well. As a result, the chosen equivalent ϕ value should be chosen based on the deformation the designer allows in the foundation soil of the embankment.

Similar to determining equivalent ϕ angles for the GEC and OSC improved foundations, also equivalent ϕ angles were determined for cyclic loading conditions. All the figures for obtaining the equivalent ϕ angles are given in Appendix A. When we compare the internal friction angles determined from the cyclic loading based on the shear stresses at 35 mm displacement, we can see that they were higher for all the cases, when compared to the friction angles determined for monotonic loading at 35 mm. It is further observed that also in cyclic shearing, the ϕ angle values are increasing with increasing horizontal displacement. The coefficient of regression values for all trendlines used in the calculation of ϕ angles were more than 80%.

Table 4.7. ϕ Angles of Benchmark Unit Cells, Unit Cells with OSC, J35, J400 and J1000 at +5 mm, +10 mm, +35 mm and +60 mm Horizontal Displacement in Monotonic Shearing.

	ϕ Angles			
	+5 mm	+10 mm	+35 mm	+60 mm
Benchmark	19.5	20.8	20.6	20.1
OSC	19.8	21.4	23.2	24
J35	19.7	21.1	24.1	27.8
J400	26	27.2	29.9	33.7
J1000	36	37.4	40.8	43.4

Table 4.8. ϕ Angles of Benchmark Unit Cells, Unit Cells with OSC, J35, J400 and J1000 at +5 mm, +10 mm and +35 mm Horizontal Displacement in Cyclic Shearing.

	ϕ Angles		
	+5 mm	+10 mm	+35 mm
Benchmark	13.7	15.4	23.9
OSC	13	15.9	26
J35	15.7	17.1	28.6
J400	18.1	20.3	33.8
J1000	19.4	21.7	42.1

4.2.4. Strain Measurements

In section 4.2, the behavior of GECs is evaluated by comparing the shear resistance the horizontal displacement values. It is seen from these that the yield and peak shear strength of the unit cell models is increasing with the inclusion of stone columns. Furthermore, the enhancement is further increasing with the intersection of GECs. The enhancement level also increases with increasing stiffness of the encasement geotextile. For the GECs, there is an increasing behavior of shear strength values with increasing strain after yielding. In order to understand the reasons of this behavior, the strain measurements on the geosynthetic encasements will be given in this section.

In order to determine the stresses in the geotextile encasements, the strains developing on the geotextile encasements are measured during the loading of the models. The strains on the geotextiles are measured with the help of strain rosettes. These are placed on a line which is closest to the monotonic or cyclic actuators and at 500 mm, 600 mm and 700 mm depths from the bottom. It should be noted that the strain rosettes at 600 mm depth are exactly on the shear plane.

In Table 4.9 Table 4.10 and Table 4.11, the vertical strain values on the strain gauges at 500 mm, 600 mm and 700 mm depth are presented after the normal loading before monotonic shear loading. For all geosynthetic encasements at any depth, with increasing normal load the strains are decreasing. The encasement in the vertical

direction at this stage is in compression. This is understandable, since the geotextile encasement is not stretched during the installation. When we compare the amount of compressions, we can easily see that the compressive strains are larger for weaker geotextile. This can be also the result of much stiffer geotextile keeping its shape during installation phase. Another observation is that with increasing vertical consolidation pressure (in other words increasing cohesion of the clay) the compressive strains also reduce in magnitude in the installation phase, because of the clay holding itself up much better.

Table 4.9. Vertical Strain Values (%) after Normal Loading at 700 mm depth (Before Monotonic Shear Loading).

	Normal Load		
	15 kPa	25 kPa	35 kPa
J35	0.9	0.73	0.63
J400	0.37	0.23	0.14
J1000	0.16	0.1	0.06

Table 4.10. Vertical Strain Values (%) after Normal Loading at 600 mm depth (Before Monotonic Shear Loading).

	Normal Load		
	15 kPa	25 kPa	35 kPa
J35	0.87	0.71	0.62
J400	0.35	0.22	0.12
J1000	0.16	0.09	0.05

Table 4.11. Vertical Strain Values (%) after Normal Loading at 500 mm depth (Before Monotonic Shear Loading).

	Normal Load		
	15 kPa	25 kPa	35 kPa
J35	0.85	0.72	0.61
J400	0.33	0.21	0.12
J1000	0.15	0.08	0.05

The horizontal strain values on the strain rosettes are presented after normal loading before monotonic shear loading, in Table 4.12, Table 4.13, Table 4.14. The hoop is in tension at all depths. The strains are increasing with decreasing normal load. This is also expected, because the higher the cohesion, the less the confinement by the encasement is needed.

Table 4.12. Horizontal Strain Values (%) after Normal Loading at 700 mm depth (Before Monotonic Shear Loading).

	Normal Load		
	15 kPa	25 kPa	35 kPa
J35	-0.99	-0.76	-0.59
J400	-0.25	-0.19	-0.11
J1000	-0.12	-0.07	-0.03

Table 4.13. Horizontal Strain Values (%) after Normal Loading at 600 mm depth (Before Monotonic Shear Loading).

	Normal Load		
	15 kPa	25 kPa	35 kPa
J35	-0.98	-0.76	-0.57
J400	-0.22	-0.16	-0.09
J1000	-0.11	-0.07	-0.02

Table 4.14. Horizontal Strain Values (%) after Normal Loading at 500 mm depth (Before Monotonic Shear Loading).

	Normal Load		
	15 kPa	25 kPa	35 kPa
J35	-0.98	-0.75	-0.54
J400	-0.22	-0.15	-0.08
J1000	-0.12	-0.09	-0.02

The vertical strain values at + 60 mm displacement after monotonic loading are presented in Table 4.15, Table 4.16, Table 4.17. The geosynthetic encasements are under tension in longitudinal direction. The vertical strain values at 500 mm and 700

mm depth are smaller than the vertical strain values. This is expected because the tensile stress due to shear appears mainly at the shear plane and the locations 10 mm above and below are the anchorage zones. These evaluations lead to the concept that as the GEC is sheared, the geotextile orients its direction with the shear plane and contributes to the resistance against the shear force applied significantly. With increasing stiffness of geosynthetic encasement, the vertical strains are decreasing like in the vertical strain values after normal loading. On the contrary of the case after normal loading, the strain values are increasing under increasing normal load.

Table 4.15. Vertical Strain Values (%) at +60 mm Displacement at 700 mm depth (After Monotonic Shear Loading).

	Normal Load		
	15 kPa	25 kPa	35 kPa
J35	-0.91	-1.06	-1.58
J400	-0.41	-0.42	-0.6
J1000	-0.16	-0.24	-0.31

Table 4.16. Vertical Strain Values (%) at +60 mm Displacement at 600 mm depth (After Monotonic Shear Loading).

	Normal Load		
	15 kPa	25 kPa	35 kPa
J35	-1.69	-2.31	-3.19
J400	-0.72	-0.86	-1.26
J1000	-0.35	-0.5	-0.59

Table 4.17. Vertical Strain Values (%) at +60 mm Displacement at 500 mm depth (After Monotonic Shear Loading).

	Normal Load		
	15 kPa	25 kPa	35 kPa
J35	-0.96	-1.02	-1.49
J400	-0.43	-0.48	-0.66
J1000	-0.19	-0.22	-0.29

In Table 4.18, Table 4.19, Table 4.20, the horizontal strain values at +60 mm displacement after monotonic loading are represented. It is seen that the encasements at any depth are under tension. This indicates that the geotextile encasement provides an additional confinement to the granular infill. The strain values are increasing with increasing normal load. This is also in alignment with additional need for confinement by the geotextile encasement. Again, 100 mm under and above the shear plane, the strain values are less than the ones at shear plane.

Table 4.18. Horizontal Strain Values (%) at +60 mm Displacement at 700 mm depth (After Monotonic Shear Loading).

	Normal Load		
	15 kPa	25 kPa	35 kPa
J35	-0.58	-0.67	-1.11
J400	-0.21	-0.39	-0.49
J1000	-0.05	-0.11	-0.18

Table 4.19. Horizontal Strain Values (%) at +60 mm Displacement at 600 mm depth (After Monotonic Shear Loading).

	Normal Load		
	15 kPa	25 kPa	35 kPa
J35	-0.8	-1.02	-1.8
J400	-0.31	-0.52	-0.75
J1000	-0.09	-0.16	-0.24

Table 4.20. Horizontal Strain Values (%) at +60 mm Displacement at 500 mm depth (After Monotonic Shear Loading).

	Normal Load		
	15 kPa	25 kPa	35 kPa
J35	-0.6	-0.7	-1.08
J400	-0.24	-0.41	-0.49
J1000	-0.04	-0.13	-0.16

In Table 4.21, Table 4.22 and Table 4.23, the vertical strain values on the strain gauges after normal loading before cyclic loading are presented. The strain values are very close to the strain values after normal loading before monotonic shear loading as expected. This also gives a hint, that the test results are repeatable.

Table 4.21. Vertical Strain Values (%) after Normal Loading at 700 mm depth
(Before Cyclic Shear Loading).

	Normal Load		
	15 kPa	25 kPa	35 kPa
J35	0.86	0.72	0.64
J400	0.38	0.22	0.15
J1000	0.15	0.11	0.06

Table 4.22. Vertical Strain Values (%) after Normal Loading at 600 mm depth
(Before Cyclic Shear Loading).

	Normal Load		
	15 kPa	25 kPa	35 kPa
J35	0.87	0.72	0.65
J400	0.36	0.21	0.13
J1000	0.16	0.1	0.06

Table 4.23. Vertical Strain Values (%) after Normal Loading at 500 mm depth
(Before Cyclic Shear Loading).

	Normal Load		
	15 kPa	25 kPa	35 kPa
J35	0.89	0.73	0.62
J400	0.36	0.2	0.13
J1000	0.14	0.09	0.05

In Table 4.24, Table 4.25, Table 4.26, the horizontal strain values on the strain rosettes after normal loading before cyclic loading are presented. These strain values

are consistent with the same strain values of the unit cells prepared for monotonic shear loading.

Table 4.24. Horizontal Strain Values (%) after Normal Loading at 700 mm depth (Before Cyclic Shear Loading).

	Normal Load		
	15 kPa	25 kPa	35 kPa
J35	-1	-0.75	-0.57
J400	-0.25	-0.2	-0.12
J1000	-0.13	-0.08	-0.04

Table 4.25. Horizontal Strain Values (%) after Normal Loading at 600 mm depth (Before Cyclic Shear Loading).

	Normal Load		
	15 kPa	25 kPa	35 kPa
J35	-0.99	-0.76	-0.56
J400	-0.23	-0.16	-0.09
J1000	-0.1	-0.08	-0.03

Table 4.26. Horizontal Strain Values (%) after Normal Loading at 500 mm depth (Before Cyclic Shear Loading).

	Normal Load		
	15 kPa	25 kPa	35 kPa
J35	-1.00	-0.77	-0.58
J400	-0.23	-0.16	-0.10
J1000	-0.11	-0.09	-0.03

The vertical strain values at + 35 mm displacement after 10th cycle of cyclic loading are presented in Table 4.27, Table 4.28, Table 4.29. There is a similar behavior in comparison with monotonic loading case. The geosynthetic encasements are also

under tension in longitudinal direction. To the left and to the bottom of the table the strains are decreasing. Generally, the strain values are smaller than the strain values of monotonic shear loading at +60 mm displacement.

Table 4.27. Vertical Strain Values (%) at +35 mm Displacement at 700 mm depth (After Cyclic Shear Loading).

	Normal Load		
	15 kPa	25 kPa	35 kPa
J35	-0.77	-0.93	-1.3
J400	-0.35	-0.41	-0.48
J1000	-0.13	-0.12	-0.24

Table 4.28. Vertical Strain Values (%) at +35 mm Displacement at 600 mm depth (After Cyclic Shear Loading).

	Normal Load		
	15 kPa	25 kPa	35 kPa
J35	-1.39	-1.91	-2.73
J400	-0.57	-0.69	-1.08
J1000	-0.29	-0.42	-0.51

Table 4.29. Vertical Strain Values (%) at +35 mm Displacement at 500 mm depth (After Cyclic Shear Loading).

	Normal Load		
	15 kPa	25 kPa	35 kPa
J35	-0.81	-0.92	-1.31
J400	-0.37	-0.4	-0.51
J1000	-0.11	-0.14	-0.23

In Table 4.30, Table 4.31, Table 4.32, the horizontal strain values at +35 mm displacement after 10th cyclic loading are represented. The strain values are decreasing

with increasing tensile stiffness of the encasements. At the shear plane, the strains are higher. If these values are compared with horizontal strain values after monotonic loading, horizontal strain values at 10th cyclic loading are slightly smaller than horizontal strain values at +60 mm displacement of monotonic loading.

Table 4.30. Horizontal Strain Values (%) at +35 mm Displacement at 700 mm depth (After Cyclic Shear Loading).

	Normal Load		
	15 kPa	25 kPa	35 kPa
J35	-0.55	-0.66	-1.12
J400	-0.19	-0.39	-0.53
J1000	-0.07	-0.12	-0.17

Table 4.31. Horizontal Strain Values (%) at +35 mm Displacement at 600 mm depth (After Cyclic Shear Loading).

	Normal Load		
	15 kPa	25 kPa	35 kPa
J35	-0.71	-0.98	-1.74
J400	-0.28	-0.44	-0.69
J1000	-0.1	-0.13	-0.23

Table 4.32. Horizontal Strain Values (%) at +35 mm Displacement at 500 mm depth (After Cyclic Shear Loading).

	Normal Load		
	15 kPa	25 kPa	35 kPa
J35	-0.53	-0.71	-1.07
J400	-0.21	-0.39	-0.5
J1000	-0.05	-0.09	-0.14

5. CONCLUSION

In this study, the shear behavior of GECs embedded in soft clay soils are investigated. Unit Cell Shear Device designed by Dr. Cihan Cengiz is used to exert monotonic or cyclic shear loads on the unit cells prepared by only clay, OSC surrounded by clay or GECs surrounded by clay. Shear load data is taken together with displacement data and strain data on geosynthetics.

First the shear strength properties of pure clay samples are determined in the Unit Cell Shear Device (UCSD) as benchmark tests. The same clay is also tested in a direct shear apparatus under same loads and similar results are obtained. Thus, the UCSD results are validated. In the stress vs displacement graph for monotonic benchmark unit cells, it is seen that most of the shear strength is mobilized in relatively small horizontal deformations and specially so for the model consolidated under the vertical load of 35 kPa.

It was determined that the shear strength of the unit cell is clearly increased under the same normal load by installing Ordinary Stone Columns (OSCs) and Geosynthetic Encased Columns (GECs). In the tests three different geosynthetic encasements are used, namely J35, J400 and J1000, where these refer to geotextiles with stiffnesses of 35 kN/m, 400 kN/m and 1000 kN/m respectively. The peak shear strengths measured in monotonic shear loading for the various soil improvement options can be compared with each other as follows: shear strength of unit cell with OSC < shear strength of GEC with J35 < shear strength of GEC with J400 < shear strength of GEC with J1000. Under the monotonic shear loading, the shear strength is already mobilized for small horizontal displacement values and this was most obvious for the models consolidated under a vertical load of 35 kPa. Already for a horizontal displacement of + 5 mm the shear force ? horizontal displacement curves pass the yield point. Therefore +5 mm displacement was chosen to compare the shear strength of different models. It was determined that the value for the unit cell with J1000 column has a shear strength of approximately 2.5 times more than the benchmark unit cell under the same normal

load. The main reason is the contribution 57 of the tensile strength of the encasement. Furthermore, the shear strength values increase with increasing displacement for unit cells with OSCs and GECs.

In order to be able to utilize the enhancement of GECs in edge slope stability calculations, an equivalent strength parameter is needed. Since the unit cell represents a combined behavior of the soft clay + stone infill + geosynthetic encasement, the results obtained from the UCSD can be used directly. So the shear strength values obtained from UCSD model under different vertical models were used to calculate an equivalent strength parameter to represent the improved foundation soil. Based on these analyses it was determined that the pure clay can be represented by $\phi = 19.5^\circ$. The inclusion of OSCs increase the equivalent shear strength parameter to $\phi = 19.8^\circ$, and for GECs with J35, J400 and J100 these values are $\phi = 19.7^\circ$, $\phi = 26.0^\circ$, $\phi = 36.0^\circ$ respectively. These equivalent values were obtained for a horizontal displacement of 5 mm.

However, the shear resistances of the unit cells continue to increase with increasing horizontal deformations for models enhanced with OSCs and GECs. The equivalent strength parameters for example for the maximum horizontal displacement of 60 mm can be given for OCS, GEC with J35, J400 and J1000 respectively as $\phi = 24.0^\circ$, $\phi = 27.8^\circ$, $\phi = 33.7^\circ$, $\phi = 43.3^\circ$.

In the cyclic load tests, the behavior of OSC and GEC are investigated in terms of global stability under earthquake loading. The results of the 10th cycle of the loading is taken in all tests for comparison. In the cyclic tests with unit cells consolidated under 35 kPa normal load, the shear strength values at 0 mm displacement are close to each other regardless of presence of a column or not or the stiffness of the geotextile encasement. But the shear strength values increased and differentiated drastically as the displacement values reached +35 mm or -35 mm, respectively. Similar behavior is seen for the unit cells prepared under 25 kPa and 15 kPa normal loads, but the shear strength values are lower. It is also observed that the shear resistance of the stone columns under cyclic loading increase as the stiffness values of the geosynthetic

encasements increases.

Again for the cyclic loading equivalent ϕ angle values for different unit cell models under cyclic loading are determined. It was also seen for cyclic loading conditions that the equivalent ϕ angle values increase as the tensile stiffness of the geosynthetic encasement are increasing. It is further observed that the dynamic equivalent ϕ angle values increase as the tensile stiffness of the geosynthetic encasement are increasing. It is further observed that the dynamic equivalent ϕ angle values are slightly higher than the values obtained from monotonic tests. For the comparison of the equivalent ϕ angles, the values at 35 mm deformation are determined for OCS, GEC with J35, J400 and J1000 respectively as $\phi = 23.2^\circ$, $\phi = 24.1^\circ$, $\phi = 29.9^\circ$, $\phi = 40.8^\circ$ for monotonic loading and as $\phi = 26.0^\circ$, $\phi = 28.6^\circ$, $\phi = 33.8^\circ$, $\phi = 42.1^\circ$ for cyclic loading.

Vertical and horizontal strain values are in consistence before both cyclic and monotonic loading. The vertical strains before shear loading are compressive because geotextile encasements are not stretched before shearing and these values are decreasing as the consolidation pressure are increasing. This can be the result of the stiffer clay that holds better the geosynthetic due to contact forces. The horizontal strain values before shear loading are tensile and decrease as the consolidation pressure increases due to the stiffer clay that can hold the stone columns much stronger.

In monotonic shear loading, both vertical and horizontal strain values are in tension. During the shear loading, it is expected that the vertical strains are in tension because the geotextile encasements are orienting its direction with the shear plane and contributes to the shear resistance. The horizontal strain values for GECs under 15 kPa normal load decrease as the shearing begins. However, the horizontal strain values for GECs under 35 kPa normal load are increasing after monotonic shear loading.

In cyclic shear loading, also, both vertical and horizontal strain values are in tension. The strains are increasing as the consolidation load increases and they are decreasing as the stiffness of the geotextile increases.

So as a general conclusion it can be stated that GEC inclusion helps improve the edge stability of the embankments on soft clays and this enhancement can be quantified by the equivalent internal friction angle, which is a parameter of geotextile encasement stiffness.



REFERENCES

- Abusharar, S.W., J. Han, “Two-Dimensional Deep-Seated Slope Stability Analysis of Embankments Over Stone Column-Improved Soft Clay”, *Engineering Geology*, Vol. 120, pp. 103-110, 2011.
- Alexiew, D., D. Brokemper, S. Lothspeich, “Geotextile Encased Columns (Gec): Load Capacity, Geotextile Selection and Pre-Design Graphs”, *Proceedings of the Geo-Frontiers Conference, Geotechnical Special Publication*, Austin, TX, USA, pp. 497-510, 2005.
- Alexiew, D., G. Thomson, “Geotextile Encased Columns (GEC): Why, Where, When, What”, How Fourth International Conference on Geotechnique, *Construction Materials and Environment Brisbane*, Australia, pp. 484-489, 2014.
- Almeida, M., M. Riccio, I. Hosseinpour, D. Alexiew, “Geosynthetic Encased Columns For Soft Soil Improvement”, *CRC Press/Balkema*, London, UK, 2019.
- Ambily, A.P., S.R. Gandhi, “Behavior of Stone Columns Based on Experimental and FEM Analysis Journal Geotech Geoenviron Engineering”, *American Society of Civil Engineering*, Vol. 133, No. 4, pp. 405-415, 2007.
- Baker, W.E., P.S. Westine, F.T. Dodge, “Similarity Methods in Engineering Dynamics e Theory and Practice of Scale Modeling, Revised Edition”, *Elsevier Science Publishers B.V.*, the Netherlands, 1991.
- Barksdale, R.D., R.C. Bachus, “Design and Construction of Stone Columns”, *Federal 147 Highway Administration*, Vol. 1, pp. 194, 1983.
- Bauman, V., G.E. Bauer, “The Performance of Foundations on Various Soils Stabilized by the Vibrio-Compaction Method”, *Can Geotech Journal*, Vol. 11, No. 4, pp. 509-530, 1974.

- Black, J.V., V. Sivakumar, A. Bell, “The Settlement Performance of Stone Column Foundations”, *Geotechnique*, Vol. 61, No. 11, pp. 909-922, 2011.
- Brauns, J., “Initial Bearing Capacity of Stone Columns and Sand Piles”, Soil Reinforcing and Stabilizing Techniques in Engineering Practice”, *Sydney I*, Vol. 1, pp. 497-512, 1978.
- Castro, J., “Modeling Stone Columns”, *Materials*, Vol. 10, pp. 782-805, 2017.
- Cengiz, C., E. Guler, “Seismic Behavior of Geosynthetic Encased Columns and Ordinary Stone Columns”, *Geotext. Geomembranes*, Vol. 46, pp. 40-51, 2018a.
- Cengiz, C., I.E. Kilic, and E. Guler, “On the Shear Failure Mode of Granular Column Embedded Unit Cells Subjected To Static and Cyclic Shear Loads”, *Geotextiles and Geomembranes*, Vol. 47, No. 1, pp. 193-202, 2019.
- Cimentada, A., A. Da Costa, J. Canizal, C. Sagaseta, “Laboratory Study on Radial Consolidation and Deformation in Clay Reinforced with Stone Columns”, *Can Geotech Journal*, Vol. 48, pp. 36-52, 2011.
- Frikha, W., M. Bouassida, J. Canou, “Observed Behaviour of Laterally Expanded Stone Column in Soft Soil”, *Geotechnical and Geological Engineering*, Vol. 31, pp. 739-752, 2013.
- Gniel, J., A. Bouazza, “ Construction of Geogrid Encased Stone Columns: A New Proposal Based on Laboratory Testing”, *Geotextiles and Geomembranes*, Vol. 28, No. 1, pp. 108-118, 2010.
- Hausmann, M.R., “Engineering Principles of Ground Modification”, McGraw-Hill Publishing Company, Singapore, 1990.
- Hughes, J.M.O., N.J. Withers, “Reinforcing of Soft Cohesive Soils with Stone Columns”, *Ground Engineering*, Vol. 7, No. 3, pp. 42-49, 1974.

- HUESKER Synthetic GmbH, *Ringtrac*, <https://www.huesker.co.uk/products/geosynthetics/woven/ringtrac.html>, 2019.
- Miranda, M., A. Da Costa, J. Castro, C. Sagasetta, “Influence of Geotextile Encasement on the Behaviour of Stone Columns Laboratory Study”, *Geotextiles and Geomembranes*, Vol. 45, pp. 14-22, 2017.
- Murugesan, S., K. Rajagopal, “Shear Load Tests on Stone Columns With and Without Geosynthetic Encasement”, *Geotechnical Testing Journal*, Vol. 32, pp. 76-85, 2009.
- Murugesan, S. and K. Rajagopal, “Studies on the Behavior of Single and Group of Geosynthetic Encased Stone Columns”, *Journal of Geotechnical and Geoenvironmental Engineering*, Vol. 136, No. 1, pp. 129-139, 2010.
- Murugesan, S., K. Rajagopal, “Model Tests on Geosynthetic-Encased Stone Columns”, *Geosynthetics International*, Vol. 14, pp. 346-354, 2007.
- Murugesan, S., K. Rajagopal, “Performance of Encased Stone Columns and Design Guidelines for Construction on Soft Clay Soils”, *In Proceedings of the 4th Asian Regional Conference on Geosynthetics*, Vol. 1, pp. 729-734, 2008.
- Najjar, S.S., “A State-of-the-Art Review of Stone/Sand-Column Reinforced Clay Systems”, *Geotechnical and Geological Engineering*, Vol. 31, pp. 355-386, 2013.
- Raithel, M., H.G. Kempfert, “Calculation Models for Dam Foundations with Geotextile Coated Sand Columns”, *In Proceedings of the International Conference on Geotechnical and Geological Engineering*, Geoengg 2000.
- Van Impe, W., “Improving of the Bearing Capacity of Weak Hydraulic Fills by Means of Geotextile”, *Third International Conference on Geotextiles*, Vienna, 1986.
- Van Impe, W., “Soil Improvement Techniques and their Evolution”, A.A. Balkema, Rotterdam, Brookfield, 1989.

Vesic, A.S., "Expansion of Cavities in Infinite Soil Mass", J Soil Mech Found Div ASCE 98(SM3), pp. 265-290, 1972.

Watts, K.S., D. Johnson, L.A. Wood, A. Saadi, "Instrumental Trial of Vibrio Ground Treatment Supporting Strip Foundations in a Variable Fill", *Geotechnique*, Vol. 50, No. 6, pp. 699-709, 2000.



APPENDIX A: MOHR-COULOMB ENVELOPES

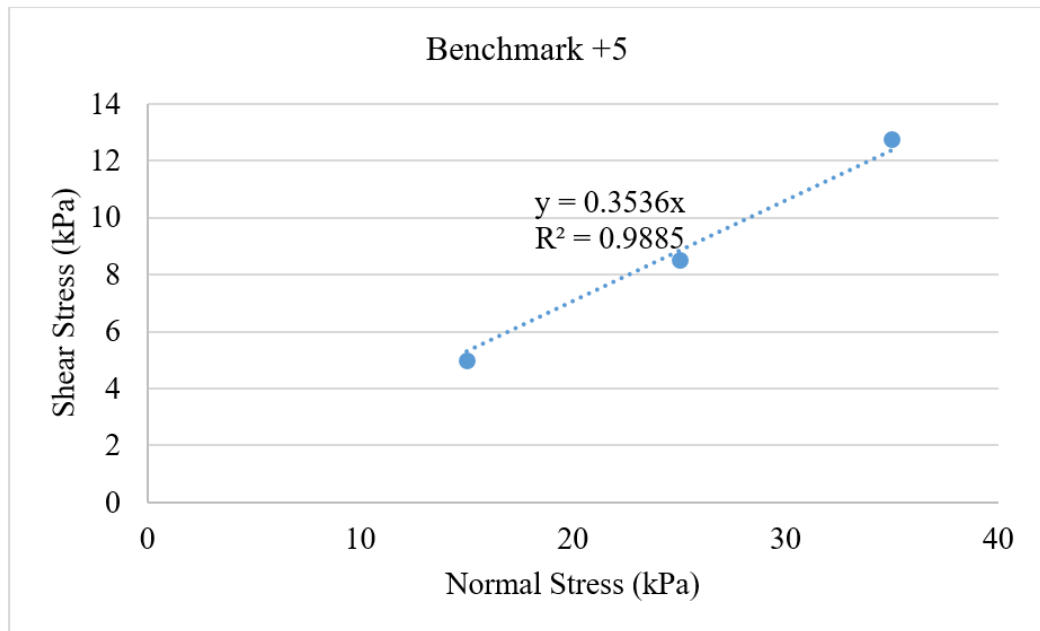


Figure A.1. Mohr-Coulomb Envelope for the Benchmark Unit Cell at +5 mm Horizontal Displacement during Monotonic Shearing.

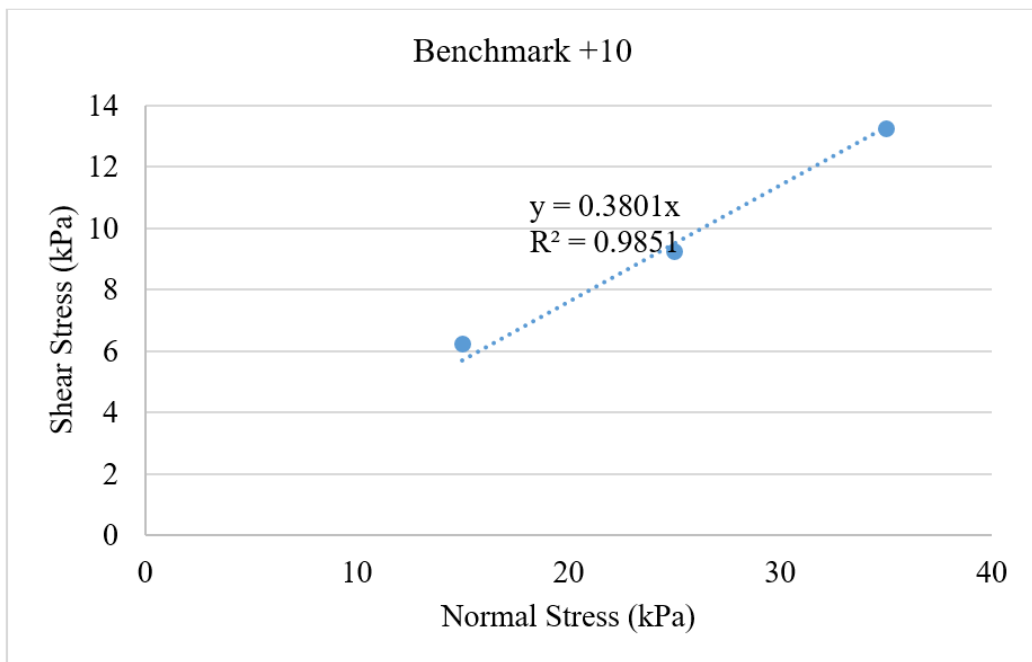


Figure A.2. Mohr-Coulomb Envelope for the Benchmark Unit Cell at +10 mm Horizontal Displacement during Monotonic Shearing.

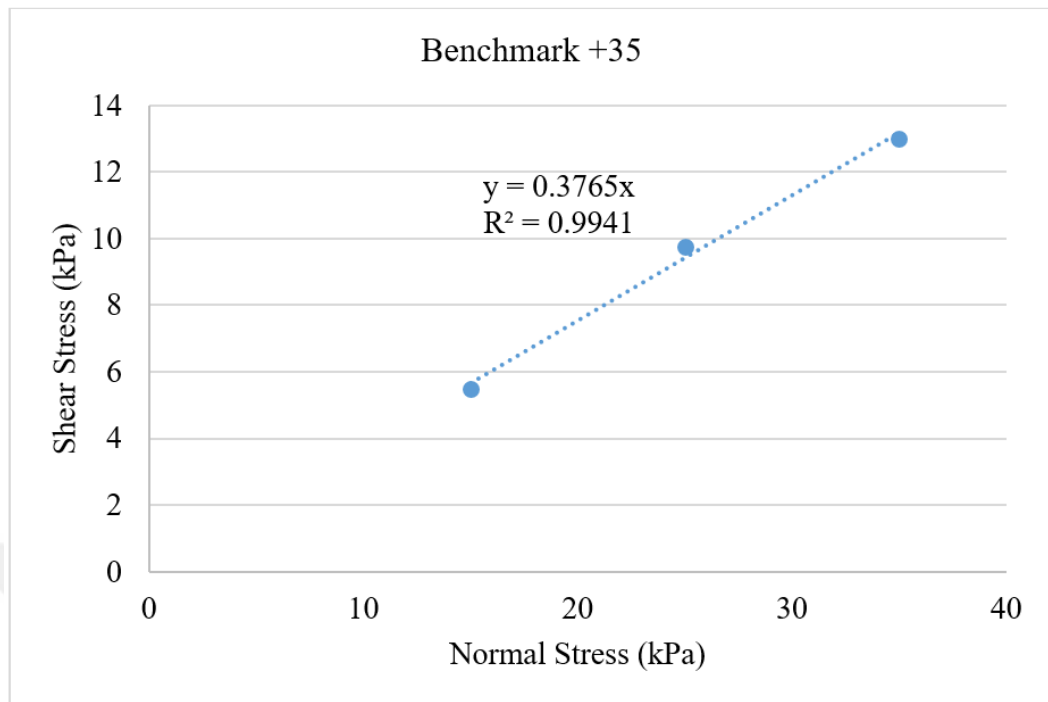


Figure A.3. Mohr-Coulomb Envelope for the Benchmark Unit Cell at +35 mm Horizontal Displacement during Monotonic Shearing.

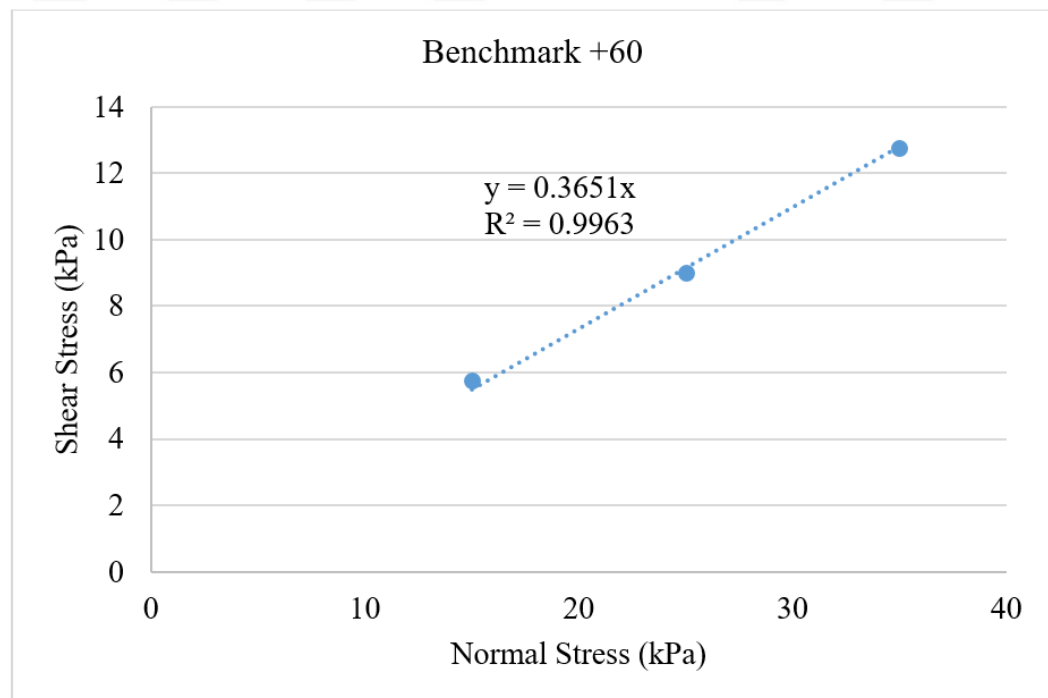


Figure A.4. Mohr-Coulomb Envelope for the Benchmark Unit Cell at +60 mm Horizontal Displacement during Monotonic Shearing.

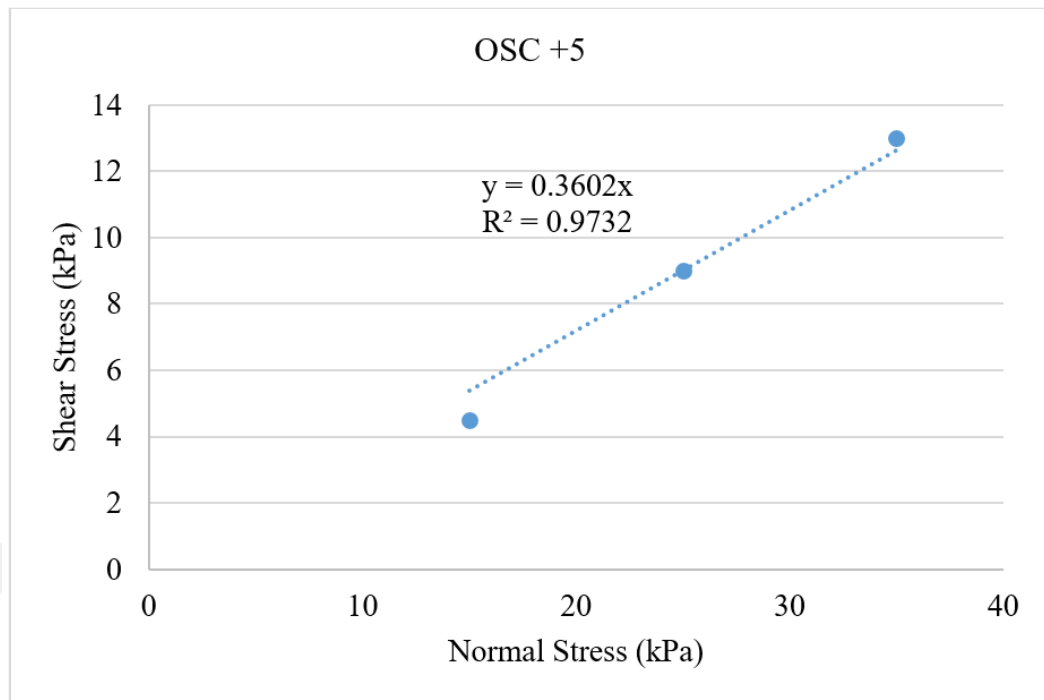


Figure A.5. Mohr-Coulomb Envelope for the Unit Cell with OSC at +5 mm Horizontal Displacement during Monotonic Shearing.

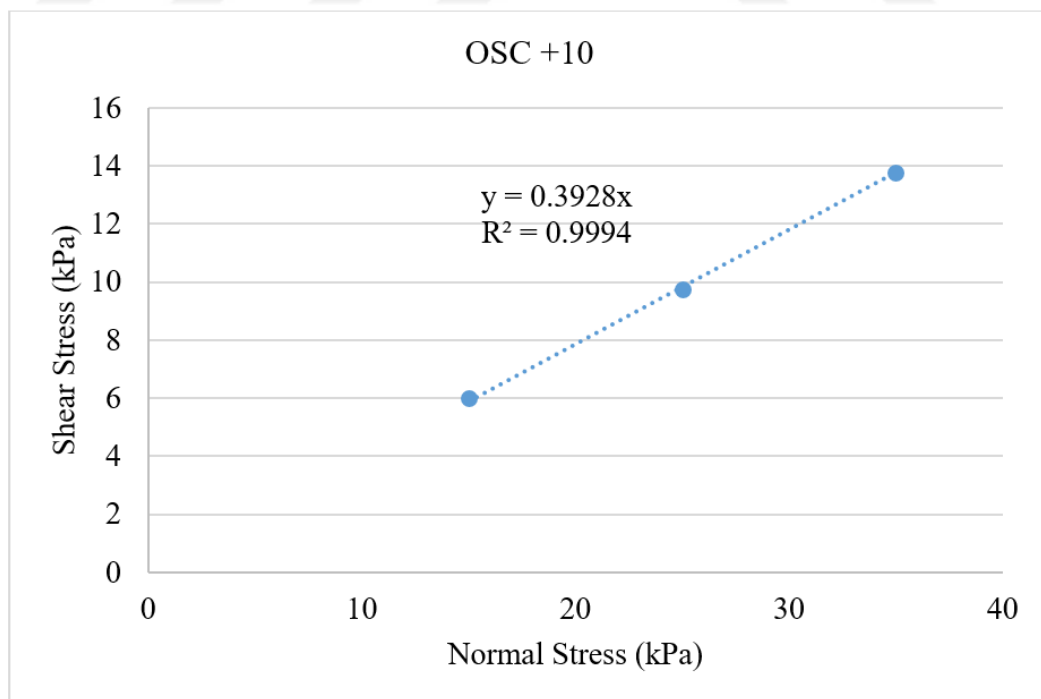


Figure A.6. Mohr-Coulomb Envelope for the Unit Cell with OSC at +10 mm Horizontal Displacement during Monotonic Shearing.

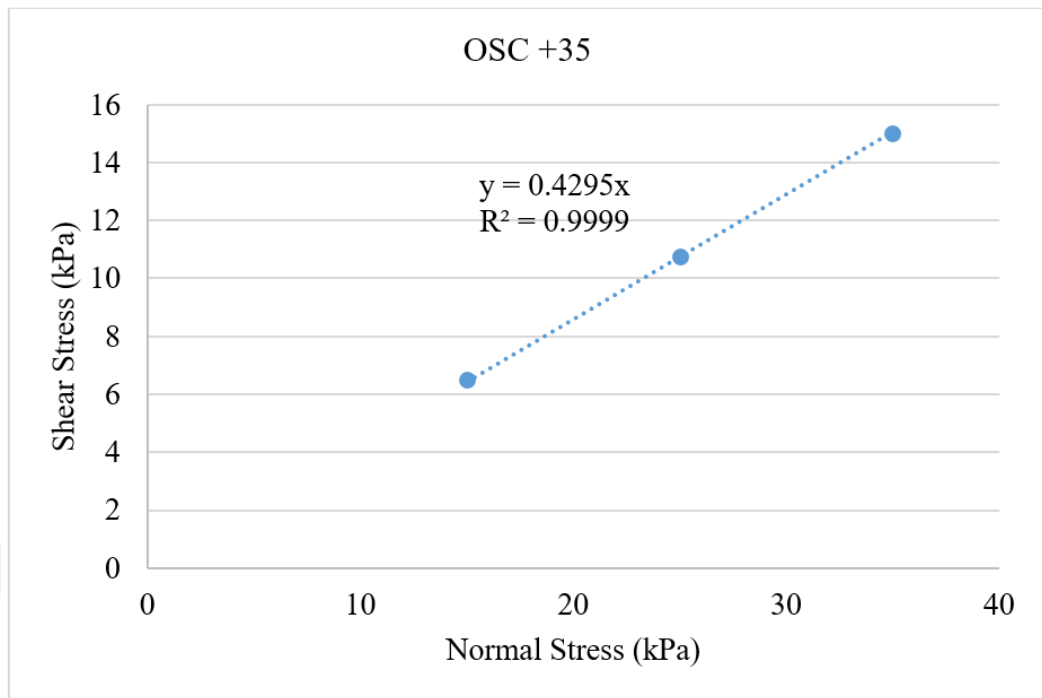


Figure A.7. Mohr-Coulomb Envelope for the Unit Cell with OSC at +35 mm Horizontal Displacement during Monotonic Shearing.

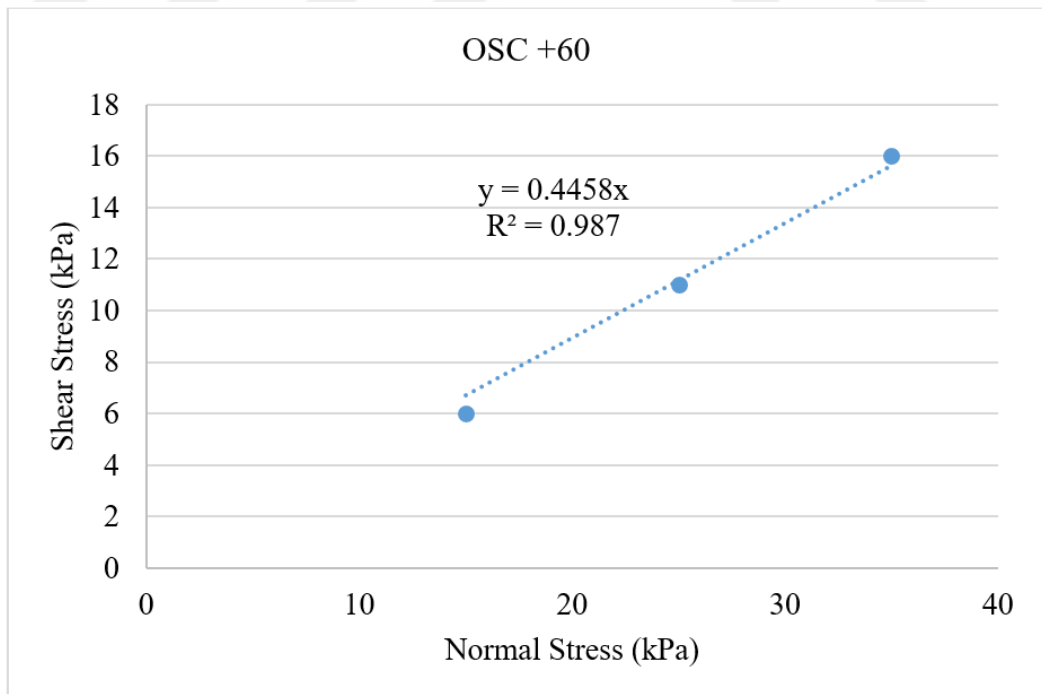


Figure A.8. Mohr-Coulomb Envelope for the Unit Cell with OSC at +60 mm Horizontal Displacement during Monotonic Shearing.

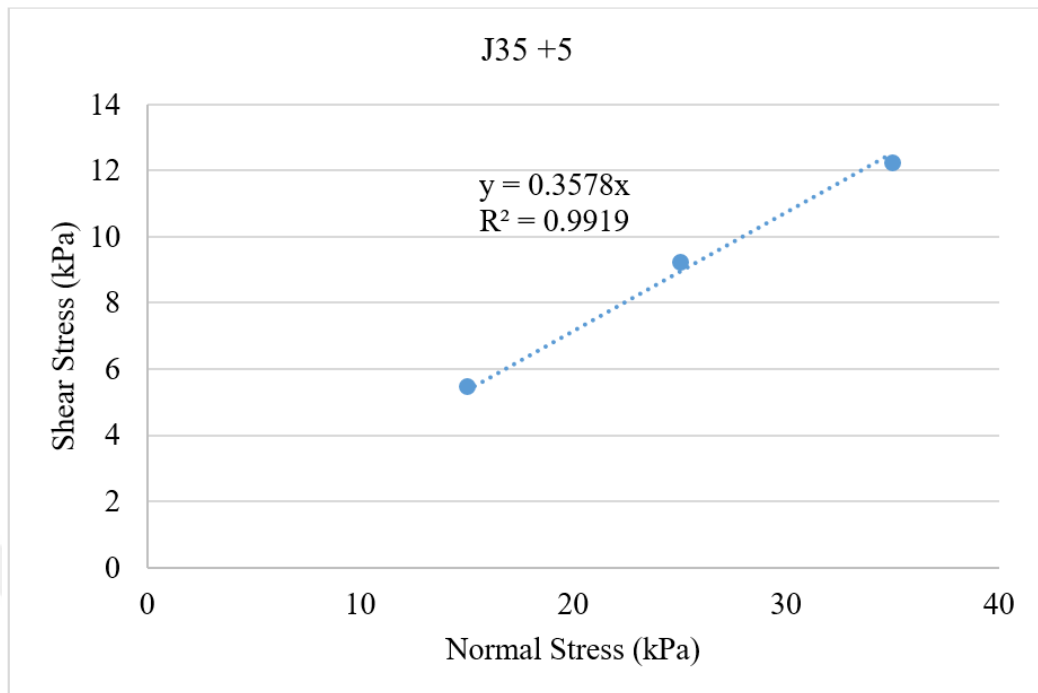


Figure A.9. Mohr-Coulomb Envelope for the Unit Cell with J35 at +5 mm Horizontal Displacement during Monotonic Shearing.

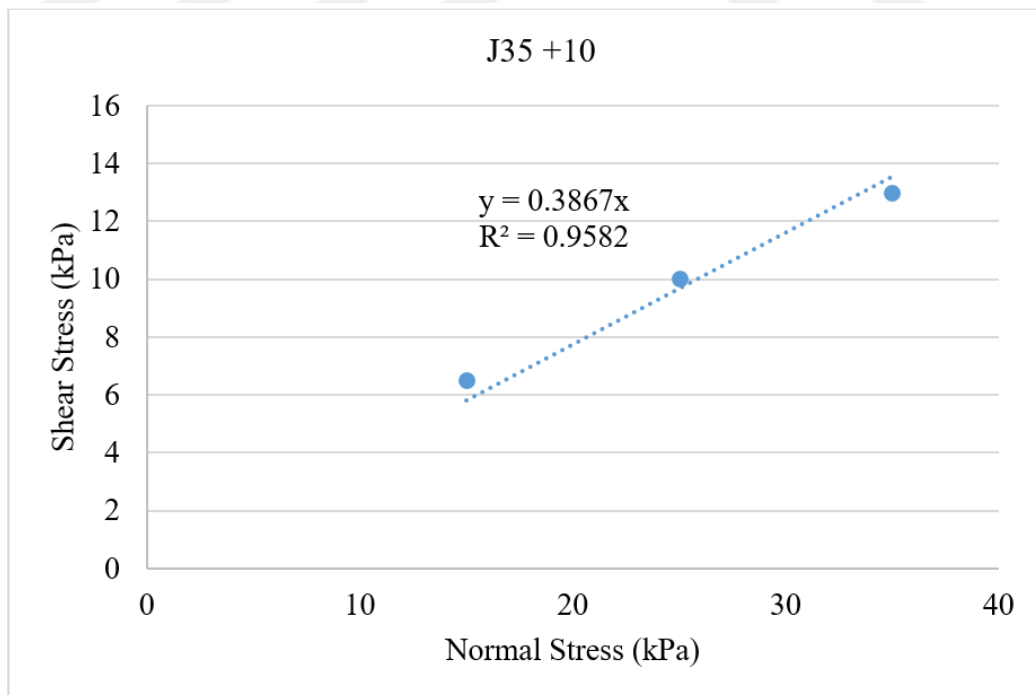


Figure A.10. Mohr-Coulomb Envelope for the Unit Cell with J35 at +10 mm Horizontal Displacement during Monotonic Shearing.

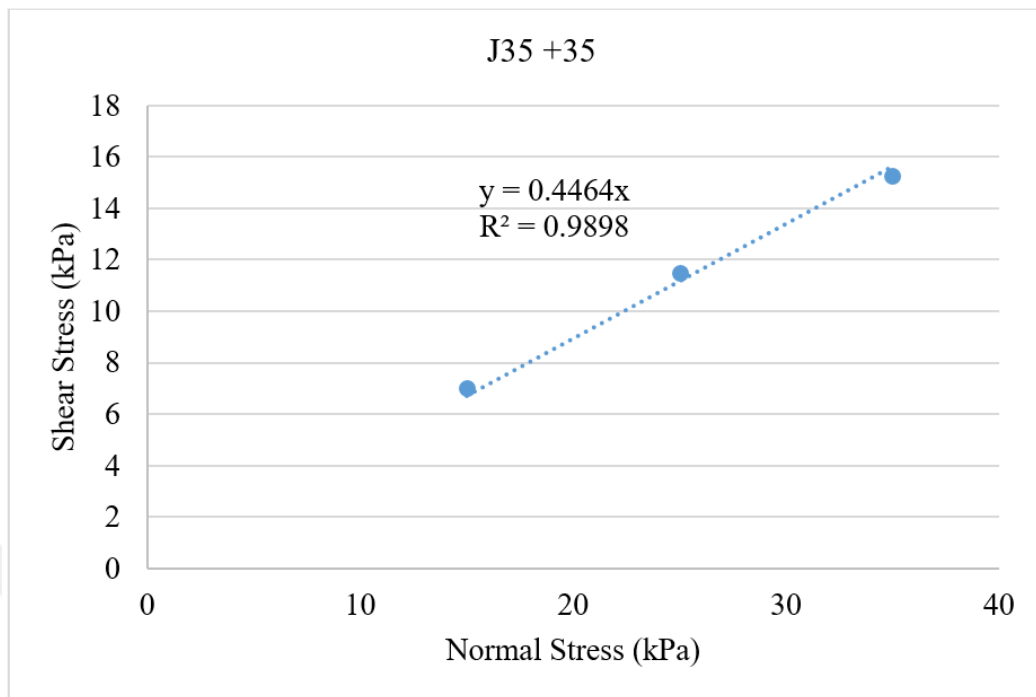


Figure A.11. Mohr-Coulomb Envelope for the Unit Cell with J35 at +35 mm Horizontal Displacement during Monotonic Shearing.

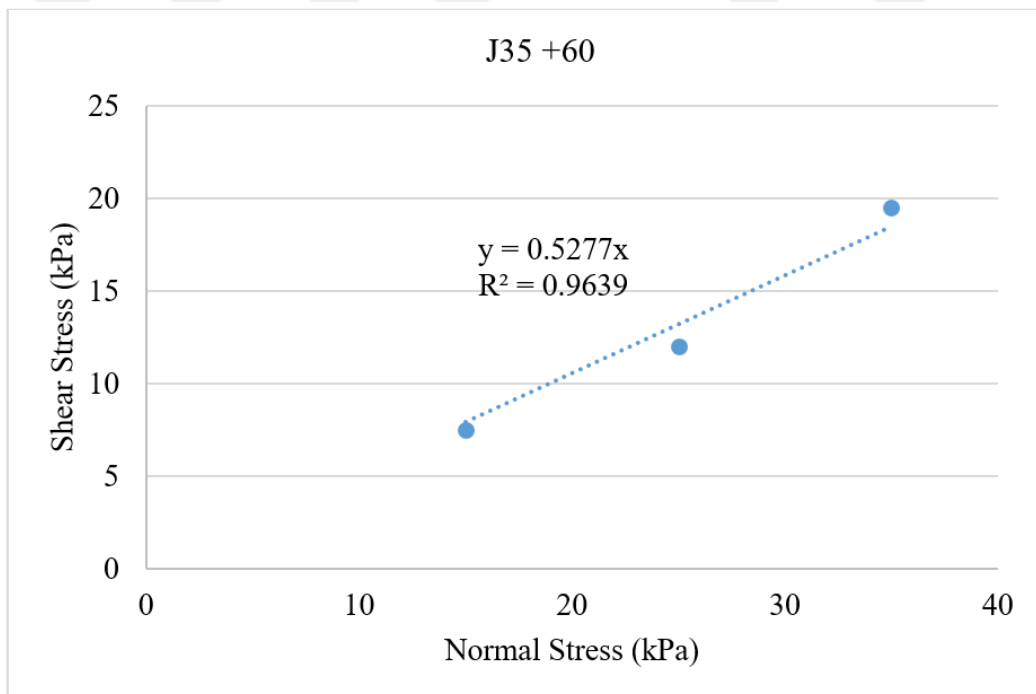


Figure A.12. Mohr-Coulomb Envelope for the Unit Cell with J35 at +60 mm Horizontal Displacement during Monotonic Shearing.

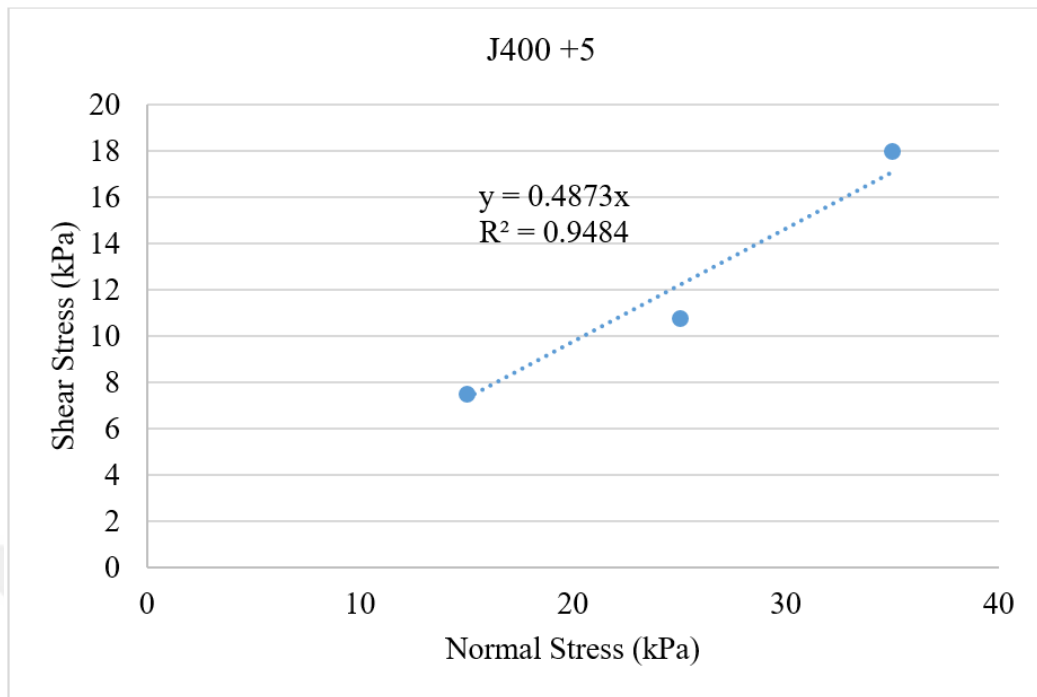


Figure A.13. Mohr-Coulomb Envelope for the Unit Cell with J400 at +5 mm Horizontal Displacement during Monotonic Shearing.

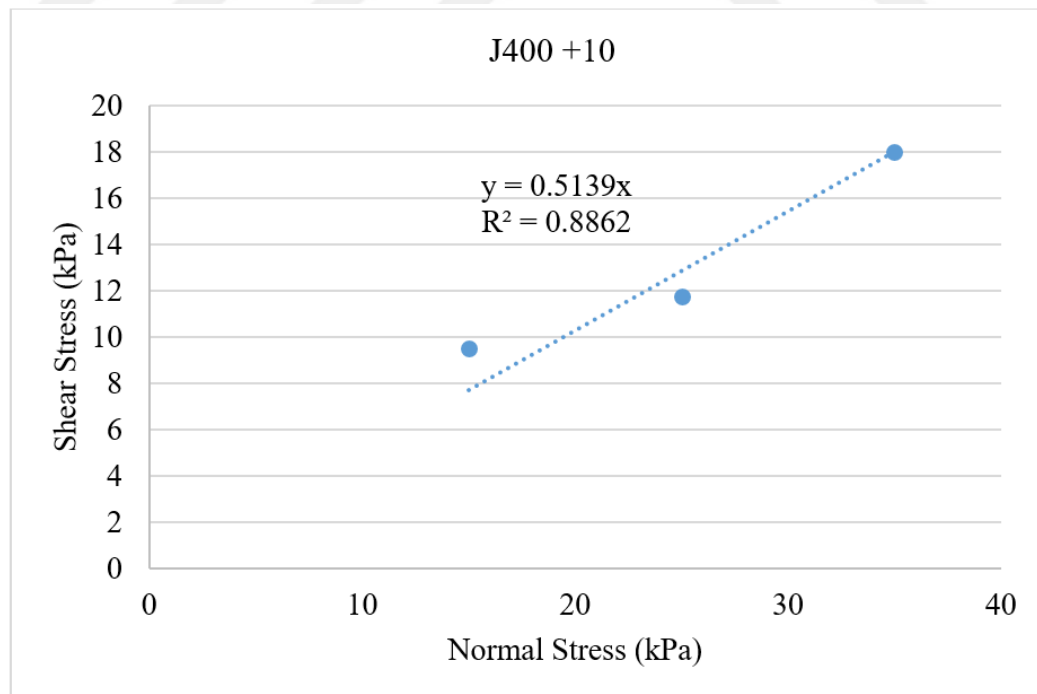


Figure A.14. Mohr-Coulomb Envelope for the Unit Cell with J400 at +10 mm Horizontal Displacement during Monotonic Shearing.

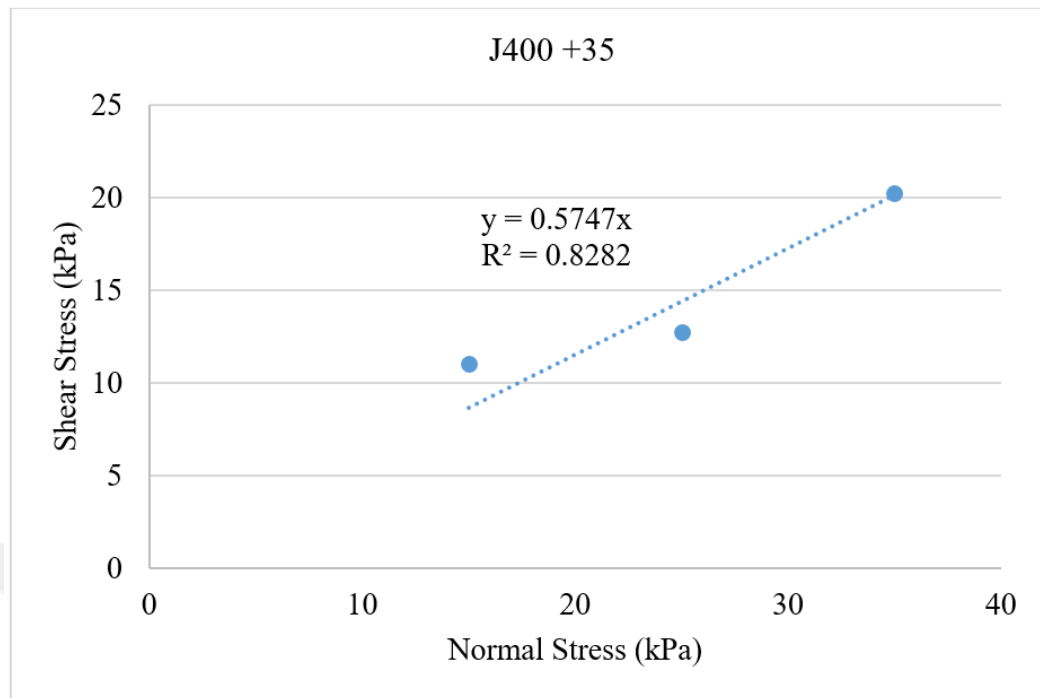


Figure A.15. Mohr-Coulomb Envelope for the Unit Cell with J400 at +35 mm Horizontal Displacement during Monotonic Shearing.

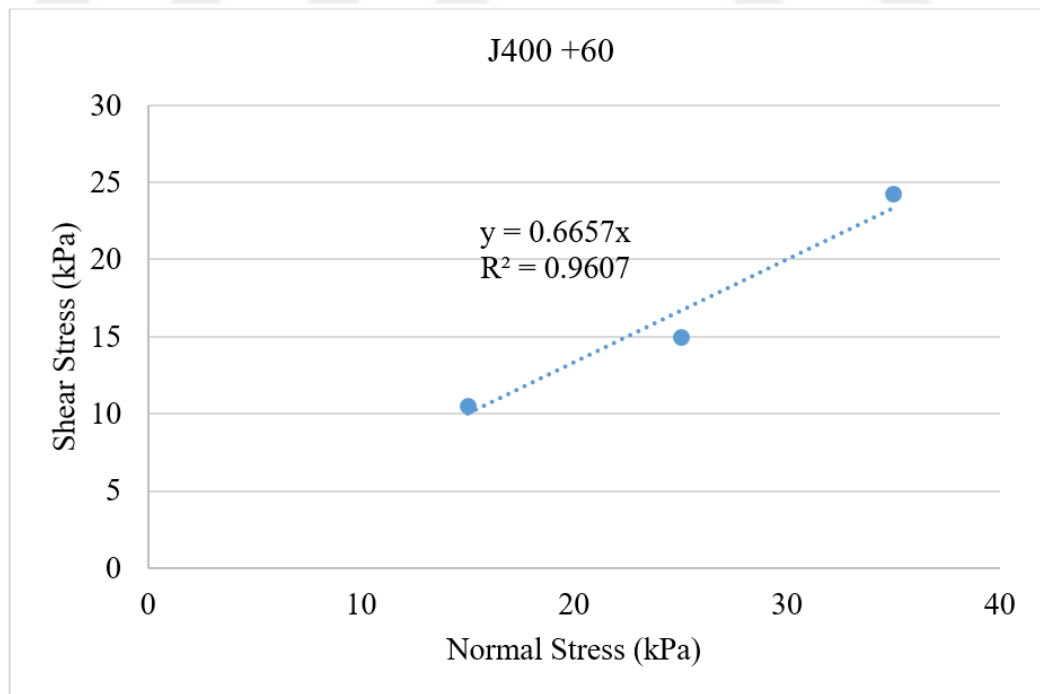


Figure A.16. Mohr-Coulomb Envelope for the Unit Cell with J400 at +60 mm Horizontal Displacement during Monotonic Shearing.

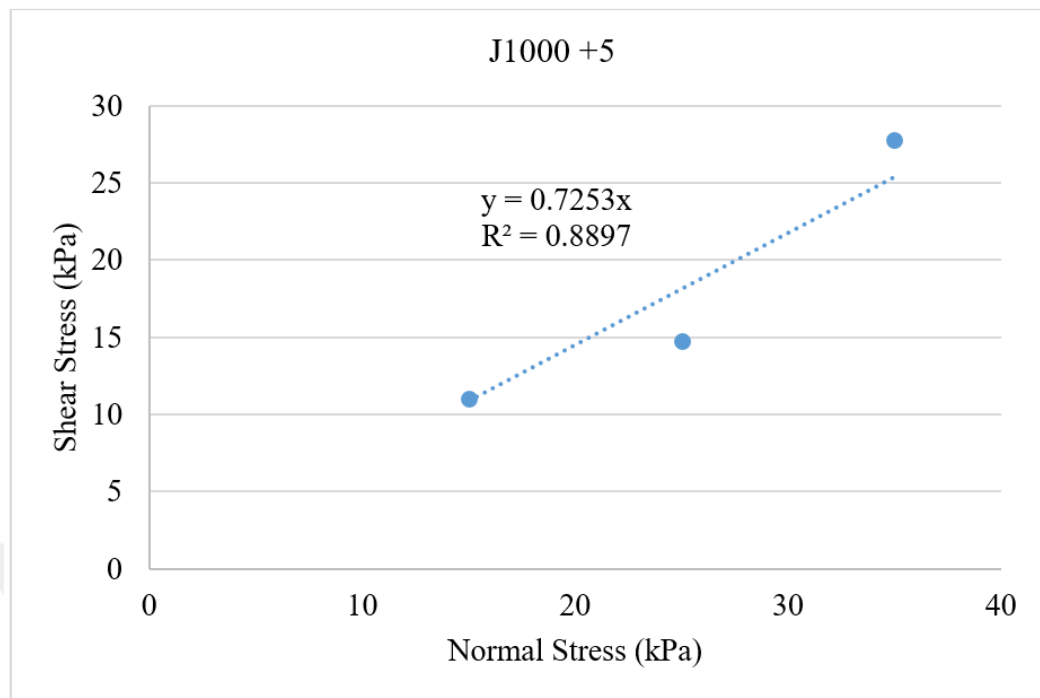


Figure A.17. Mohr-Coulomb Envelope for the Unit Cell with J1000 at +5 mm Horizontal Displacement during Monotonic Shearing.

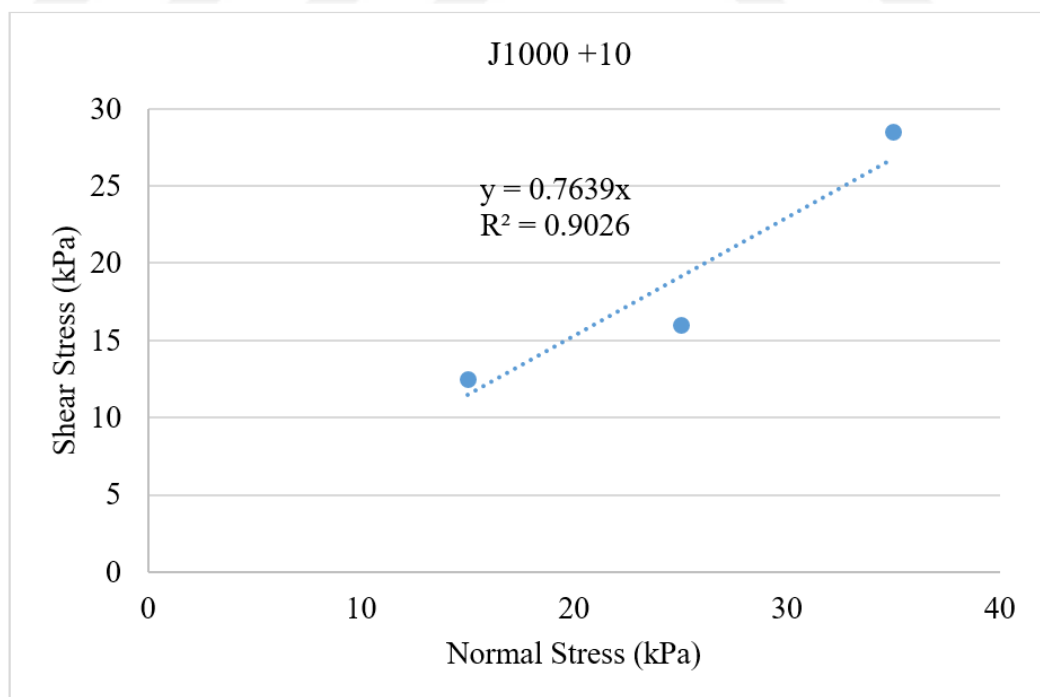


Figure A.18. Mohr-Coulomb Envelope for the Unit Cell with J1000 at +10 mm Horizontal Displacement during Monotonic Shearing.

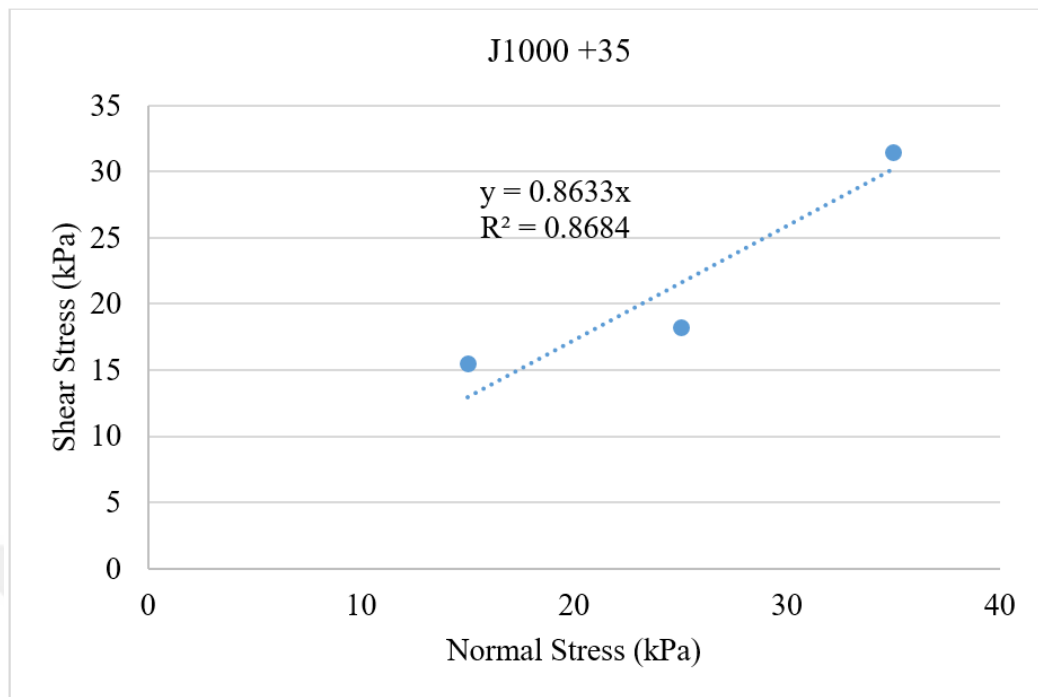


Figure A.19. Mohr-Coulomb Envelope for the Unit Cell with J1000 at +35 mm Horizontal Displacement during Monotonic Shearing.

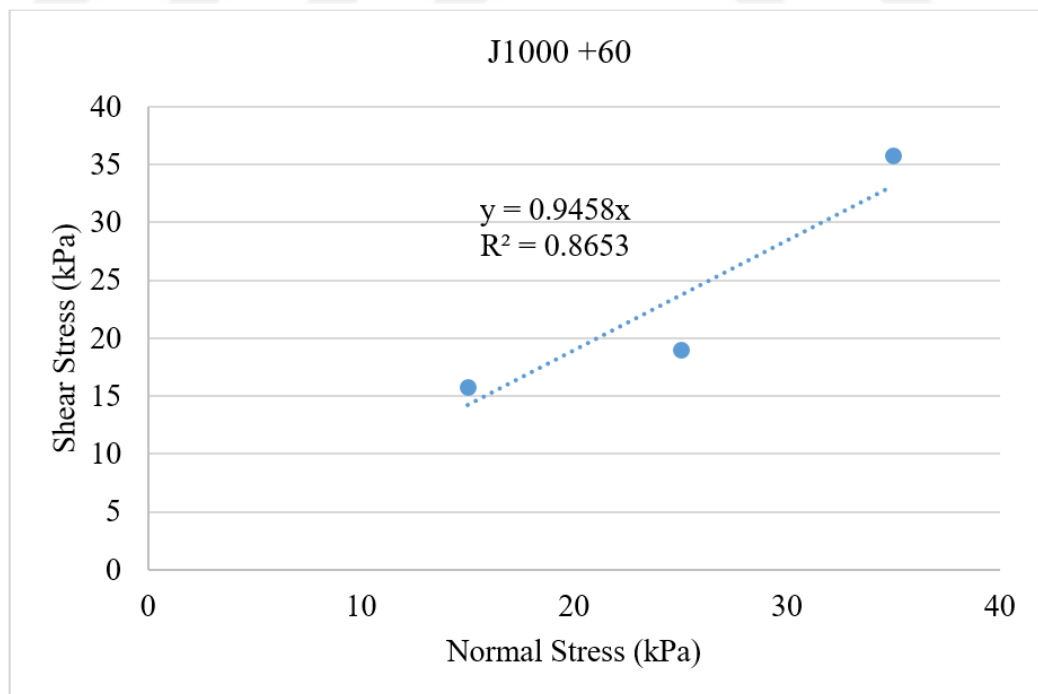


Figure A.20. Mohr-Coulomb Envelope for the Unit Cell with J1000 at +60 mm Horizontal Displacement during Monotonic Shearing.

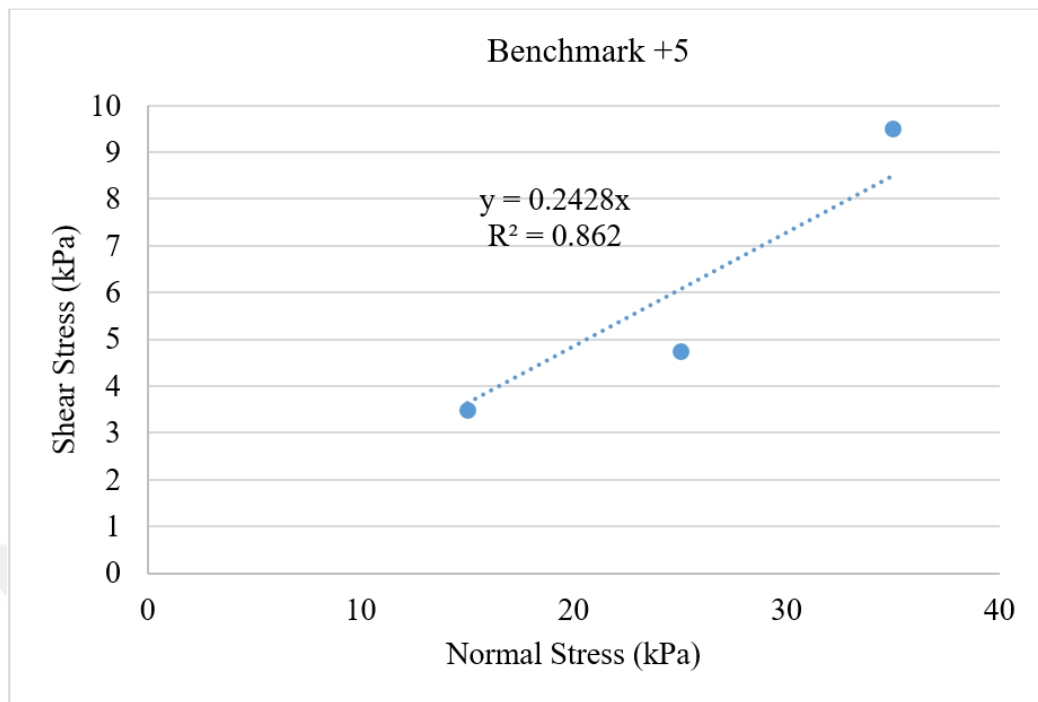


Figure A.21. Mohr-Coulomb Envelope for the Benchmark Unit Cell at +5 mm Horizontal Displacement during Cyclic Shearing.

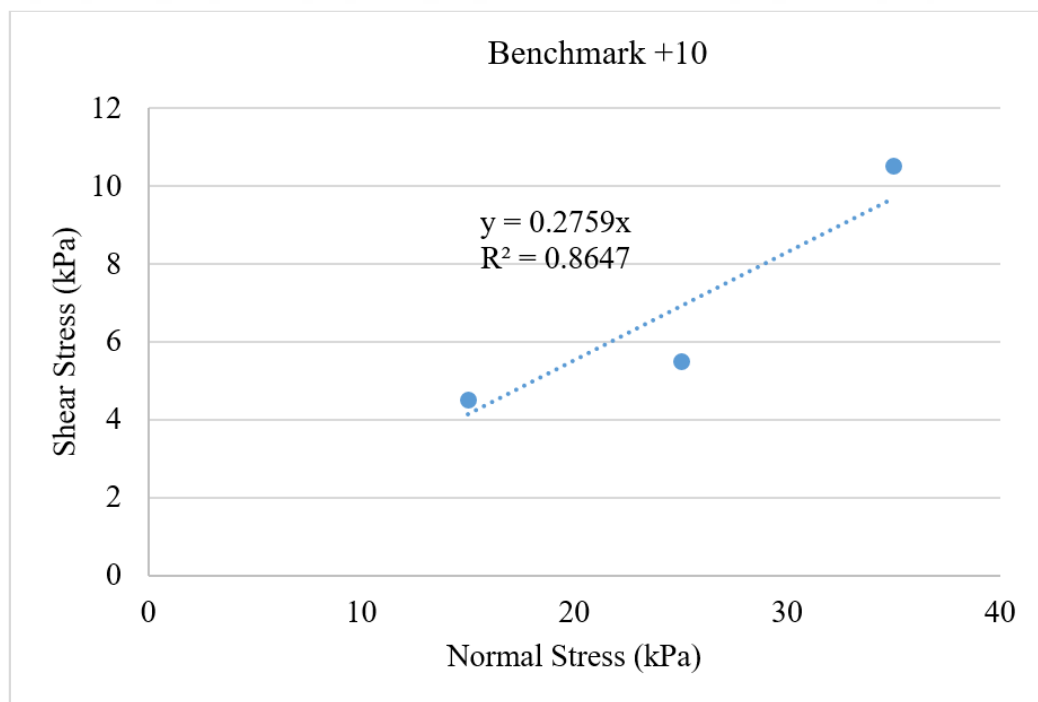


Figure A.22. Mohr-Coulomb Envelope for the Benchmark Unit Cell at +10 mm Horizontal Displacement during Cyclic Shearing.

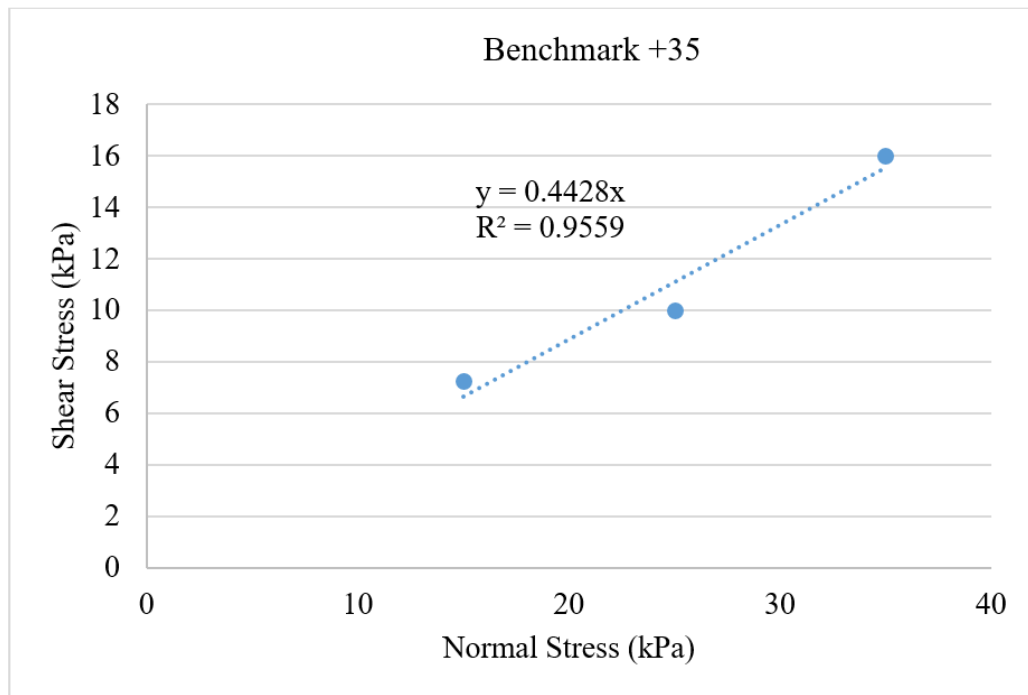


Figure A.23. Mohr-Coulomb Envelope for the Benchmark Unit Cell at +35 mm Horizontal Displacement during Cyclic Shearing.

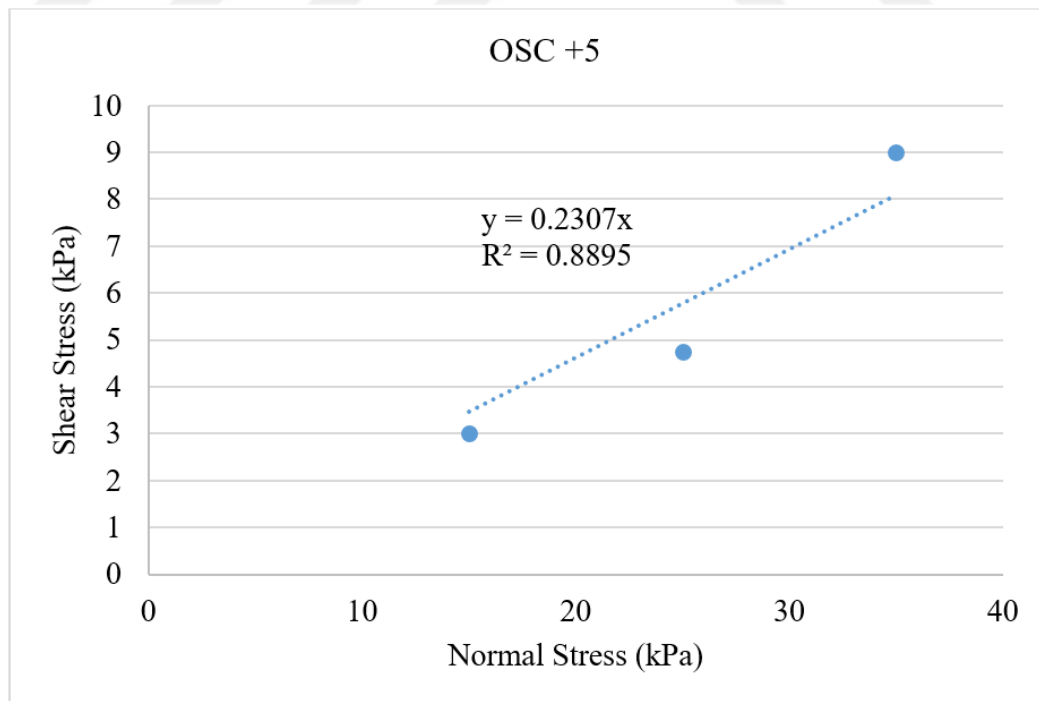


Figure A.24. Mohr-Coulomb Envelope for Unit Cell with OSC at +5 mm Horizontal Displacement during Cyclic Shearing.

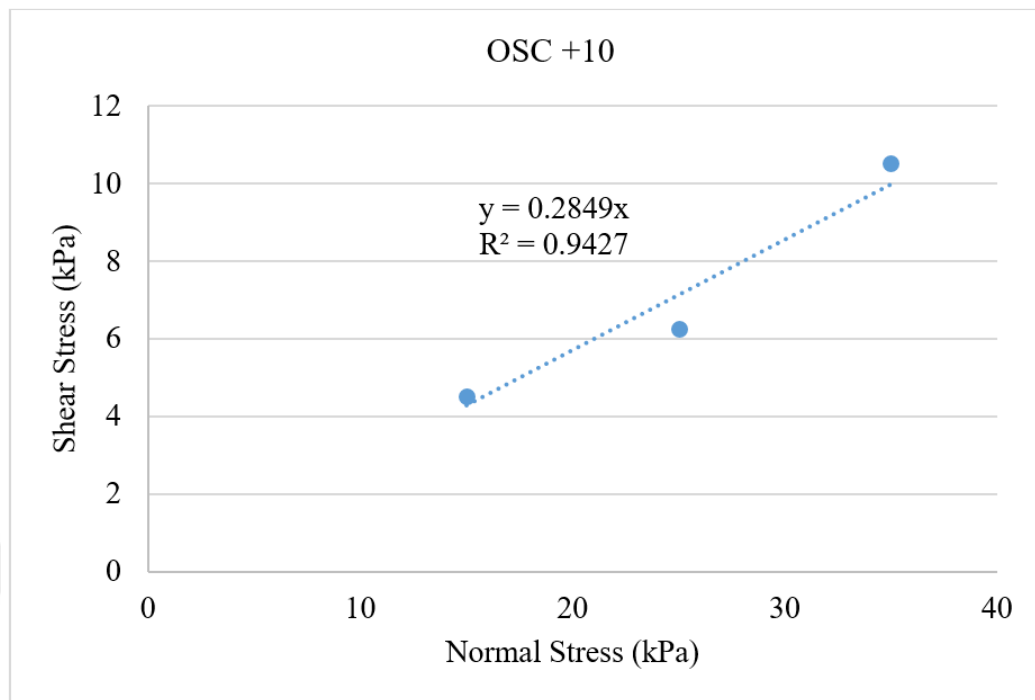


Figure A.25. Mohr-Coulomb Envelope for Unit Cell with OSC at +10 mm Horizontal Displacement during Cyclic Shearing.

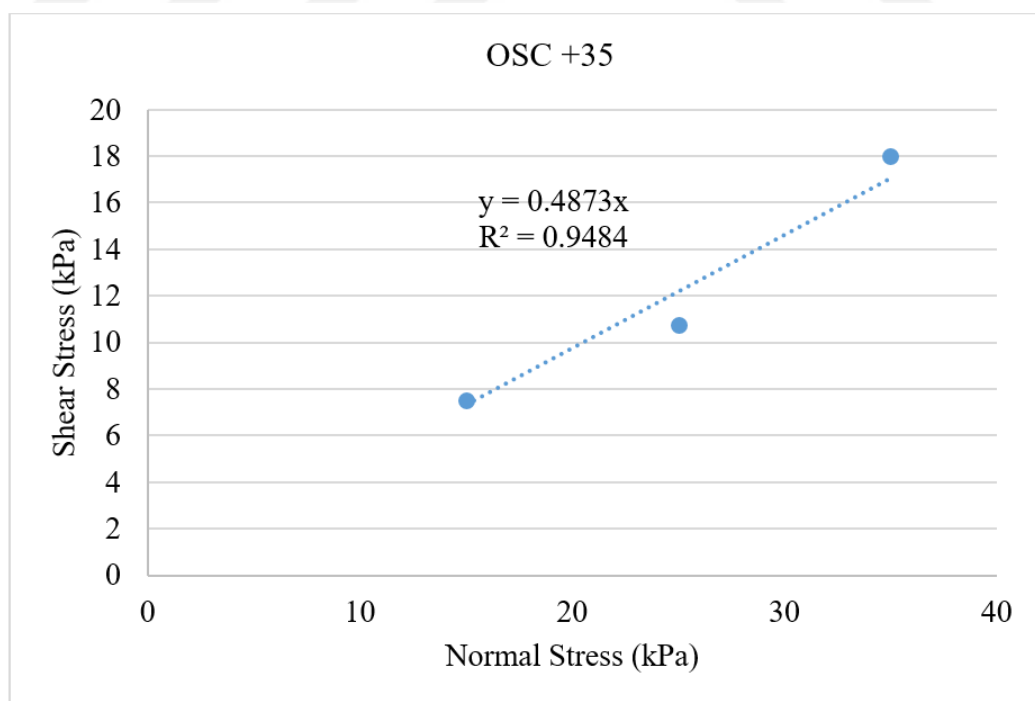


Figure A.26. Mohr-Coulomb Envelope for Unit Cell with OSC at +35 mm Horizontal Displacement during Cyclic Shearing.

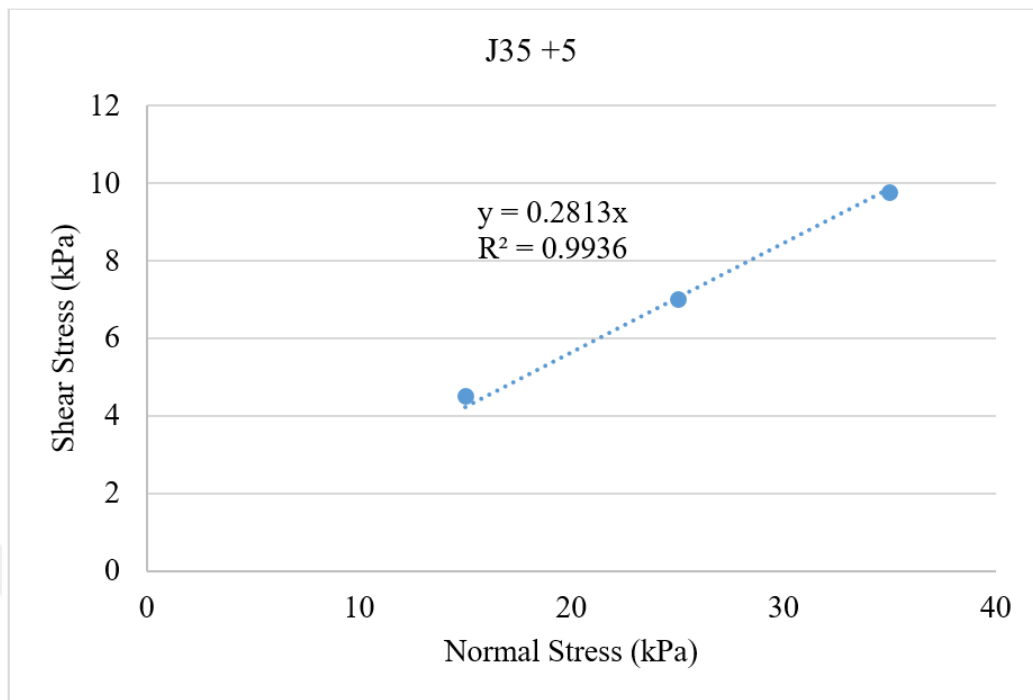


Figure A.27. Mohr-Coulomb Envelope for Unit Cell with J35 at +5 mm Horizontal Displacement during Cyclic Shearing.

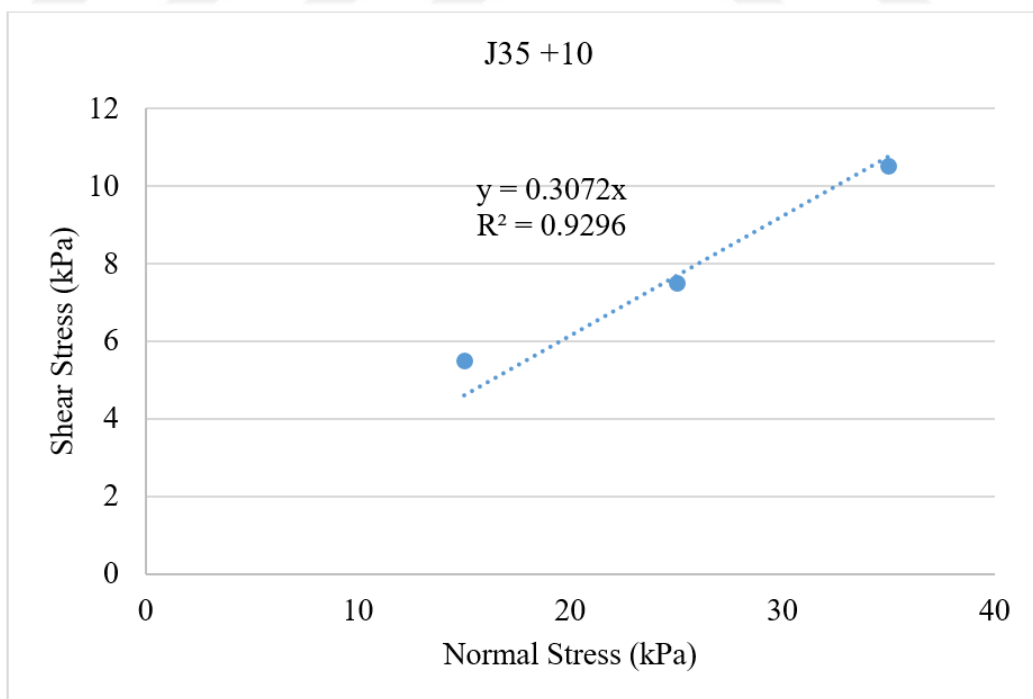


Figure A.28. Mohr-Coulomb Envelope for Unit Cell with J35 at +10 mm Horizontal Displacement during Cyclic Shearing.

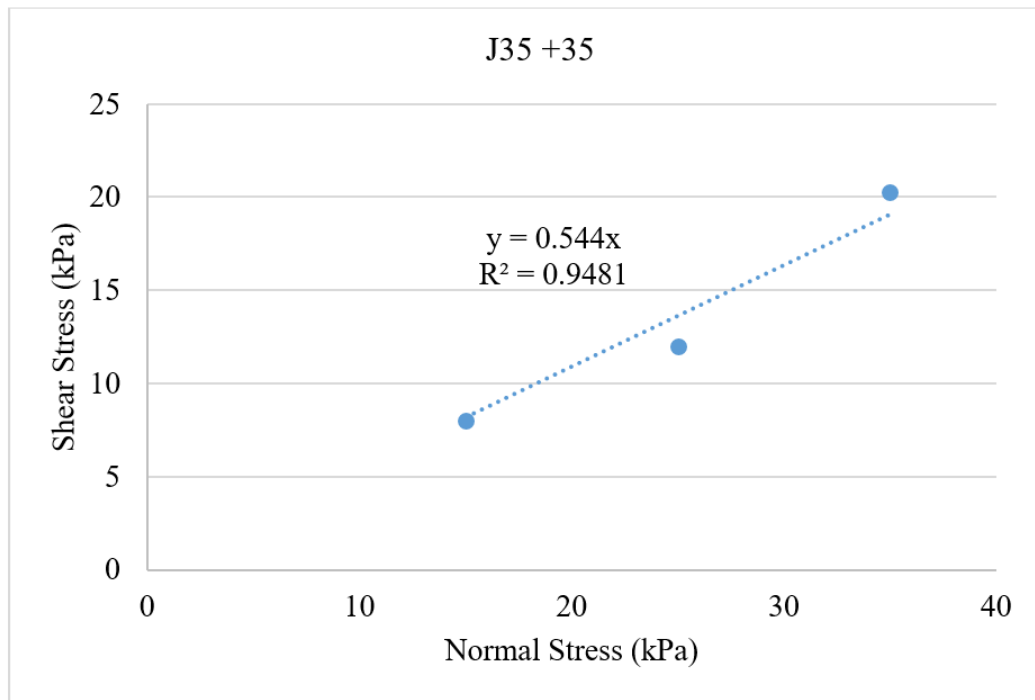


Figure A.29. Mohr-Coulomb Envelope for Unit Cell with J35 at +35 mm Horizontal Displacement during Cyclic Shearing.

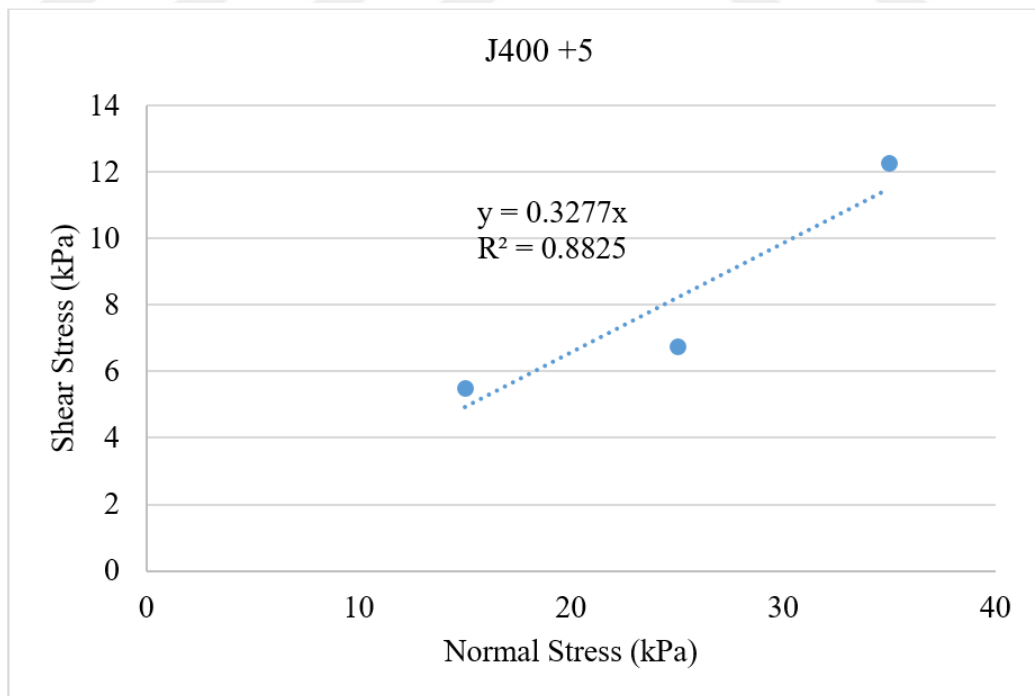


Figure A.30. Mohr-Coulomb Envelope for Unit Cell with J400 at +5 mm Horizontal Displacement during Cyclic Shearing.

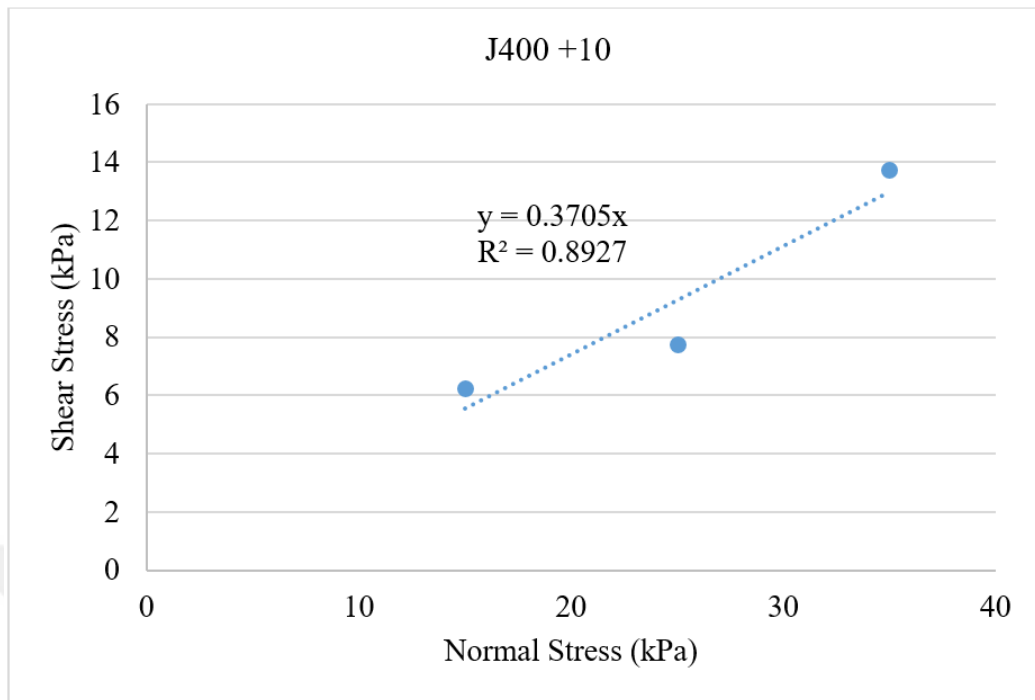


Figure A.31. Mohr-Coulomb Envelope for Unit Cell with J400 at +10 mm Horizontal Displacement during Cyclic Shearing.

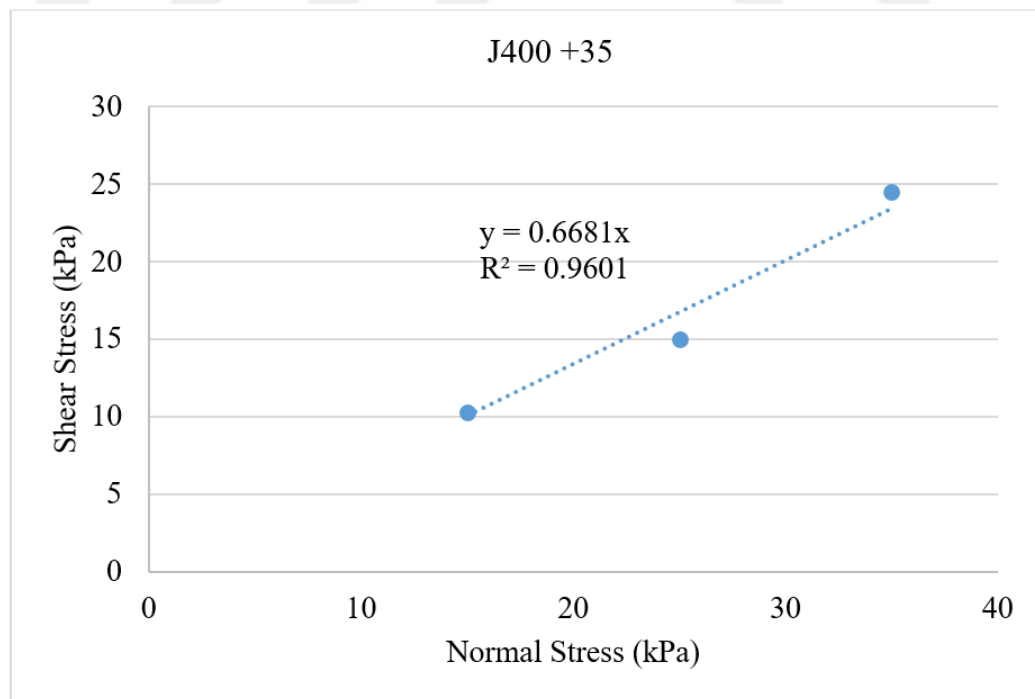


Figure A.32. Mohr-Coulomb Envelope for Unit Cell with J400 at +35 mm Horizontal Displacement during Cyclic Shearing.

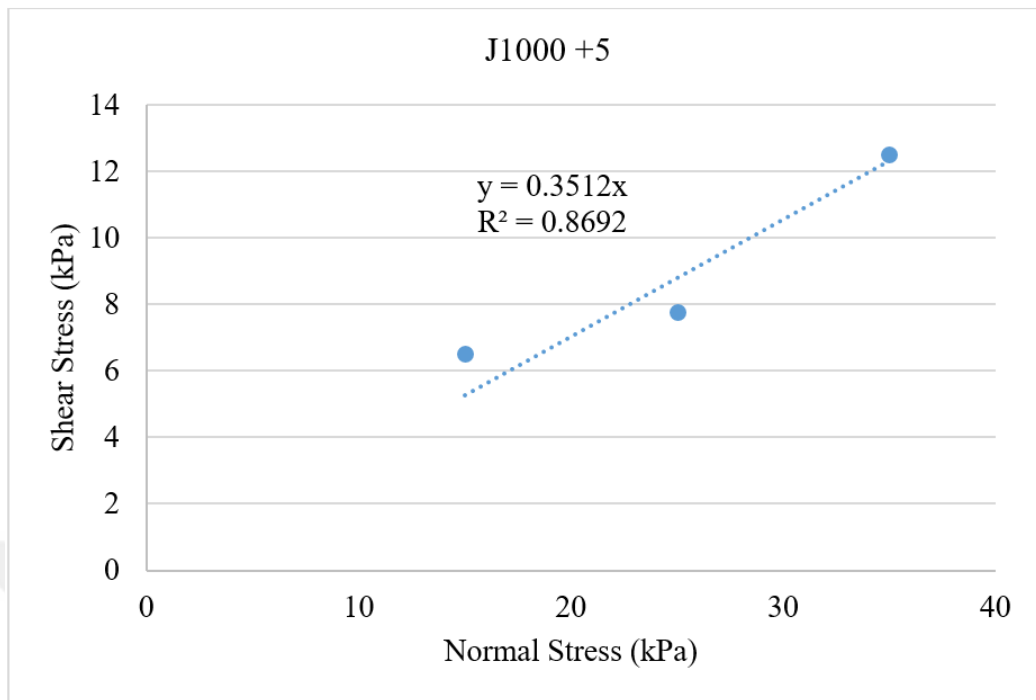


Figure A.33. Mohr-Coulomb Envelope for Unit Cell with J1000 at +5 mm Horizontal Displacement during Cyclic Shearing.

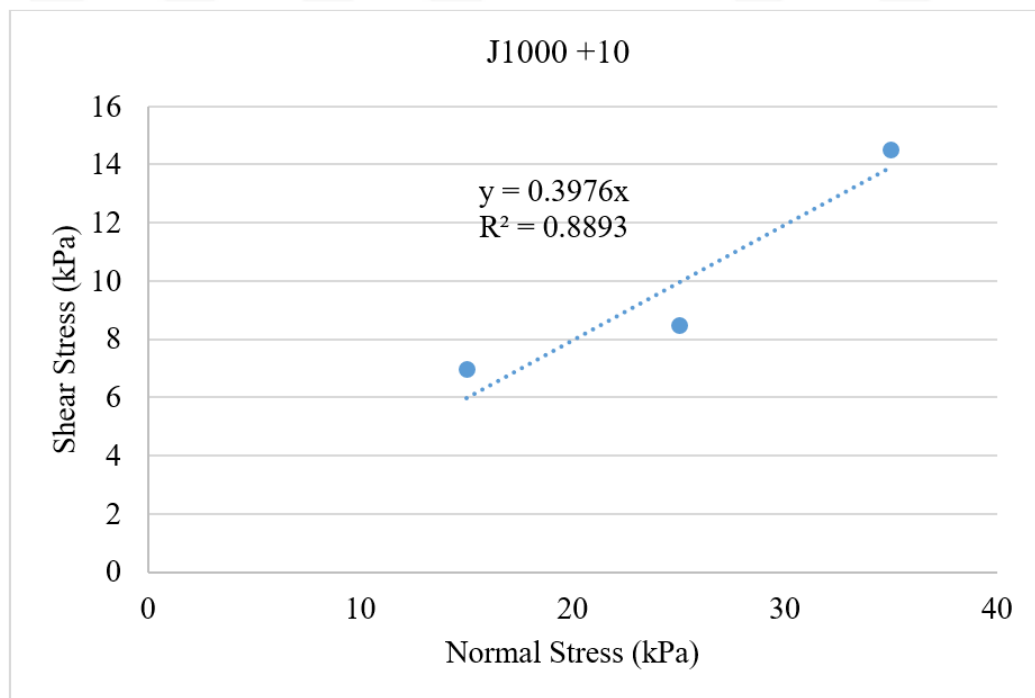


Figure A.34. Mohr-Coulomb Envelope for Unit Cell with J1000 at +10 mm Horizontal Displacement during Cyclic Shearing.

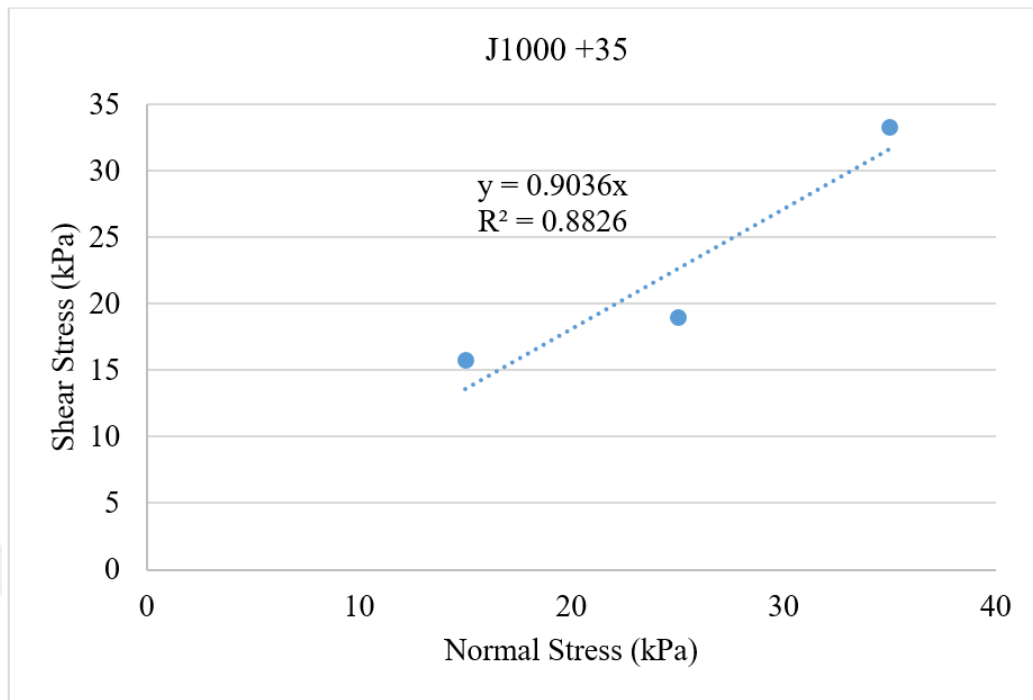


Figure A.35. Figure A.34. Mohr-Coulomb Envelope for Unit Cell with J1000 at +35 mm Horizontal Displacement during Cyclic Shearing.